PFC/RR-83-35 DOE/ET/51013-109

INTRODUCTION TO TANDEM MIRROR PHYSICS

Massachusetts Institute of Technology

J. Kesner

M.J. Gerver B.G. Lane

B.D. McVey

Science Applications, Inc.

Boulder, CO

R.E. Aamodt

P.J. Catto D.A. D'Ippolito

J.R. Myra

September 1983

Plasma Fusion Center

Massachusetts Institute of Technology

Cambridge, Massachusetts 02139

Summary

This monograph, prepared jointly by the MIT Plasma Fusion Center Mirror Fusion group and SAI, Boulder, Colorado, presents a review of the development of mirror fusion theory from its conception some thirty years ago to the present. Pertinent historic experiments and their contribution are discussed to set the stage for a detailed analysis of current experiments and the problems which remain to be solved in bringing tandem mirror magnetic confinement fusion to fruition.

In particular, Chapter III discusses in detail the equilibrium and stability questions which must be dealt with before tandem mirror reactors become feasible, while Chapters IV and V discuss some of the current machines and those under construction which will help to resolve critical issues in both physics and engineering whose solutions are necessary to the commercialization of tandem mirror fusion.

We acknowledge the valuable assistance of A.M. Dawson in preparing and editing the text, and R.S. Post for important observations and support. We thank Lawrence Livermore National Laboratory's Mirror Fusion Division for assistance with illustrations and Vera Schultz and Patricia Fina for typing the manuscript.

CONTENTS

CONTENTS (cont.)

CONTENTS (cont.)

List of Figures

List of Figures (cont.)

List of Figures (cont.)

List of Figures (cont.)

List of Tables

I. INTRODUCTION: THE DEVELOPMENT OF THE TANDEM MIRROR CONCEPT IN THE UNITED STATES

I.A General Comments

Thirty years have passed since the first laboratory experiment demonstrated that a plasma in a straight solenoid configuration with uniform central magnetic field remained for a longer time when the field strength was increased at the ends by energizing magnetic mirror coils [Post and Steller, 1952]. During this time span the research in mirror containment of a hot plasma has advanced at an accelerating rate from a program initially aimed at establishing the qualitative feasibility of the mirror fusion concept to the present broadly-based program aimed at eventually determining the economic aspects of a mirror fusion power reactor. While the ultimate mirror configuration may yet be discovered, the current tandem mirror design appears to offer optimistic and satisfactory solutions to the envisaged problems of a fusion power economy; it is presently one of the principal design approaches of the U.S. magnetic fusion energy program. The purpose of this monograph is to present the physics concepts, review the principal experimental data bases, and discuss some of the attendant engineering scenarios which have led to these conclusions.

In the early 1950's the world–wide impetus to create a self–sustaining controlled thermonuclear reaction generated a considerable number of different magnetic design configurations, all based on the notion that the transport of plasma across field lines should be slow enough that the fusion nuclei would have time to burn adequately. The U.S. mirror program thereby began with a straight

solenoidal magnetic field design and the idea of stopping the unrestricted flow of particles parallel to the radially-confining DC magnetic field with rf field pressure [York, 1952]. However, in order to reduce the required intensity of rf to reasonable values for systems at thermonuclear temperatures and densities, DC mirror coils were conceptually added to constrict the parallel particle momentum flux [Post and Steller, 1952; Budker, 1954]. It then appeared that, without rf stoppering, a simple mirror device of the type shown in Fig. I.A.1, while having large and perhaps troublesome particle losses parallel to the field, would ultimately have a sufficient number of nuclei fuse before leaving the system and achieve a net power gain if the mirror fields were made strong enough and the fusing nuclei were made extremely energetic. Furthermore, at these earliest stages of the mirror program it appeared that the linear geometry offered the energy economics opportunity of being able to "pay" for the end stoppering by simply adding more (fusion-power) length in the middle [Post, 1954]. These basic mirror principles originally determined the need for high magnetic fields, very energetic particles and possible long central cell volumes and initiated a research and development program which emphasized high-energy, high-current particle beam injection (originally charge-neutralized ion beams) into solenoidal magnetic geometries with high field mirrors, high vacuum, and radial and axial compression (and decompression) capabilities for heating the plasma and for adiabatically-trapping the injected ion beams [Post, 1954]. Today's tandem mirror reactor appears, at first sight, to be surprisingly similar to this original, three-decades-old scenario. The basics today involve energetic high current steady state (neutral) beam injection into a high vacuum, high field system with a long solenoid and with supplemental rf heating. Additionally, today's reactor

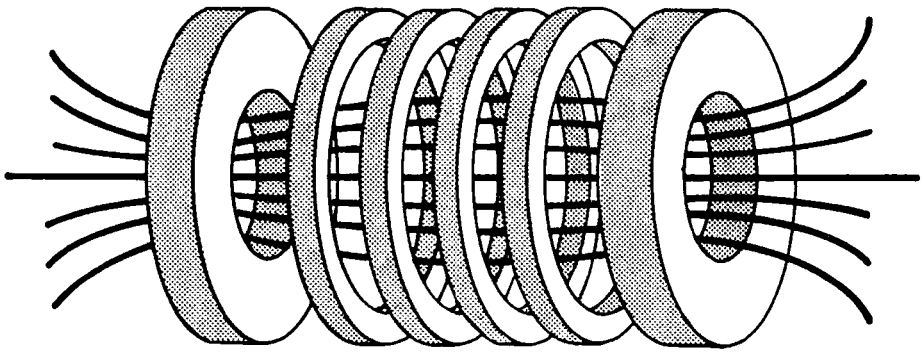

Figure I.A.1 A simple mirror device without rf stoppering

concept still takes advantage of the directed particle end losses by employing efficient electrical direct converter designs on the mirror ends, a concept conceived early in the initial phases of the world's mirror program [Budker, 1954]. However, the differences are enormous because today's design is based on augmenting mirror fields with longitudinal electrostatic confinement, an extensive knowledge of the need for stability and where to find it in parameter space, and a set of engineering and technological design criteria which appear to be achievable. Critically important, too, is that the present design has a predicted power amplification factor, Q, defined as the ratio of fusion power output to the total power input, an order of magnitude larger than the original design was ever capable of reaching. Both the higher Q and the reduced technology requirements for today's mirror reactor are a direct consequence of the concept of longitudinal electrostatic confinement which dramatically reduces energy and particle losses parallel to the confining magnetic field and thereby alleviates the need for ultra-high temperature plasmas and concomitantly reduces the high technology required to produce and sustain them. It is *this* principle of longitudinal electrostatic confinement which is the essential feature of the tandem mirror design and as such forms the main physics theme of this monograph.

I.B Early Experiments and Technology Development

The early progress in the mirror program came as a direct result of attempting to create, sustain and diagnose the very high temperature plasmas required for effective mirror containment. Initially there was a lack of high energy plasma or beam injectors with adequate particle currents, so the early experiments centered on creating a hot plasma by plasma injection into the region between mirrors, trapping the injected plasma with a pulsed mirror field, and then heating the trapped plasma by compressing the magnetic field by factors as large as 10^3. These experimental programs led to the development of high-field pulsed magnets and high-powered condenser banks, microwave interferometry as a plasma density diagnostic, and the development of ultra-high-vacuum techniques including titanium gettering with application to large fusion devices. This latter development resulted from the observations that (1) charge exchange events, not mirror containment physics, were dominating the mirror experiments and (2) an extraordinarily low level of neutrals would have to be maintained in order for charge exchange times to be significantly longer than the short mirror containment times. This would be especially true in later experiments where large currents of neutral beams would be used to heat and sustain the plasma.

While the possible importance of a magnetic well was theorized soon after the mirror program started [Teller, 1954; Post, 1954; Budker, 1959] the initial experiments were done in symmetric mirror traps having an axial but not a radial well configuration. The earliest injection, trapping and compression experiments turned out to be hot electron plasma devices (see Table I.1), and these were

Table I.1 Early (circa 1958) Mirror Machines

Name	$n(cm^{-3})$	T_i(keV)	Type of Plasma Injection	Type of Heating	Purpose of Experiment
ARGUS	Earth's magnetosphere		Nuclear explosion into magnetosphere	None	Confinement
TABLE TOP	2×10^{13}	3.5	Washer Gun	Compression	Trapping, Heating, Confinement
DCX	10^5	300	Molecular Ion Breakup	No additional	Very High Energy Plasma Containment
OGRA I	10^5	80	Molecular Ion Breakup	No additional	– – –

observed to persist stably for millisecond–long time periods. While this apparent gross stability property unfortunately temporarily misled the mirror program into ignoring the requirement of a magnetic well for MHD stability and, in fact, made MHD theory totally suspect, the instrumental and technological advance achieved during this period laid a strong base for subsequent experimental progress in the mirror field.

Throughout this same era important theoretical advances were being made which would allow quantitative analyses of mirrors, forewarn of critical stability problems, and improve operating performances. These included: the calculation of collisionally-induced end losses [Rosenbluth *et al.*, 1957; Budker, 1959]; the development of the guiding center theory of adiabatic particle confinement in mirrors [Northrup and Teller, 1960]; the low frequency interchange stability criterion [Rosenbluth and Longmire, 1957; Bernstein *et al.*, 1958; Berkowitz *et al.*, 1958; Kadomtsev, 1959]; and the idea of creating high temperature fusion plasmas with energetic neutral beams [Colgate *et al.*, early 50's], ion beams followed by compression [Post, 1954], and molecular beam injection with trapping by dissociation [Luce, 1956; Barnett *et al.*, 1959].

A critical period for the mirror fusion program followed this initial phase, for the all–important problems of macro– and microstability began to influence both the experimental results and the fusion reactor performance predictions. The experimental progress which led the program into this new regime came as a result of improved methods of injection trapping and compression and high energy beam injection (see Table I.2). The net result was the creation of hot ion, rather than hot electron, plasmas, but now there was an attendant loss of

Table I.2 Axisymmetric Mirror Machines

Name	Year	n	T_i(keV)	T_e(eV)	Type of Plasma Injection	Type of Plasma Heating	Purpose of Experiment
ALICE	1962	2×10^8	20	–	Neutral beam injection		Flute instability studies
OGRA III	1972	5×10^9	20	–	Neutral beam	Neutral beam	Feedback stabilization
PR-2	Early 60's	10^9	1.2	10	Arc	Turbulent	Confinement
PHOENIX 1A	1964	3×10^8	20	–	Neutral beam injection		– – –
MISE I	1964	4×10^{10}	1	–	Coax-gun	Trapped gun plasma	MHD stabilization
DECA II	1964	$10^{13}/10^{14}$	2	–	Gun	Compressor	Plasma Losses

stability in the symmetric mirror traps, with measured lifetimes now orders of magnitude shorter than predicted by classical collisional processes in a mirror, and even much shorter than the lifetimes observed in the hot electron machines.

In some of the devices cited, a gross deformation of the plasma occurred, and in these cases it was clear that the MHD interchange mode had been activated. However, the extremely short times predicted for the interchange mode to cause the plasma to strike the container walls were never realized [Rosenbluth and Longmire, 1957; Kadomtsev, 1961]. Apparently, the effects of "line-tying" the plasma by charge conduction across field lines by cold, conducting plasma or metal walls outside the mirror regions slowed the nonlinear deformation [Post *et al.*, 1960; Lehnert, 1966; Kunkel and Guillory, 1965; Scott, *et al.*, 1965], and in some of the devices this appeared to suppress totally the interchange mode. Some of the observations can be explained by the finite Larmor radius (FLR) of the hot particles destroying the phase coherence between ions and electrons in an interchange motion, and thereby reducing subsequent plasma distortion [Rosenbluth *et al.*, 1962]. However, an $m = 1$ distortion in a symmetric mirror trap is predicted to be unaffected by FLR effects and so this mechanism cannot explain, by itself, all of the observations.

The interchange mode syndrome vanished when the Russian mirror program dramatically ushered in the so-called minimum-B mirror design which followed the ideas of early theoretical work [Berkowitz *et al.*, 1958; Teller, 1954; Post, 1954; Rosenbluth and Longmire, 1957; Kadomtsev, 1959] that predicted interchange mode stabilization when the plasma is located in a minimum-B system, *i.e.*, at the minimum of a three-dimensional magnetic well. Equivalently,

it had been shown by both a fluid-like MHD approach and a particle picture of a plasma that when a plasma is contained in a magnetic field with convex curvature, the system will be interchange stable. It is easily demonstrated that without sufficiently strong currents internal to the plasma a magnetic well cannot exist in an axisymmetric device and so a plasma can easily be displaced radially towards the wall. In the classic experiment of Ioffe and co-workers [Gott *et al.*, 1961], the "good" curvature region was created by superimposing six linear conductors carrying opposing currents in adjacent rods onto a standard symmetric coil mirror system as shown in Fig. I.B.1a. A pulsed plasma source was used and the plasma decay monitored with and without the current turned on in the six conductors which are now referred to as "Ioffe bars." When the current in the Ioffe bars was raised to a value at which a magnetic well was formed at the plasma boundary, the low frequency fluctuation level in the plasma dropped by orders of magnitude and the plasma lifetime increased dramatically as shown in Fig. I.B.1b.

Within months, Ioffe's interchange stabilizing success was duplicated elsewhere and over the next few years increases in plasma lifetimes were observed worldwide as machines were converted to minimum-B configurations [Biguet *et al.*, 1964; Colchin *et al.*, 1970; Francis *et al.*, 1964, 1965; Damm *et al.*, 1964; Barr and Perkins, 1965]. The major devices of this type are listed in Table I.3. However, the relative increases in lifetimes were not always as dramatic as those reported by Ioffe, and it appeared that in some instances confinement was being limited by problems other than MHD stability. In some of the Ioffe-bar-modified mirrors, for instance, a new problem in the form of impurity contamination

Name	Year	n	T_i(keV)	T_e(eV)	Type of Plasma Injection	Type of Plasma Heating	Purpose of Experiment
2X, 2XII	1964-73	10^{13}	8	–	Gun	Compression	Confinement
2XIIB	1975-78	10^{14}	10	100	Neutral beam	Neutral beam	Confinement
BASEBALL	1966-76	5×10^{9}	20	–	Neutral beam injection		Microstability target plasmas
TABLE TOP	1968	10^{11}	–	25,000	Gun	Compression	Hot electron plasma
PR-6	Middle 60's	10^{12}	–	–	Arc discharge	Turbulent	Confinement & stability
PR-7	1970	10^{12}	–	–	Arc discharge and stability	Turbulent	Confinement & stability
MISE II	1971	5×10^{12}	1.5	15	Gun injected	Trapped gun plasma	Plasma losses in magnetic wells
OGRA II T	1973	10^{13}	2–6	–	Gun	Turbulent	Stability of turbulently heated plasmas
BILLE-EN-TETE	1973	6×10^{11}	1.5	–	Gun	Compression	Confinement & stability
DECA II	1964-70	10^{13}	2	—	Gun	Compression	Plasma losses
DECA IIA	1970-74	10^{12}	1	30	Gun	—	Confinement & stability
PHOENIX II	Late 60's	5×10^{9}	20	20	Neutral beam		– – –
DCX 1.5	–	4×10^{8}	15	–	Neutral beam		High energy confinement
DCX 2	–	5×10^{9}	500	–	Molecular Ion Breakup		High energy confinement

Table I.3 Minimum B – major experiments

of the hot plasmas now arose. As had been recognized theoretically earlier, impurity radiation losses were a critical problem at high temperatures and a very small contamination would create a significant temperature barrier to the necessarily hot mirror-contained plasmas. While, in fact, the Ioffe bars were providing a stabilizing magnetic well for these devices, some of the field lines were now leaving the confinement region radially, before the mirror maximum. High energy particles were thereby leaving the confinement region along these lines, bombarding the walls and creating impurity ions which now could follow the distorted field lines back into the plasma. In earlier symmetric mirror designs the field lines were pulled out of the ends, past the mirror maxima, so that during the usual positive ambipolar potential operation of a mirror device the cold impurities on returning field lines encountered strong repulsive forces and were seldom a significant problem.

This impurity problem was solved by designing new and improved magnetic well configurations, the first of which was the baseball (originally called tennis ball coil) magnet conceived of in the U. K., where the coil was shaped like a baseball seam. Some time later, the more flexible design named the "yin-yang" coil, which involved two independent coils instead of the one "seam" coil of the baseball, was invented and tested [Moir and Post, 1969]. The yin-yang magnet is still a key component of most mirror reactor designs.

Having apparently satisfactorily removed the interchange issue from the mirror fusion approach, critical questions still remained on the technology of how to create and sustain a high temperature mirror fusion plasma. Additionally, theory predicted that other instabilities, driven by the velocity space anisotropies

and radial density gradients inherent in simple mirror-confined plasmas would enhance particle end losses out of the mirrors and greatly reduce the particle and energy confinement times [Rosenbluth, 1956; Post and Perkins, 1961; Weibel, 1959; Harris, 1959; Mikhailovskii and Timofeev, 1963; Rosenbluth and Post, 1965; Post and Rosenbluth, 1966; Berk *et al.*, 1969a]. Solving these technology and microinstability physics problems took the mirror program into its next important phase and these solutions set the stage for the development of the tandem mirror reactor concept.

Studies of the fusion technology questions showed that neutral or molecular beam injection could ideally solve all of the problems of creating, heating and sustaining a steady state fusion grade plasma in a mirror machine which had no anomalous instability-induced mirror end losses and a development program was launched for designing and building high current and energetic beam sources. This program was a dramatic success culminating in the 2XIIB experiment with 600 equivalent amperes of 15 keV particles being injected consistently into the magnetic well. Paralleling these beam accomplishments were successful developments in extremely high vacuums (10^{-10} torr in ALICE) and the design, construction and operation of the superconducting Baseball II magnet. These improvements laid the foundation for the successful running, in 1982, of the gigantic 325-ton MFTF superconducting yin-yang magnet which stores 410 MW of energy, produces a 7.68 tesla B field, and operates at a vacuum of 10^{-8} torr.

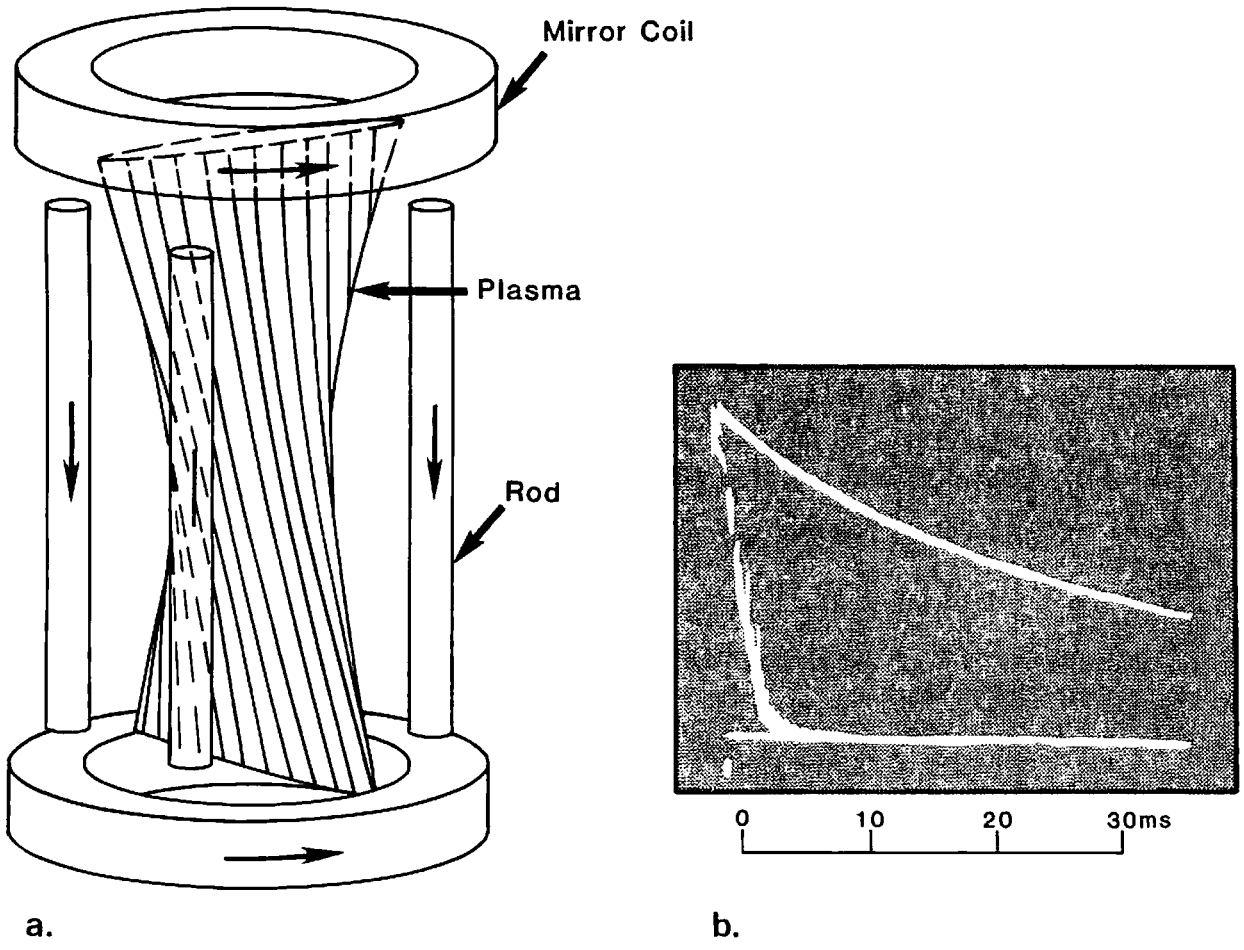

Figure I.B.1 Magnetic mirror with Ioffe bars. (a) Mirror–quadrupole stabilization; (b) Plasma decay oscillograms in the PR–5 (upper curve with stabilizing hexapole field, lower curve without).

Along with the progress in technology during this era came mixed success with the physics issues. While ion temperatures as high as 500 keV were achieved in beam–injected plasmas, in fact the density was found to be limited to low values, of order 10^9 particles/cm^3 or less, in these experiments. On the other hand, high densities, of order 10^{13} particles/cm^3, were achieved in injection and compression experiments but ion temperatures were found to be limited to less than 8 keV; and when good vacuum conditions were maintained the plasma decay was always faster, by orders of magnitude, than that classically predicted. In both of these classes of minimum–B experiments and other colder plasma injection experiments, high frequency microinstabilities with frequencies of the order of the ion cyclotron frequencies, were observed to be present in the plasmas when either the neutral beam build–up was being limited, or in the anomalously fast decays of the injected devices. Subsequent studies of the low density plasmas showed that quiescent classical density decays could be achieved at low enough temperatures [Post, 1981a]. Similarly, it was found that high density decays could be improved, an approach predicted by classical collisional processes, if the vacuum conditions were sufficiently degraded [Post, 1981b].

These experimental scenarios were consistent with the detailed microinstability picture which had been evolving over the years; however, it has to be appreciated that in lieu of extensive and difficult–to–obtain instantaneous data, explicit comparisons with theory are not always possible and explanations may not necessarily be unique. This is particularly true for microinstabilities where details such as the particle velocity space distribution functions are essential features of theory. In an experiment which studies the effects on confinement of changing

the vacuum conditions, for instance, a large number of changes take place as the vacuum degrades: the ions are cooled by increased charge exchange; the electrons are cooled because of less ion collisional heating, thermal ionization with cold electrons, line radiation, and collisions with the increased number of cold impurities; a low energy, microstabilizing, ion component is generated; the plasma is better coupled to the end walls by conduction along field lines; and the halo of cold plasma surrounding the hot plasma is increased in density. To interpret uniquely which of these effects is affecting containment is clearly very difficult, especially when it is additionally realized, for example, that lowering the electron temperature alone both increases classical two-body scattering rates and decreases the size of the ion–expelling ambipolar potential, which itself reduces the reservoir of energy available to ion microstabilities. Therefore, simply lowering the electron temperature should increase classical rates and decrease microstability activity; hence the mirror confinement should become less anomalous. On the other hand, identifying which elemental physics effects are responsible for the observed confinement changes is critical for understanding a plasma and for the extrapolation of the physics to larger machines. In the case of the example given, for instance, to proceed towards the mirror fusion reactor goal, it is clearly desirable to reduce microinstability activity, not increase classical losses. What the implications are for a given experimental result is therefore not always obvious, and sometimes they are not universally accepted. However, when multiple diagnostics are used judiciously and the results are carefully compared and correlated with detailed state–of–the–art theories, more confidence on the proper interpretation and allowed extrapolation is developed. With these caveats, the early results of controlling microinstabilities in mirror machines can be reviewed.

The true essence of high–frequency microinstabilities lies in details of the plasma particle distribution functions. For mode frequencies of the order of the ion gyrofrequency and for questions concerning ion mirror containment, the ion distribution function is the important quantity. Excellent agreement between observations and theory was first achieved in the DCX series of experiments and appeared to explain the density limits of these devices [Dunlap *et al.*, 1962]. The first experiments specifically directed at modifying the ion distribution in order to study the control of ion microinstabilities began by varying the background vacuum conditions [Baiborodov *et al.*, 1971, 1973; F. Coensgen, 1973], the ion temperature [Coensgen, 1975a; Kanaev and Yushmanov, 1972], the ambipolar potential [Damm *et al.*, 1970; Thompson *et al.*, 1971; Kanaev *et al.*, 1973; Ioffe, et al., 1974] and the injection of warm ion plasma streams into the plasma [Baiborodov *et al.*, 1973a; Ioffe *et al.*, 1974; Coensgen *et al.*, 1975b; Kanaev, 1979]. A characteristic oscilloscope trace of the ion cyclotron fluctuations in the Russian PR6 device is shown in Fig. I.B.2, and indicates the dramatic suppression of ion microinstabilities caused by the injection of a warm plasma stream. By developing simple qualitative and sometimes quantitative theoretical models for explaining the observed behavior on the basis of distribution modifications and subsequent microstability changes, a convincing picture evolved out of all these experiments which gave great credence to the theoretical microstability picture and a confidence that they could be advantageously controlled. However, this conclusion needed further quantitative studies and verification in higher temperature regimes with as close to steady state conditions as possible. It was decided that the best way to accomplish this task was again through new technology, so in the U.S. a program was launched to build twelve, 50–ampere–

equivalent sources of 15 keV neutral beams to be mounted on the 2XII device. In principle these beams would be used to simply blast the way into a satisfactory parameter regime where appropriate fusion-oriented scaling studies could be performed. The resulting device was designated 2XIIB, indicating the beam additions.

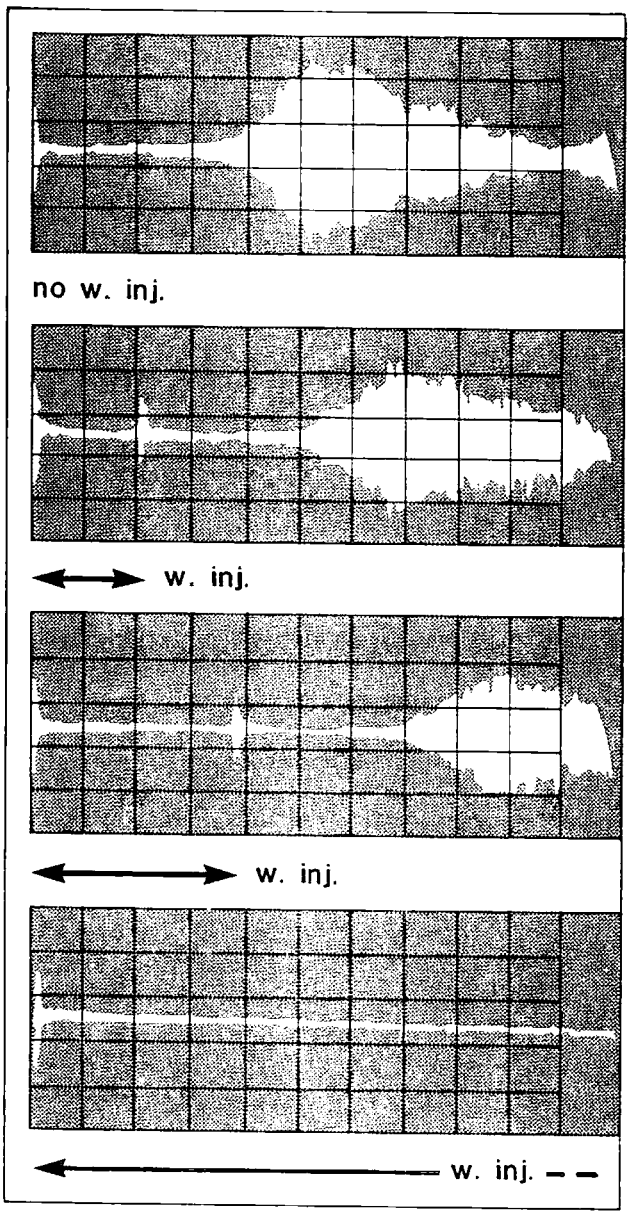

Figure I.B.2: Experimental observation of microinstability in mirrors: (a) ion–cyclotron fluctuations vs. time in PR–6, with stabilizing warm plasma stream injected (w.inj.) and without injection (no w.inj.).

I.C 2XIIB, the Big Bonanza

Twenty years of technology development, pioneering theoretical and experimental physics, and international discovery and cooperation led to the 2XIIB experiment (see Fig. I.C.1 a and b). A maximum of 9 MW of neutral beam power was focused on a plasma one–half liter in volume. (Of course, this experiment was short pulsed with a lifetime of about ten milliseconds.) Record ion temperatures of 13 keV were obtained at plasma densities of about 5×10^{13} particles cm^{-3}, and when microinstabilities were suppressed, a record mirror machine Lawson fusion power parameter, $n\tau_E$, value of about 10^{11} $s{\cdot}cm^{-3}$ was achieved. Additionally, beta, the ratio of plasma energy density to vacuum magnetic energy density, and hence a critical measure of the effectiveness of the expensive confining magnetic field could be made to exceed unity, indicating an extremely efficient use of the minimum-B mirror's magnetic field [Logan *et al.*, 1976].

In the earlier 2XII experiment which injected and compressed plasma, it had been observed that at low ion energies ($T_i \approx 1$ keV) the plasma could be found to decay smoothly and close to the rate calculated by classical scattering processes [Coensgen *et al.*, 1975a]. However, as the ion energy was increased tenfold the Lawson fusion power parameter, $n\tau_E$, did not scale as $T_i^{\frac{3}{2}}$, the classical prediction, but remained rather constant, indicating the dominance of some anomalous processes. While rf diagnostics were not used with the proper frequency response to observe the high frequency convective waves theoretically predicted to be inherent in a small radius mirror such as 2XII [Post and Rosenbluth, 1966], it was speculated that such waves were indeed present and dominated classical

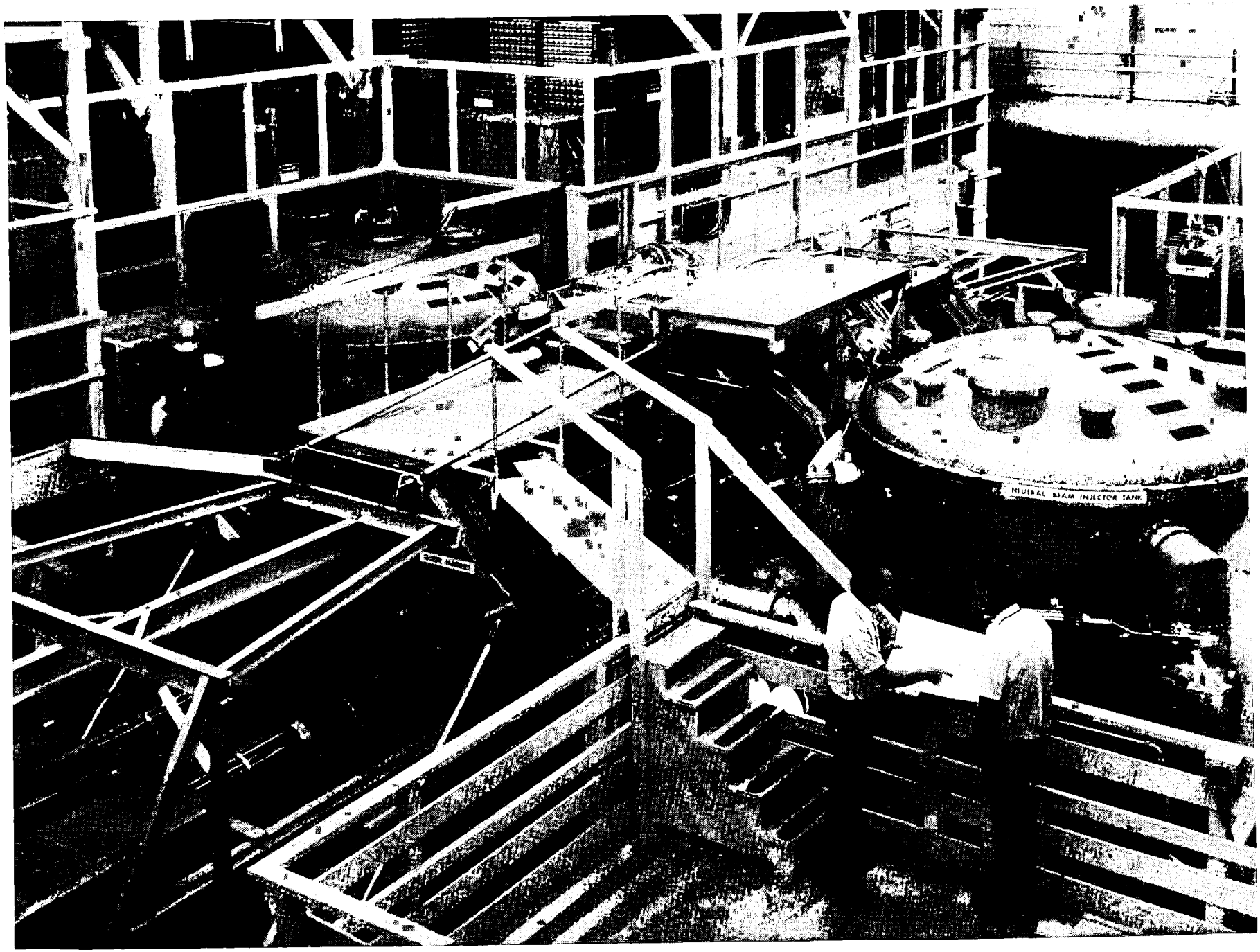

Figure I.C.1a The 2XIIB experiment: the machine

Figure I.C.1b The 2XIIB experiment: an artist's cutaway

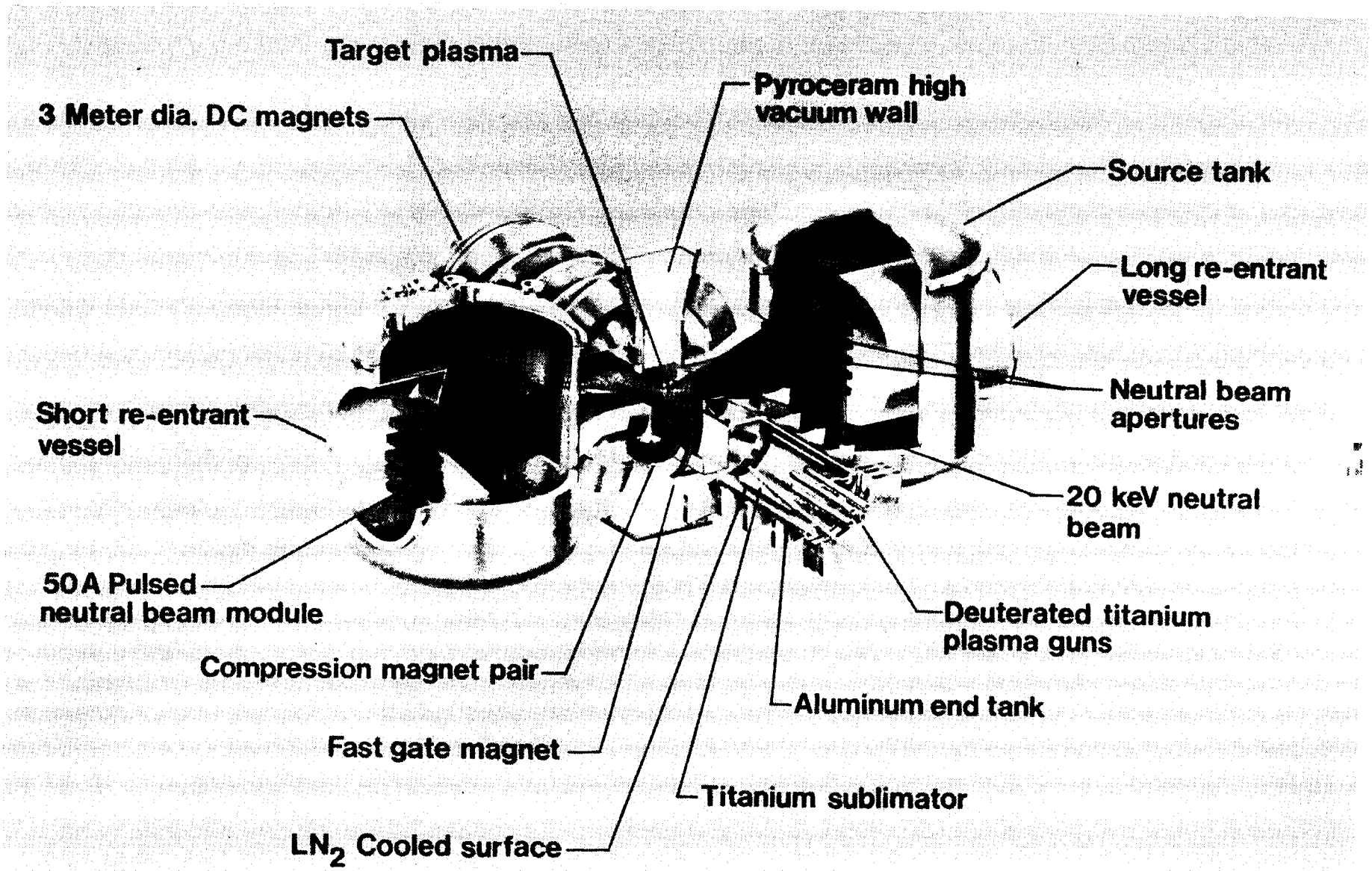

scattering which became weaker at the higher ion energies. The quasilinear anomalous loss rates due to the waves [Baldwin and Callen, 1972] were shown to be reasonably consistent with 2XII data [Coensgen *et al.*, 1975b], and furthermore their diffusion formula predicted that classical loss rates could be approached by obtaining higher density plasmas and/or higher electron to ion temperature ratios. With these loss formulae and scaling laws, it was predicted that the 2XII plasma density could be sustained with 600 A equivalent of neutral beams [Coensgen *et al.*, 1973], an extremely fortuitous result seeing that the 2XII magnetic design would only allow twelve 50–A neutral beam modules to fit into the system when the additionally–required diagnostics were also added.

Based on this understanding of the observed 2XII confinement, the 2XIIB experiment ("B" for beams) was conceived. It was understood that these loss formulae excluded the possibility of other predicted microstabilities dominating the 2XIIB plasma behavior as new temperature and density regimes were entered and the anomalous high frequency convective–wave–induced losses were reduced. Other microinstability–induced rapid anomalous plasma decays had been observed in the 2XII plasma, but appeared to be explainable as a double–humped instability [Dory *et al.*, 1965] and easily controllable by plasma injection procedures [Coensgen *et al.*, 1972]. The improvements in confinement with vacuum degradation in 2XII and the ion microinstabilities observed in other mirror traps of course forewarned of pending problems in 2XIIB. While higher temperatures and densities were initially achieved in 2XIIB, enhancement of rf activity at the ion cyclotron frequency was observed to be correlated with enhanced plasma end losses, and the limitation of $n\tau_E$ to a value an order of magnitude below classical.

Extensive diagnostics and correlation procedures identified that the ion cyclotron rf activity had the characteristics of the drift cyclotron loss cone (DCLC) modes, predicted earlier [Rosenbluth and Post, 1965; Post and Rosenbluth, 1966]. Additionally this particular microinstability had been shown theoretically [Post, 1967; Berk *et al.*, 1969b; Pastukhov, 1974a] to be stabilizable by injection of a warm plasma with the proper density and temperature depending on the characteristics of the contained hot ion plasma and ambipolar potential magnitude. It was, presumably, this type of stabilization mechanism which had been achieved indirectly through vacuum degrading and rf microwave electron heating [Baiborodov, 1973a; Ioffe *et al.*, 1974; Coensgen *et al.*, 1973] and directly through warm plasma injection [Ioffe *et al.*, 1974]. With a long pulse modification of a 2XII plasma injection gun, a suitable warm plasma stream was injected into 2XIIB, and $n\tau_E$ confinement factor increased tenfold. Figure I.C.2 illustrates the dramatic confinement enhancement used by stream injection. With the addition to the experiment of a gas box, which self-generated a warm plasma component through ionization of a controlled gas flow by the escaping hot plasma, even higher warm plasma densities were achieved; concomitantly, the highest hot ion densities and β values for a mirror plasma were recorded. Important also was the fact that $n\tau_E$ was shown to again increase with increasing ion energy as shown in Fig. I.C.3 [Coensgen *et al.*, 1976].

The significance of the 2XIIB experiment was not only in setting record performance factors and the demonstration that microinstabilities could be suppressed by various laboratory techniques, but the experiment also tested and verified numerous fundamental scaling laws predicted by theoretical analyses of

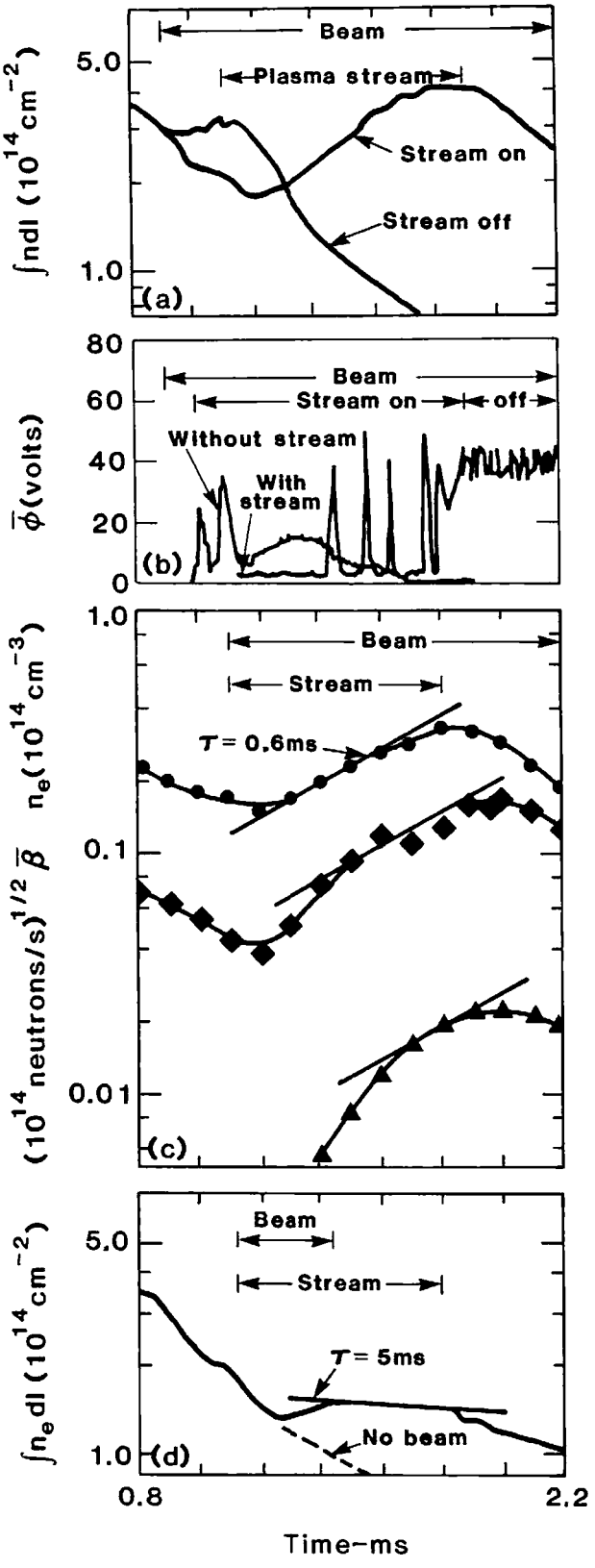

Figure I.C.2: Confinement enhancement obtained with warm stream injection.

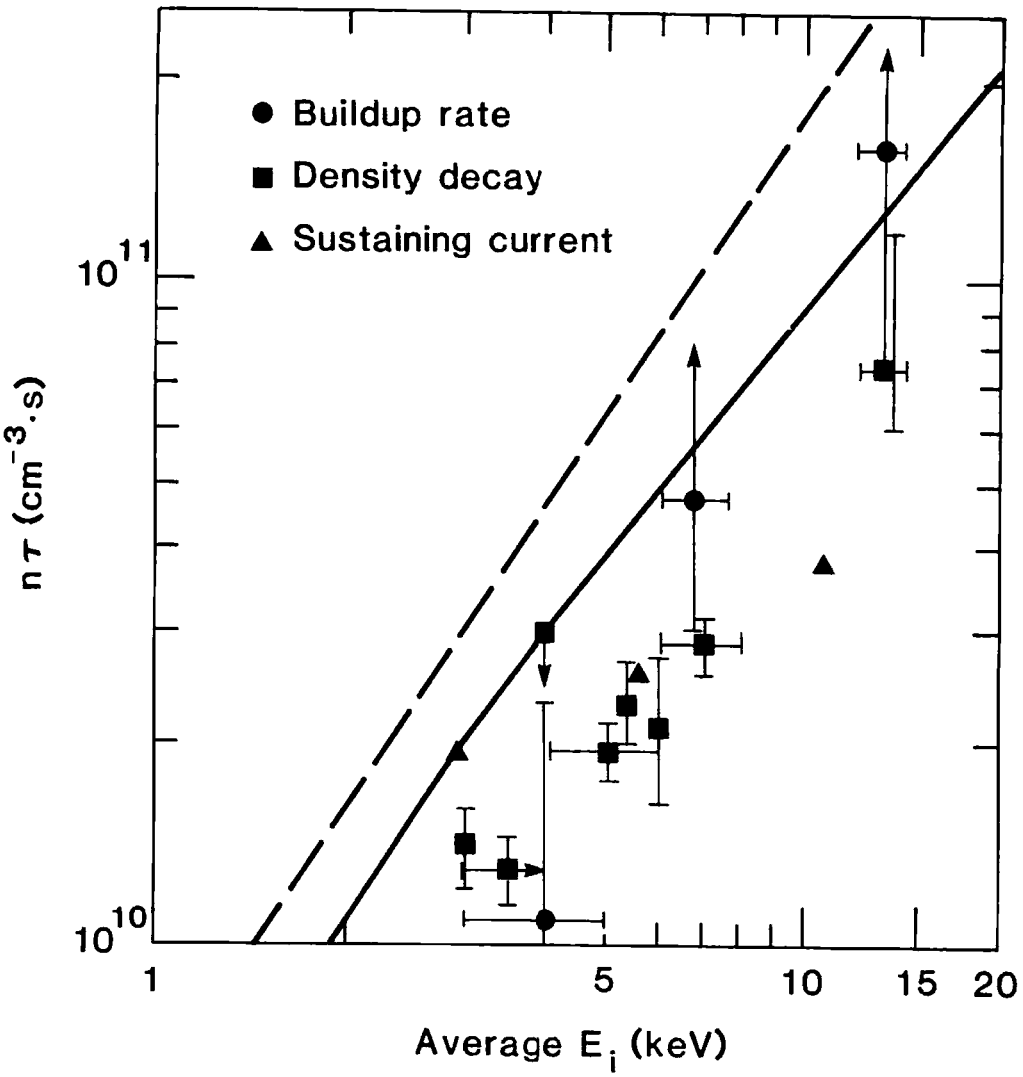

Figure I.C.3: $n\tau_E$ in the 2XIIB experiment was shown to increase dramatically with increasing ion energy.

the DCLC mode [Baldwin *et al.*, 1976]. While there still remained some unanswered questions about the fundamental nonlinear theory of the DCLC mode in the 2XIIB geometry and environment, with some adjustable parameters the theory could be normalized and then had predictive capabilities in excellent agreement with the experiment, as illustrated in Fig. I.C.4. This agreement gave great credence to the DCLC theory and therefore to the extrapolations thereof into the mirror fusion reactor parameter regime. Here the theory predicted that the DCLC mode would be stable or easily stabilized by warm plasma streams depending on the exact parameter values of the design.

The conclusion that was drawn by the end of the 2XIIB experiment was that the qualitative feasibility of mirror fusion containment had been established, instabilities could be adequately controlled and a dense plasma at thermonuclear temperatures could be created and sustained. The critical quantitative question of the economics of a mirror fusion power-producing reactor with a 2XIIB scenario now became a key issue, particularly in light of the possible need for supplementary warm plasma stream stabilization which not only requires additional power for its sustenance, but also creates another energy loss channel for electrons.

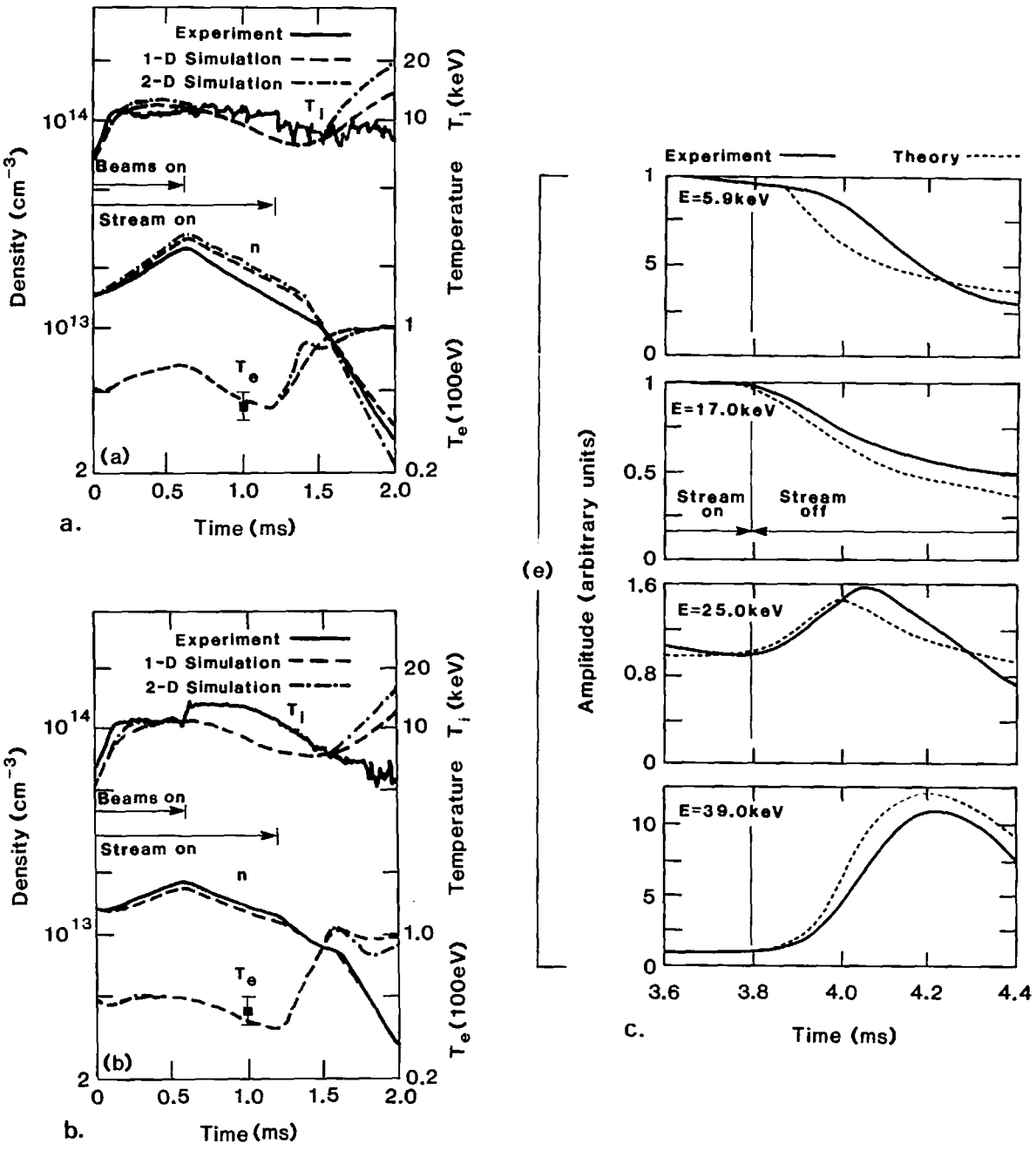

Figure I.C.4a-c: These figures show the excellent agreement between the theoretical predictions of the DCLC theory for the 2XIIB geometry and the experimental results.

I.D " 'Q' and Limitations of the Simple Mirror"

The ultimate purpose of the fusion power research and development program is to provide a net power producing fusion reactor which can operate in a consistent fashion and produce economical electrical and/or advanced concept energy units. An important fact is that in a simple mirror reactor the plasma temperature cannot be maintained directly by energy deposition of the fusion reaction products in the plasma, because the mean confinement time of the reaction products (α particles in a D–T system) is always less than the collisional thermalization time [Post, 1962]. (It is assumed here that the mirror machine is short enough that scattering into the loss cone time is long compared to an ion transit time.) Hence, a simple mirror can never reach the self–sustaining "burn" condition, where $Q \rightarrow \infty$, but inherently requires maintaining the plasma temperature by beam injection or heating processes exterior to the plasma and therefore it can act only as a power amplifier. However, the very high temperatures inherent to mirror devices and the relatively enhanced directed end losses of the linear open geometry in principle can lead to large electrical power conversion efficiencies. In fact, directly converting energy end losses by employing a proper succession of decelerating electrostatic grids which can very efficiently recover the kinetic energy of the end exiting ions is a natural system component of most mirror machine reactor designs [Budker, 1959; Moir *et al.*, 1975; Post, 1969; Post, 1981c]. On the other hand, these same enhanced end losses usually imply the need for a mirror device to have a large fraction of recirculating power to energize neutral beams and rf sources and hence necessarily add additional system inefficiencies which degrade this latent conversion potential of the mirror

containment system.

The fundamental energy sources in a deuterium tritium (D–T) thermonuclear power system are determined by the energy released in the fusion reaction in the plasma, $D + T \rightarrow n^0 + 17.58$ MeV, and the energy released in the surrounding lithium blanket, $n^0 + Li^6 \rightarrow He^4 + T + 4.8$ MeV. This tritium breeding blanket is a necessary component of the D–T reactor system because of the large quantities of naturally scarce tritium needed for fueling the basic reaction. In order to sustain these reactions an adequate plasma must be contained in the mirror geometry with the attendant large mirror end losses as well as the loss of the kinetic energy of the fusing nuclei themselves. These fusion sources and these inherent energy losses define the basic "bare" power gain factor, Q. Q equals unity defines scientific breakeven for a device, but inefficiencies in systems for converting the fusion radiation power and for driving the beams and heating systems degrade the overall gain factor. A typical engineering requirement is that the bare Q of a device should be of the order of five or greater for the device to be realistically considered as a contender for reliably producing electrical power.

The original bare Q calculations neglected the effects of electron drag on the ions and ion ambipolar losses and found Q values in excess of 10 [Post, 1962] well within needed engineering design limits. Unfortunately, subsequent calculations [Fowler and Rankin, 1965] showed that each of these mentioned neglected processes reduced Q by a factor of 2 or more, and found that Q maximized at ion energies of 200–300 keV at a value of about 1.5. Further investigations, including supplementary electron heating to reduce the electron drag effect on the ions [Werkoff, 1972], found no significant improvement in the

value of Q which then necessarily included all of the necessary power inputs.

It was evident by now that very innovative ideas were needed to improve the bare Q of a simple mirror machine. One of the earliest designs to use a set of colinear mirrors, much like the current tandem mirror design, proposed three mirror sections with the central trap to be held at zero ambipolar potential by maintaining a cold ion population at the interior mirror throats with the use of a cold neutral beam feed [G. G. Kelley, 1967]. The purpose was strictly to reduce the ambipolar losses of the central trap ions and essentially eliminate the factor of two reduction in Q brought about by ambipolar losses [Fowler and Rankin, 1965]. With better end containment the electron temperature would also increase and reduce ion drag losses. This design was not investigated further until the tandem mirror era had matured.

When the 2XIIB experiment operating at maximum neutral beam power started to show beta values exceeding unity, the concept of field- reversed mirrors began to be studied actively as a method of increasing simple mirror Q values. In this system (see Fig. I.D.1) it is expected that the closing of a large fraction of the magnetic field lines within the plasma will provide better confinement than that provided by a simple mirror. However, realistic Q predictions consistent with equilibrium and stability requirements need detailed knowledge of plasma behavior in the vicinity of magnetic separatrices and are still being researched. Experimental p.ograms for field- reversed configurations are additionally being carried out, but presently both theory and experiment are in an early developmental stage.

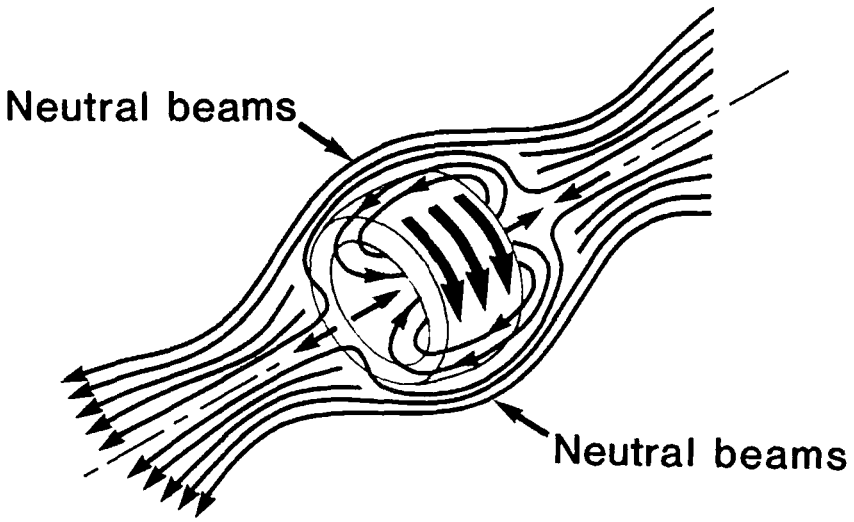

Figure I.D.1: Field reversed mirrors are used to increase Q values. By closing a large fraction of the magnetic field lines within the plasma, better isolation will be provided than that in a simple mirror.

I.E The Tandem Mirror

The key ideas for the tandem mirror did not develop until the mid 1970's. Building on the confidence of single cell operation brought about by the performance of the 2XIIB experiment and the supporting theory, configurations were sought that took advantage of the single cell but were not restricted by its inherent bare Q limitations. The tandem design closely represented a return to the original idea in the early mirror program where a reactor design consisted of a long center solenoid wherein the fusion reactions take place, the ends of which are plugged not by the initial idea of simple mirror coils, but now, like Kelley's device, the end plugs are MHD-stabilizing mirror cells.

The essence of the tandem design is to use the positive ambipolar potentials which are created by magnetically-confined hot ions and electrostatically-contained electrons of a single mirror cell in order to create two positive electrostatic barriers at the ends of a center solenoid. These single cell "plugs" then serve as potential barriers for the colder ions in the center solenoid region [Dimov et al., 1976; Fowler and Logan, 1977]. This configuration with minimum |B| end cells is illustrated in Fig. I.E.1.

A simple operational scenario for this configuration is that very energetic neutral beams deposit hot ions in the end cells, and cold gas and hot ions escaping from the end cells fuel the solenoid. Then, with neutral injection in the two end cells, hot plasma will accumulate in each end cell in the usual manner; a strong net positive charge also develops in each cell. This positive charge of each of the end cells establishes potential barriers that prevent the escape of loss cone ions from the solenoid, while electrons are confined by the overall positive potential

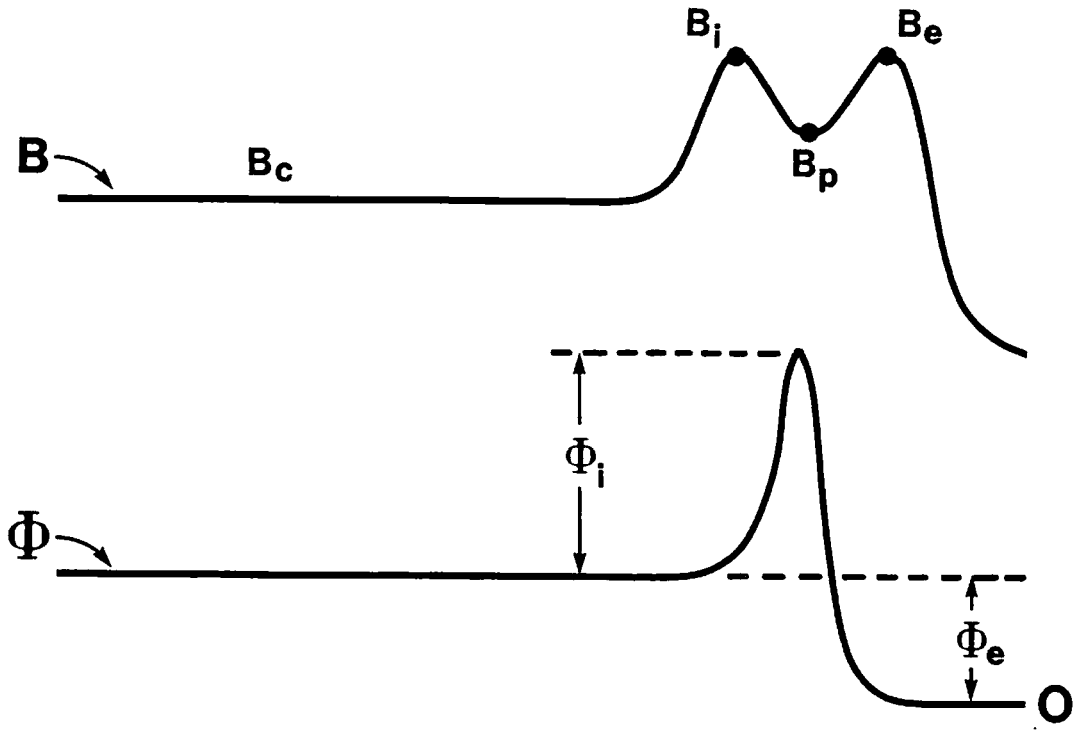

Figure I.L.1 The tandem design uses the positive ambipolar potentials created by magnetically-confined hot ions and electrostatically-confined electrons to create single cell "plugs" which serve as potential barriers for the colder ions in the central solenoid.

end–to–end. Once established, a steady–state could be sustained in which neutral injection maintains the hot ions in the end cells; the hot ions heat the electrons, and the electrons, which communicate throughout the whole system, ionize and heat cold fuel continuously injected into the solenoidal region. The end result is that the electron temperature is approximately constant throughout the system while the ions, having little thermal contact between regions, are much hotter in the end cells.

In order to escape out of the ends of the solenoid the electrostatically-confined ions must diffuse upward in energy until they reach an energy exceeding their barrier height, denoted ϕ_i in Fig. I.E.1. The rate of collisional scattering necessary for this ion energy end loss process is known as the "Pastukhov" time [Pastukhov, 1974b; Catto and Bernstein, 1981; Cohen *et al.*, 1978; Galbraith and Kammash, 1978] and, if the barrier height is large compared to the solenoidal ion temperature, it was shown that the Pastukhov lifetime is much longer than the ion–ion scattering time. It is just this electrostatic enhancement of the ion confinement time in a mirror device that allows the tandem configuration to outperform the single cell mirror and produce higher Q's at lower magnetic field strengths and neutral beam powers.

These theoretical developments led to an aggressive international experimental program (see Table I.4) in the tandem concept, and the initial experiments indeed demonstrated enhanced central cell ion confinement due to the establishment of an electrostatic potential well along the field [Miyoshi *et al.*, 1976; Coensgen *et al.*, 1980]. In the same time period, reactor studies showed that while bare Q's of order 5 were possible in this configuration, high current neutral

Table I.4 Parameters of tandem mirror experiments in operation[1], construction[2], or design stage[3].

	Gamma 6[1] JAPAN	TMX[1] USA	Phaedrus[2] USA	AMBAL[2] USSR	MFTF-B[3] USA
PLUG					
B_0 (kG)	4	10	4	12	20
B_{mirror} (kG)	10	20	–	–	40
R_p (cm)	4	10	7	12	48
$L_{mirror\text{-}to\text{-}mirror}$ (cm)	–	75	105	–	360
Heating method	Beam, RF, REB	Beam	ICRF	Beam	Beam / ECR
Heating power (MW)	0.5	9	0.1	0.1	60 / 2
Duration (ms)	2.5	25	1	–	30 sec
n (cm^{-3})	5×10^{13}	5×10^{13}	5×10^{12}	3×10^{13}	5×10^{12}
W_i (keV)	0.4–10	26	2	20	375
T_e (eV)	20–2000	200	40	1000	90,000
n					10^{13}
$Q - Q_{DT}$					1
SOLENOID					
B (kG)	1.5	0.5–2.0	0.2	2	15
$L_{plug\text{-}to\text{-}plug}$ (cm)	315	640	390	–	4,000
R_p (cm)	2×20	30	30	30	30
n (cm^{-3})	1×10^{13}	1×10^{13}	2×10^{12}	1×10^{13}	2×10^{13}
W_i (eV)	–	80	15	500–1000	15,000
T_e (eV)	300	200	40	–	12,500
n					10^{15}
Q					

beam injection energies in the order of an MeV and maximum magnetic field strengths in excess of 15 tesla were needed to achieve such a power performance factor [Logan *et al.*, 1978]. To develop systems for delivering these kinds of reliable steady state neutral beam energies and magnetic field strengths from noncircular coil sets (which are still necessary to produce the minimum-B fields), a very substantial extrapolation of present day engineering and technology is required with associated large costs and nontrivial uncertainties in the ultimate results. One straightforward way to reduce the engineering problems is to use only circular coil sets, so a program in symmetric, e-ring-stabilized tandems was initiated and is currently at an intermediate development stage [Lazar *et al.*, 1980]. Clearly, a better alternative is to reduce the technology requirements by improving the basic physics of longitudinal mirror confinement.

One critical technology constraint of the standard tandem mirror design is brought about by the fact that the hot end plug electrons interact freely with the central cell electrons thereby maintaining a uniform axial temperature. The ion confining potential is therefore determined strictly by the logarithm of the density ratios along the axis, and the numbers are such that a very high plug density is required for effective ion containment. Again fundamental 2XIIB data provided the key to a means for alleviating this high plug density constraint and thereby, in principle, allow a lowering of the required supporting magnetic field intensities and neutral beam energies and also a substantial increase in Q. The unexpected observations were that large axial electron temperature variations (factors of three) were present even in the long electron mean free path operating conditions of 2XIIB [Clauser, 1979], and that axially local density depres-

sions occurred naturally [Stallard and Logan, 1976]. The axial temperature observations were subsequently explained by including self-consistent ambipolar potential effects along with the axial placements of stream-stabilizing particle and energy sinks and sources of 2XIIB [Rognlien and Brengle, 1981], while the sustained density depression (and associated ambipolar potential reduction) appeared to be explainable by local cold ion pump-out due to latent ion cyclotron fluctuations. Similar axial gradient observations were being made in "double layer" experiments studying shock wave phenomena in space plasmas [Coakley and Hershkowitz, 1979].

In the context of the tandem configuration, this axial electron temperature variation, or more fundamentally, the local ambipolar variations lead to a new means, other than just axial density ratios, for setting the overall axial ion-confining potential. This phenomenon of "ambipolar (containment) enhancement" culminated in the thermal barrier concept [Baldwin and Logan, 1979] where the hot plug electrons are presumed to be isolated axially from the relatively colder central cell electrons by locally depressing the ambipolar potential. The depression can, in principle, be induced by ion sloshing techniques [Kesner, 1973] or resonant ECRH application [Ioffe *et al.*, 1974], or both, and the depression sustained by pumping out ions that collisionally scatter into the local well by a number of conceived methods. The key changes are best illustrated by the design shown in Fig. I.E.2. This modification of a tandem design had the immediate impact of enhancing Q and reducing required neutral beam energies for DT breakeven to the order of a hundred keV as well as reducing the required plug fields. Thus, design constraints are clearly relaxed from the standard tandem mirror. However, the price paid for relaxing the technology requirements

is that additional components need to be added to sustain modifications such as those shown in Fig. I.E.2. For this particular thermal barrier resonant ECRH is required to energize some electrons and magnetically trap them, and also heat the end plug electrons. Additionally, neutral beams are necessary to "pump" trapped ions out of the potential depression (by the process of charge exchange of low-energy trapped ions on the high parallel energy neutral beam particles) so that the electrostatic potential dip will not be suppressed.

While the technology for these new components is well in hand, these supplements do add considerable physics complications and thereby new experimentally untested uncertainties. Nevertheless, the thermal barrier and its generalization termed "ambipolar enhancement" add greatly to the viability of a tandem mirror fusion reactor and are now considered key elements of all designs. With the advent of the TMX-U, TARA, Γ-10, and MFTF-B experiments, data bases will be established for a working knowledge of ambipolar enhancement.

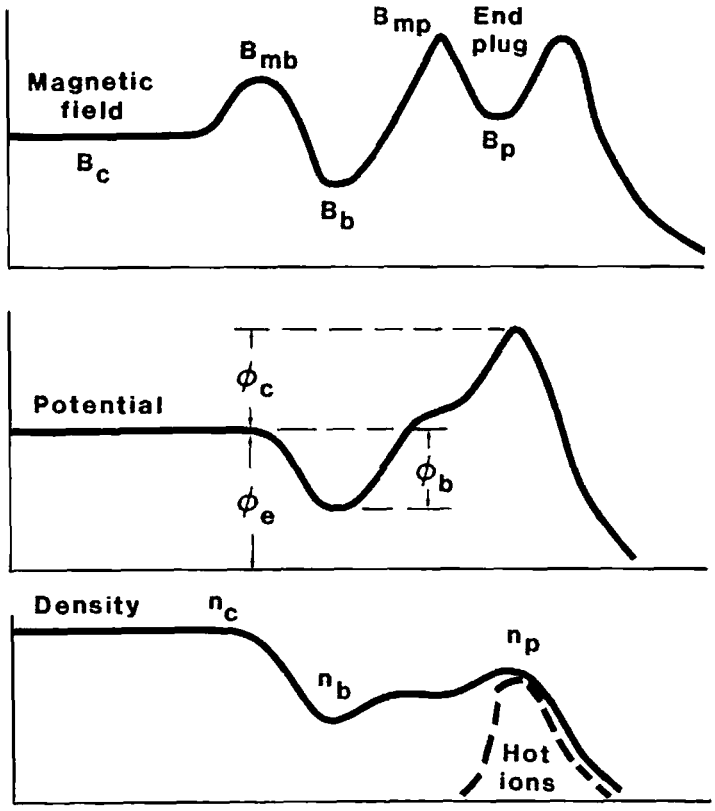

Figure I.E.2: These curves show the magnetic field, potential and density in the thermal barrier of a tandem mirror.

I.F General Issues and Future Outlook

The past 30 years of the dynamic, rapidly evolving mirror program have just been reviewed briefly. At this time the program stands at a critical position, with important tests of high Q, low technology elements of a tandem reactor to be tested and their limits verified. No doubt the optimal design has yet to be discovered, and substantial scientifically and technologically innovative ideas have yet to be added to the final product. Nevertheless, certain fundamental properties of the mirror program have persisted at every stage and can be expected to persist in an actual tandem reactor design.

The advantages of the tandem mirror configuration are: high β plasmas, implying an efficient use of the (expensive) magnetic field; linear cylindrical geometry implying easy access for engineering considerations and reactor maintenance; and steady state operation for improved duty cycles and reduction of structural problems that result from the thermal cycling of the first wall.

Of course these basic advantages of mirror devices have to be balanced against the inherently expensive mirror requirements for high temperature plasmas and high intensity magnetic fields, and thereby these advantages are really quantitative issues and define the key future physics issues. For example, maximizing β involves considerations of the physics of radial transport [Ryutov *et al.*, 1978; Cohen, 1979; Myra and Catto, 1982], low frequency stability [Kaiser *et al.*, 1983; Freidberg *et al.*, 1983; Ryutov, *et al.*, 1981], and efficient thermal barrier or bipolar enhancement operation [Baldwin and Logan, 1979]. These designs must also be consistent with maintaining microstability of the plasma distributions. Additionally, new stability questions concerning trapped particle modes [Berk *et*

al., 1982] and drift waves in the central cell [Horton, 1980] and their combinations are all subject to the individual characteristics of a particular design. Selection of the final design will have to consider the totality of these issues and also be consistent with the necessary supporting technology; the complete system must be simple enough to perform reliably as a power producing reactor.

The task before the mirror fusion program is truly challenging, and the first real appraisal of how close to a final product the tandem concept is lies in the detailed performance of the next generation of experiments (see Table I.4). There are many questions that can be answered in the interim, and much groundwork to be set for extrapolating the key experimental results. The remaining sections of this manuscript survey, in detail, the elemental ideas that form the basis of the research and development program and are the elements for future extrapolations and understandings.

References Section I

1. Baiborodov, T., Y. V. Gott, M. S. Ioffe, B. T. Kanaev, E. E. Yushmanov, 1973, 6th European Conf. on Contr. Fusion and Plasma Physics, Moscow, Vol. 2, p. 122.

2. Baiborodov, T., M. S. Ioffe, B. I. Kanaev, R. I. Sovolev, E. E. Yushmanov, 1973a, Proc. 4th Int. Conf. on Plasma Physics and Controlled Fusion Res., Madison, Wisconsin (IAEA, Vienna) Vol. 2, p. 647.

3. Baldwin, D. E. and J. B. Callen, 1972, Phys. Rev. Lett. 28, 1686.

4. Baldwin D. E. *et al.*, 1976, LLNL Report UCID-17038, Rev. 1.

5. Baldwin, D. E. and B. G. Logan, 1979, Phy. Rev. Lett. 43, 1318.

6. Barnett, C. F., P. Bell, J. S. Luce, E. D. Shipley, A. Simon, 1959, "Plasma Physics and Thermonuclear Research," Vol. 1, p. 196, Pergamon Press, Editors C. Longmire, J. Tuck, W. Thompson.

7. Barr, W., and W. Perkins, 1965, Bull. Am. Phys. Soc. 2, 203.

8. Berk, H. L., L. D. Pearlstein, J. D. Callen, C. W. Horton, M. N. Rosenbluth, 1969a, Phys. Rev. Lett. 22, 876.

9. Berk, H. L., T. K. Fowler, L. D. Pearstein, R. J. Post, J. D. Callen, W. C. Horton, and M. N. Rosenbluth, 1969b, Proc. 3rd Int. Conf. on Plasma Physics and Contr. Nucl. Fus. Res., Novoisikersk (IAEA, Vienna) Vol. 2, p. 151.

10. Berk, H. L., M. N. Rosenbluth, H. V. Wong, T. M.Antonsen, D.E.Baldwin, 1982, Institute for Fusion Studies Report #IFSF-59, submitted to Soviet Journal of Plasma Physics.

11. Berkowitz, J ., H. Grad, and H. Rubin, 1958, Proc. 2nd Int. Conf. on Peaceful Uses of Atomic Energy, (United Nations, Geneva), Vol. 31, p. 117.

12. Bernstein, I. B., E. A. Frieman, M. J. Kruskal, and R. Kulsrud, 1958, Proc. Roy. Soc., (London), A244, 17.

13. Biquet, A., P. Blanc, R. Gravier, P. Lecoustey, H. Luc, C. Renaud, J. Tachon, D. Vern, B. Zanfagria, 1964, CR Acad. Sci. Paris, 259, 1040.

14. Budker, G. I., 1954, as cited in Coensgen *et al.*, 1976, UCID Report, 17037.

15. Budker, G. I., 1959, as cited in Coensgen *et al.*, 1976, UCID Report, 17037.

16. Catto, P. J. and I. B. Bernstein, 1981, Phys. Fluids **29**, 1900.

17. Clauser, J. L., 1979, Bull. Am. Phys. Soc. 23, 850.

18. Coakley, P., and N. Hershkowitz, 1979, Phys. Fluids, 22, 1171.

19. Coensgen, F. H. *et al.*, 1972, UCRL Report #51208.

20. Coensgen, F. H., W. F. Cummins, A. W. Molvik, W. E. Nexsen, Jr., T. C. Simonen, 1973, LLNL, Livermore, CA, UCRL-50002-73, p. 49.

21. Coensgen, F. H. *et al.*, 1975a, Proc. Eur. Conf. Controlled Fusion Plasma Phys., Vol. 2, 167.

22. Coensgen, F. H., W. F. Cummins, B. A. Logan, A. W. Molvik, W. E. Nexsen, T. C. Simonen, B. W. Stallard, 1975b, Phys., Rev. Lett., **35**, 1501.

23. Coensgen, F. H., W. F. Cummins, W. E. Nexsen, Jr., A. W. Molvik, T. C. Simonen, 1976b, LLNL Proposal No. LLL-Prop 102, Rev. 1.

24. Coensgen, F. H. *et al.*, 1976, UCID Report 17037.

25. Coensgen, F. H. *et al.*, 1980, Phys. Rev. Lett. **44**, 1132.

26. Cohen, R. H., 1979, Nuc. Fusion **19**, 1579.

27. Cohen, R. H., M. E. Rensink, T. A. Cutler, A. A. Mirin, 1978, Nuc. Fusion **18**, 1229.

27. Colchin, R. J., J. C. Dunlop, and H. Postma, 1970, Phys. Fluids **13**, 501.

28. Colgate, S. A., W. Brobeck,D. Imhof, W. Harker, F. Bjorklund, H. Brammer, A. Stoddard, also various members of the Kurchatov Institute in the USSR (in early 50's). Specific references unavailable due in part to the classified nature of early fusion research.

29. Damm, C. C., J. H. Foote, A. H. Futch, A. L. Hunt, K. Moses, R. F. Post, J. B. Taylor, 1970, Phys. Rev. Lett. **24**, 495.

30. Damm, C. C., J. H. Foote, A. H. Futch, and R. F. Post, 1964, Phys. Rev. Lett. **13**, 469.

31. Dimov, G. I., V. V. Zakaidakov, M. E. Kishinevskii, 1976 Fizika Plasma **2**, 597 [T. K. Fowler and B. G. Logan, 1977, Comments on Plasma Physics and Controlled Fusion **2**, 167].

32. Dory, R. A., G. E. Guest, F. G. Harris, 1965, Phys.Rev. Lett. **5**, 131.

33. Dunlap, J. L.,C. F. Barnett, R. A. Dandl, H. Postma, 1962, Nuclear Fusion Supplement Part I, p. 233.

34. Fowler, T. K. and B. G. Logan, 1977, Comments on Plasma Physics and Controlled Fusion **2**, p. 167.

35. Fowler,T. K., and M. Rankin, 1966, Plasma Phys. 8, 121.

36. Francis, G., J. W. Hill, D. W. Mason, 1965, Proc. 2nd Conf. on Plasma Physics and Contr. Nucl. Fusion Res., Culham Laboratory UK, p. 53.

37. Francis, G., D. W. Mason, J. W. Hill, 1964, Nature **203**, 623.

38. Freidberg, J. R., D. A. D'Ippolito, 1983, "Rotational Stability of Tandem Mirrors," Phys. Fluids **26**, September issue (in press).

39. Galbraith, P. L. and T. Kammash, 1978, Plasma Phys. **20**, 959.

40. Gott, Y. B., M. S. Ioffe, V. G. Telkovsky, 1961, in Proc. Conf. on Plasma Physics and Contr. Nucl. Fus., Salzburg, p. 1045.

41. Harris, E. G., 1959, Phys. Rev. Lett. **2**, 34.

42. Horton, W., 1980, Nucl. Fusion **20**, 321.

43. Ioffe, M. S., B. I. Kanaev, V. P. Pastukhov, and E. E. Yushmanov, 1974, Sov. Phys. JETP **40**, 1064.

44. Kadomtsev, B. B., 1959, "Plasma Physics and the Problem of Controlled Thermonuclear Reactions," Vol. III, Leontovitch, M.A. (Editor) Pergamon Press, London, p. 340.

45. Kadomtsev, B. B., 1961, Sov. Phys. JETP **13**, 223.

46. Kaiser, I. B., W. M. Nevins, L. D. Pearstein, 1983, Physics Fluids **26**, 351.

47. Kanaev, B. I., 1979, Nucl.Fus. **19**, 347.

48. Kanaev, B. I., V. P. Pastukhov, E. E. Yushmanov, 1973, ZhETFPu. Red.

18, #6, p. 347.

49. Kanaev, B. I. and E. E. Yushmanov, 1972, Proc. 5th Eur. Conf. Contr. Fusion Plasma Physics I, p. 82.

50. Kelley, G. G., 1967, Plasma Physics **9**, 503.

51. Kesner, J., 1973, Plasma Physics **15**, 577.

52. Kunkel, W. B., and J. U. Guillory, 1965, Lawrence Berkeley Laboratory in Proc. 7th Int. Conf. on Phenomena in Ionized Gases,Belgradia.

53. Lazar, N. H. *et al.*, 1980, Bull. Amer. Phys. Soc. **25**, 993.

54. Lehnert, B., 1966, Phys. Fluids **9**, 1367.

55. Logan, B. G. *et al.*, 1976, Phys. Rev. Lett. **37**, 1468.

56. Logan, B. G. *et al.*, 1978, Proc. 7th Int. Conf. on Plasma Physics and Contr. Fus. Res., Innsbruck, August paper, IAEA-CN-37R-3.

57. Luce, J. S., 1956, Molecular Ion Breaking: Preliminary Note, July 26, 1956, ORNL - CF-56-7-119.

58. Mikhailovskii, A. B., and A. V. Timofeev, 1963, Zh. Ekop. Fiz. **44**, 919 [1963, Sov. Phy. JETP **17**, 626].

59. Miyoshi, S. *et al.*, 1976, Proc. Int. Conf. on Plasma Physics and Contr. Nuc. Fus. Res., (IAEA, Vienna), Vol. 2, p. 443.

60. Moir, R. W., and R. F. Post, 1969, Nucl. Fus. **9**, 252.

61. Moir, R. W., W. L. Barr, G. A. Carlson, 1975, Proc. Int. Conf. on Plasma

Physics and Contr. Fus. Res., (IAEA, Vienna) Vol. 2, p. 583.

62. Myra, J. R. and P. J. Catto, 1982, Phys. Rev. Lett. 48, 620.

63. Northrup, T. and E. Teller, 1966 Phys. Rev. **117**, 215.

64. Pastukhov, V. P., 1974a, Sov. Phys. JETP **39**, 85.

65. Pastukhov, V. P. 1974b, Nuc. Fus. **14**, 3.

66. Post, R. F., 1954, "Sixteen Lectures on Controlled Thermonuclear Reactions," LLNL, Livermore, CA, UCRL-4231.

67. Post, R. F., 1962, Nuclear Fusion Suppl., Part 1, p. 99.

68. Post, R. F., 1967, Proc. Int. Conf. on Plasma Confined in Open Ended Geometry, November, Gatlinburg, TN., p. 304.

69. Post, R. F. and Steller, 1952, AEC report Wash 115, p. 81, Denver Conference on Thermonuclear Reaction held on June 28.

70. Post, R. F., 1969, in Proc. Conf. on Nuc. Fus. Reactors, Culham, p. 88.

71. Post, R. F., 1981, "Fusion," Vol. I, Magnetic Confinement Part A, Academic Press, N.Y., E. Teller, Editor, (a) p. 383; (b) pp. 389, 396; (c) p. 419.

72. Post, R. F., R. E. Ellis, F. C. Ford, M. N. Rosenbluth, 1960, Phys. Rev. Lett. **11**, 166.

73. Post, R. F. and W. A. Perkins, 1961, Phys. Rev. Lett. **6**, 85.

74. Post, R. F. and M. N. Rosenbluth, 1966, Phys. Fluids **9**, 730.

75. Rognlien, T. D., and T.A. Brengle, 1981, Phys. Fluids **24**, 876.

76. Rosenbluth, M. N., N.A. Krall, N. Rostoker, 1962, Nuc. Fus. Suppl. Part 1, 143.

77. Rosenbluth, M. N., 1956, USAEC Report No.LA-2030.

78. Rosenbluth, M. N. and C. Longmire, 1957, Ann. Phys. (New York), 1, 120.

79. Rosenbluth, M. N. and R. F. Post, 1965, Phys. Fluids **8**, 547.

80. Rosenbluth, M. N., W. M. MacDonald, D.L. Judd, 1957, Phys. Rev. **107**, 1.

81. Ryutov, D. D., G. V. Stupakov, 1978, Dokl. Akad. Nauk SSSR **240**, 1086 [Sov. Phys. Dokl. **23**, 412].

82. Ryutov, D. D. and G. V. Stupakov, 1981, in Plasma Physics and Contr. Nuc. Fus. Res., (IAEA, Vienna, Austria) Vol. I, p. 119.

83. Scott, R. F., T. H. Jensen and C. B. Wharton, 1965, Proc. 2nd Conf. on Plasma Phys. and Contr. Nuc. Fus. Res., Culham, p. 6.

84. Stallard, B. W. and B. G. Logan, 1976, Internal LLNL Report.

85. Taylor, J. B., 1963, Phys. Fluids **6**, 1529.

86. Taylor, J. B., 1964, Phys. Fluids **7**, 767.

87. Teller, E., 1954, Conf. on Contr. Thermonuclear Reactors, Oct. 6, 1954, Princeton, NJ.

88. Thompson, E., J. G. Corde, D. R. Sweetman, 1971, Proc. Int. Conf. Plasma Phys. Contr. Nuc. Fusion Res., (IAEA, Vienna), Vol. II, p. 689.

89. Turner, W. C., C. N. Harman, J. W. Shearer, and J. Taska, 1979, Bull. Amer. Phys. Soc. 24, 1083.

90. Weibel, E. S., 1959, Phys. Rev. Lett. 2, 83.

91. Werkoff, F. 1972, Plasma Physics 14, 897.

92. York, H. F., 1952, "Three Lectures on Controlled Thermonuclear Power Production,", UCRL Report No. UCRL-1919.

II. PHYSICS OF A SINGLE MIRROR CELL

II.A. Confinement

The magnetic mirror effect arises when a charged particle moves into a region of increasing magnetic field parallel to the field line direction, that is when magnetic field lines converge. Such a field tends to reflect charged particles and hence has been termed a "magnetic mirror."

A mirror machine is a device that confines plasma between two such mirrors using a magnetic topology in which the flux tube has a maximum cross-sectional area at the central "midplane" region and necks down to form local minima at the mirror throats [Post, 1954; Budker, 1958] as pictured in Fig. II.A.1.

Such a device may be axially symmetric, although, as will be seen later, requirements for MHD stability have focused attention on nonaxisymmetric magnetic topologies. Typical of these are the quadruple mirror cells pictured in Fig. II.A.2 a-c.

The confinement properties of a magnetic mirror are best understood in terms of single particle dynamics. The conditions necessary for confinement can be understood in terms of invariants of the charged particle motion in a magnetic field. The first of these is the magnetic moment, μ, often referred to as the adiabatic invariant, which is associated with the rotational energy of a charged particle in its helical trajectory in a magnetic field [Alfven, 1950].

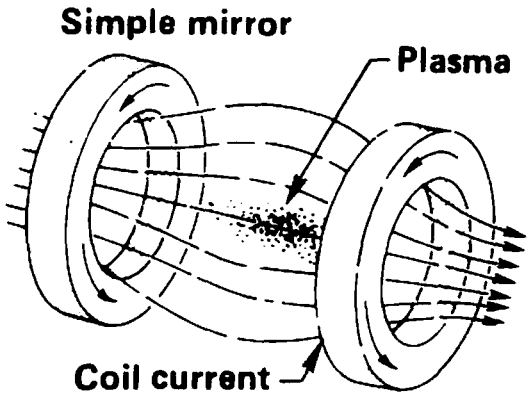

Figure II.A.1: Development of minimum-B magnet coil configurations: a simple magnetic mirror cell with axisymmetric field concentrated at the ends (the mirrors) reflects ions back toward the center.

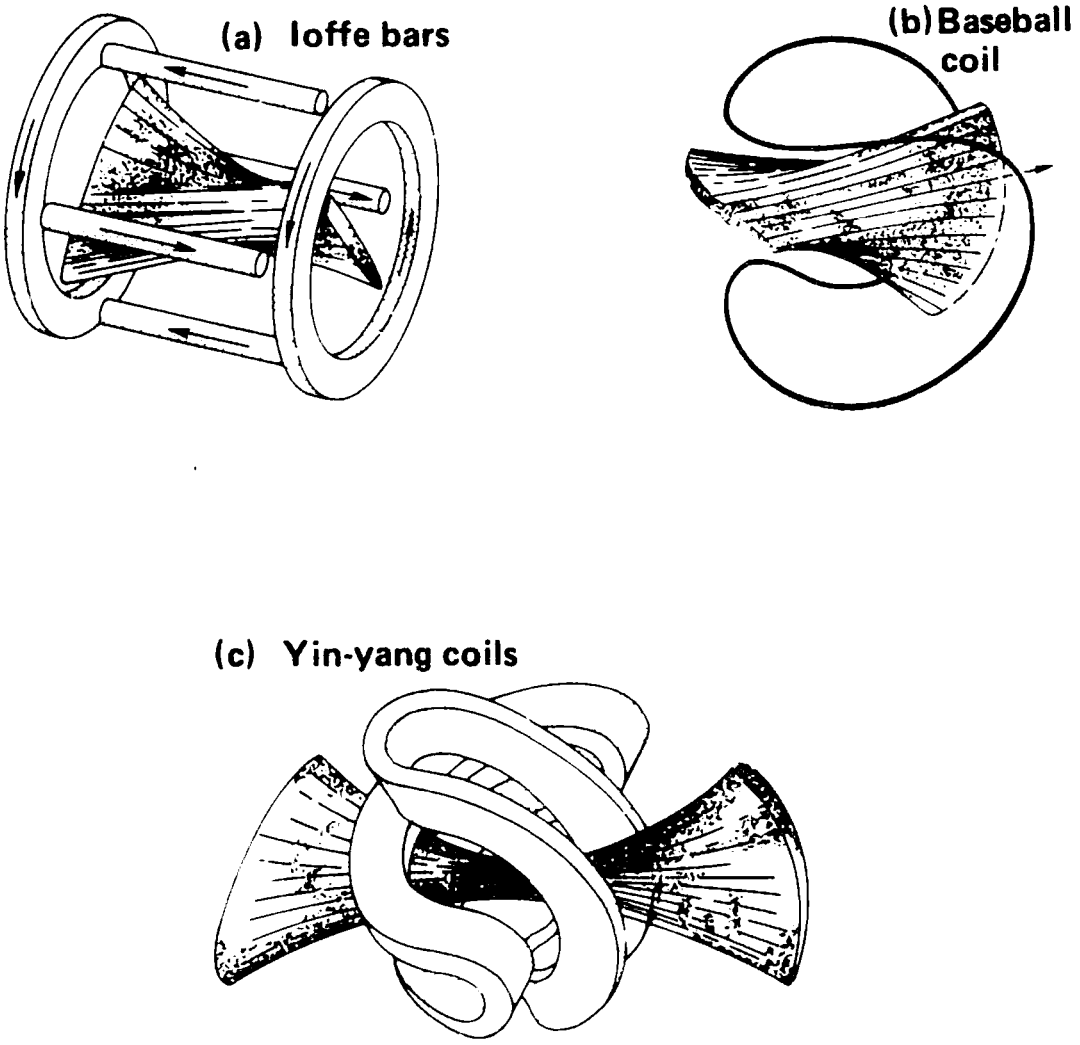

Figure II.A.2a-c: Development of minimum-B magnet coil configurations: (a) current in the Ioffe bars imposes a transverse multipole field on the simple-mirror field, forming a magnetic pocket (minimum-B) at the center; (b) the single baseball coil produces the same minimum-B field configuration more efficiently than the Ioffe-bar system, and (c) the two nested yin-yang coils produce the same minimum-B field but provide greater flexibility by permitting different currents in the two coils, thus different strengths of magnetic mirrors.

The magnitude of μ is given by the ratio of perpendicular kinetic energy to the magnetic field amplitude. Thus

$$\mu = \frac{1}{2} m v_\perp^2 / B. \tag{1}$$

with $v_\perp$ the velocity component perpendicular to the magnetic field direction and B the field magnitude. It is in fact well conserved when the magnetic field varies by a small amount during one gyrorotation period, a condition that will be discussed in more detail below. We also define the particle energy to be

$$\epsilon = \frac{1}{2} m v_\parallel^2 + \mu B(z) + \epsilon\phi(z), \tag{2}$$

with $v_\parallel$ the velocity component parallel to the field direction. ϵ is exactly conserved in steady state magnetic fields. Ignoring the effect of electrostatic fields, a gyrating particle will reach a turning point ($v_\parallel = 0$) when $\epsilon = \mu B$ so that in a magnetic mirror field (Fig. II.A.3), charged particles will be confined in the magnetic well, provided that

$$\mu B_m > \epsilon, \tag{3}$$

with B_m the magnetic field maxima.

This condition may also be expressed in terms of the mirror ratio defined as $R \equiv B_m/B_0$, the ratio of peak-to-midplane magnetic fields and the charged particle pitch angle at the minimum field point defined as $\theta \equiv \sin^{-1}(v_{\perp 0}/v)$.

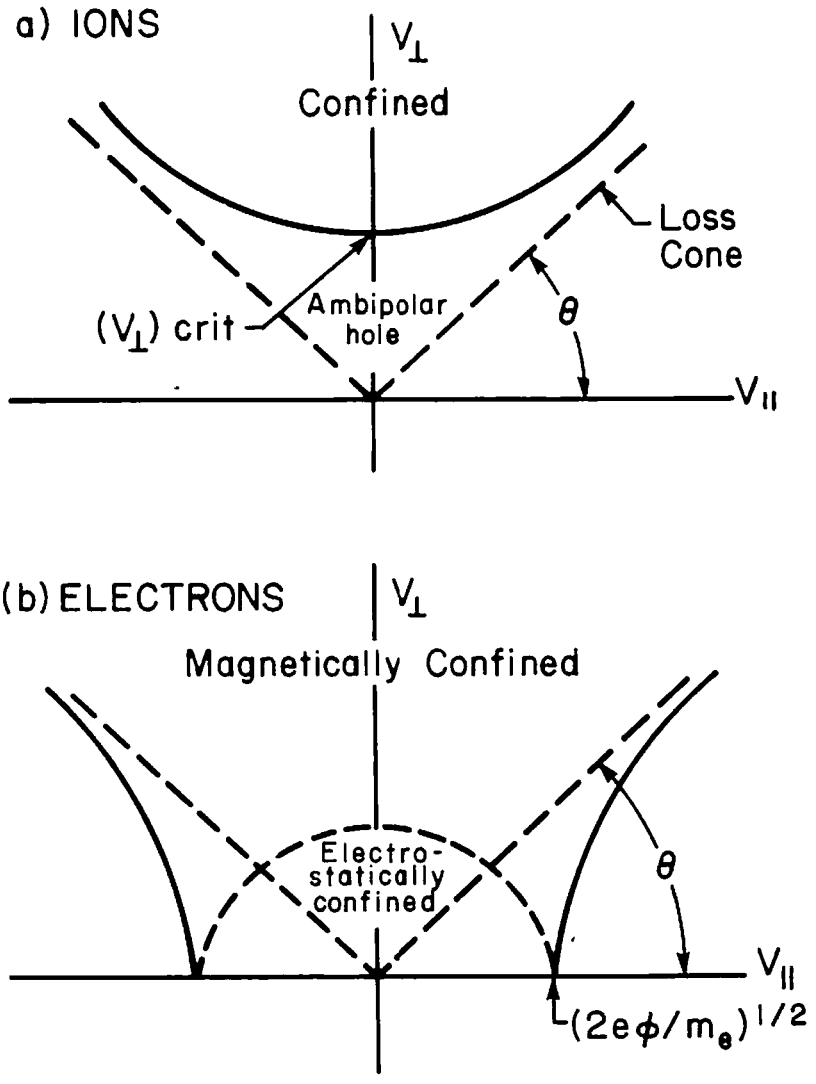

Figure II.A.3: Loss-cone and ambipolar holes that result from plasma particle loss for a) ions and b) electrons. Dashed curves are appropriate with zero ambipolar potential. Solid curves indicate modification of loss boundary in the presence of a positive potential.

Thus the condition given above in Eq. 3 may be written as

$$\theta \geq \theta_{LC} \equiv \left[\sin^{-1}\left(\frac{1}{R}\right)^{1/2}\right]. \tag{4}$$

The so-called "loss-cone" angle, θ_{LC}, defines the minimum midplane pitch angle which a confined particle can have. Thus in velocity-space the loss region presents a cone centered about the field line shown in Fig. II.A.3.

By differentiation, assuming constancy of ϵ and μ, the retarding force experienced by a confined particle can be written as

$$F = -\nabla_z(\mu B(z) + \epsilon\phi(z)). \tag{5}$$

Thus, the quantity $\mu B + \epsilon\phi$ acts as an effective potential which confines charged particles. Since the magnetic moment, μ, enters into this potential, particles with differing μ values find themselves in potential wells of differing shapes and depths.

A second "invariant" of particle motion is the generalized axial momentum (canonical with bounce motion) which may be written as

$$J = \oint P_z dz = m \oint v_{\|} dz. \tag{6}$$

In nonaxisymmetric systems, conservation of J requires that the drift frequency be small compared with the bounce frequency. J conservation determines drift orbits of confined particles which are, for example, circular in axisymmetric systems. The breakdown of this invariance can lead to radial diffusion as can occur in the central cell of a tandem mirror; this is called resonance transport.

II.B Loss Processes

Whereas, in a system with closed field lines, particle loss requires diffusion in real space (across field lines), in a mirror confinement system velocity space pitch angle diffusion results in particle loss. Thus, the best confinement that can be achieved in a mirror is dictated by a collisional pitch angle scatter time. Collisions which change both energy and magnetic moment occur between both like and unlike species. Ions will primarily pitch angle scatter on other ions and drag or slow down on electrons. Electrons pitch angle scatter on both species.

The dominant collisional process in a fully-ionized plasma is the coulomb cross section, which varies inversely with the square of the relative energy of the colliding particles. Thus plasma confinement improves markedly as the kinetic temperature is increased. The ion pitch angle self-scatter time can be estimated for small angle collisions [Spitzer, 1962] to be

$$\tau_{ii} = \frac{M^2 v^3 f(x)}{\pi n e^4 \ln\Lambda} \approx 2.5 \times 10^{11} \frac{E_i(keV)^{3/2} M^{1/2}}{n \ln\Lambda} \tag{7}$$

For ions, M and E_i are the atomic number and energy of the scattered species respectively, and $\ln\Lambda$, the coulomb logarithm ($\ln\Lambda \approx 15$ to 20). τ_{ii} depends only on ion energy, since ions can only pitch angle scatter off themselves. Clearly good confinement requires high ion energies. Notice that τ_{ii} is proportional to $\sqrt{M}$ so that more massive particles are better confined. For the same reason, electrons will tend to scatter faster than ions. Thus, for electrons

$$\tau_{ee} = 1.1 \times 10^{10} T_e^{3/2}(keV)/n \ln\Lambda \tag{8}$$

Because the loss of electrons and ions must be equal, the mirror will float up to a positive potential, resulting in primarily electrostatic confinement of the electrons. In the combined electrostatic and magnetic well the electron confinement will be that given by Pastukhov [Pastukhov, 1974],

$$\tau_p = \tau_{ee} G(R) \frac{e\phi}{T_e} \exp(e\phi/T_e), \tag{9}$$

with $G(R)$ a weak function of mirror ratio, R. Notice that the electron confinement time is enhanced over the pitch angle scatter time because the electrons near the loss boundary have a lower velocity space density (the exponential factor) and because these electrons are hotter and thus have a smaller coulomb cross section (the linear factor). Setting $\tau_p \approx \tau_{ii}$ will give an equation for potential which yields $\phi/T_e \approx 6$. The resulting distortion of velocity space loss boundaries are indicated in Fig. II.A.3.

The positive electrostatic potential in the mirror will also cause a degradation of ion confinement by ejecting low energy ions. If the ion energy is written as $\epsilon = \frac{1}{2}mv^2 + e\phi$, the condition for confinement $\epsilon < \mu B_m$ becomes

$$v_{\perp 0}^2 (R-1) - v_{\|0}^2 = 2e(\phi_0 - \phi_m), \tag{10}$$

which yields a hyperbola in velocity space shown in Fig. II.A.3. Thus, the positive ambipolar potential of a mirror will create a "hole" in velocity space which degrades ion confinement and, more importantly, creates a potential drive for ion microinstability.

Another collisional process of great importance in a mirror is the time for

energy exchange between electron and ion species, referred to as electron "drag." It is given approximately by [Spitzer,1962],

$$\tau_d = 1.8 \times 10^{13} M T_e^{3/2}(keV)/n \ln \Lambda. \tag{11}$$

τ_d depends on the electron temperature, since the electron-ion collision frequency depends on $T_e^{-3/2}$. Thus if the electrons are sufficiently hot and therefore sufficiently collisionless, ion self scatter will dominate the loss process. From Eqs. (7) and (11) this happens when $T_e > E_i/15$.

In mirrors that are maintained by injection of energetic neutral beams the source of plasma is cold electrons and hot ions. In this situation the following picture emerges for equilibrium: the mirror will float positively up to 5 to 6 T_e to provide the necessary electron confinement; hot ions will slow down on electrons and then pitch angle scatter until the ions either enter the velocity-space loss cone or the low energy hole. The electrons are heated by the hot ions. The confinement time of the electrons and ions, however, is sufficiently short that the equilibrium mean ion energy remains significantly above the electron temperature.

A detailed analysis of ion confinement resulting from small angle deflections can be described by a Fokker-Planck equation [Chandrasekhar, 1943]. The resulting velocity-space current due to collisions was first evaluated by Landau [1936] and was put in a more appropriate form for mirror application by Rosenbluth, McDonald and Judd [1957]. The latter work estimated the scattering time to be approximately of the form

$$\tau \approx t_{ii} \log_{10} R, \tag{12}$$

indicating a linear scaling of confinement for a small mirror ratio and a slower improvement for large R. The Rosenbluth form has been used in detailed computational codes which form the basic tools for the study of classical mirror confinement.

The effect of ambipolar potential on ion confinement has been shown by Kaufman [1956] to result in a modest increase in ion loss rate that can be approximated by an effective decrease in mirror ratio. Thus an effective mirror ratio $R_{eff} < R$ may be defined by

$$R_{eff} = R[1 + e\phi/mE_i]^{-1}. \tag{13}$$

Notice that the ion pitch angle scatter loss rate only increases slowly for $e\phi \sim 5T_e \ll E_i$. In a tandem mirror, this effect becomes important since a maximum potential is needed for the minimum energy of plug ions subject to retaining adequate plug confinement. Therefore one wishes to increase the plug electron temperature until ion confinement or stability begins to decline. Thus degradation of ion confinement due to the ambipolar potential is important in the optimization of tandem mirror reactor performance.

II.C Adiabaticity

It can be seen from basic principles [Alfven, 1950] that the magnetic moment remains approximately constant when the magnetic field seen by a particle varies by only a small amount during one gyroperiod. That is,

$$\frac{V_{\|}}{\Omega L_B} \approx \frac{\sqrt{2mT_{\|}}c}{eBL_B} \ll 1 \tag{14}$$

with

$$L_B = Max\left(\left(\frac{d\ln B}{dz}\right)^{-1}, \quad \left(\frac{d\ln B}{dz^2}\right)^{-\frac{1}{2}}\right)$$

and $v_{\|}$ the velocity along the field line. Thus, for a given energy particle, adiabaticity sets a lower limit on magnetic field strength and an upper limit on rapidity of axial field change.

Clearly, the mass dependence figures importantly in the adiabaticity requirements. Heavier ions are less adiabatic than protons of similar energy. Furthermore, electrons remain adiabatic up to temperatures of $\sqrt{m_i/m_e}$ times the maximum ion adiabatic temperature. Thus, in electron heating experiments, it is not uncommon to create and confine electrons at greater than 100 keV energy for modest field strengths.

Additionally, an important interrelationship is observed between adiabaticity and beta limits of mirrors. In mirror systems and particularly in the stabilizing minimum-B cell of a tandem mirror, it is desirable to maximize the ratio of plasma to magnetic pressure (defined as $\beta \equiv 8\pi nT/B^2$) which would tend to

maximize the ratio of temperature to magnetic field squared. However, it is just this ratio that is limited by adiabaticity. Thus, if the ions are heated to the adiabatic limit in a given magnetic field, further increases in beta can only result from a higher plasma density.

Optimizing high beta magnetic mirror designs requires a detailed knowledge of adiabatic limits. This question has been looked at analytically by a number of authors [Hastie *et al.*, 1969; Howard, 1971; R. Cohen *et al.*, 1978; Chirakov, 1978]. The problem is two-fold: first, to determine the change of μ during one bounce period, defined as $\Delta\mu$, and second, to determine the condition under which a stochastic velocity space diffusion of orbits would result. A detailed treatment [Chirakov, 1978] yields

$$\frac{\Delta\mu}{\mu} \sim \frac{-3\pi}{2} R_c \frac{\Omega_0}{v_{\|0}} \exp\left(\frac{-L\Omega_0 f}{v_{\|0}}\right), \tag{15}$$

with $f \sim \frac{2}{3}$ for pitch angles up to 60°. For a stochastic process, a confinement time (τ_a), against nonadiabatic losses can be estimated to be

$$\tau_a \sim \tau_b/(\Delta\mu/\mu)^2 \tag{16}$$

for τ_b the bounce time. Thus, for good adiabatic confinement compared with other losses, it is necessary that $\tau_a \gtrsim \tau_{conf}$ or

$$\frac{\Delta\mu}{\mu} \sim \sqrt{\tau_b/\tau_{conf}}. \tag{17}$$

For $\tau_{conf} \sim \tau_{ii}$ this becomes

$$\frac{\Delta\mu}{\mu} \sim \sqrt{\nu_{ii}L/v_i} \sim 0.02. \tag{18}$$

Estimating from Eq. 15 $\Delta\mu/\mu \sim 5/\epsilon \exp(-2/3\epsilon)$ with $\epsilon \equiv v_i/\Omega L \approx \rho/L$, the result is obtained that the required parabolic length of the mirror must exceed 10 ion gyroradii.

The approximations that went into the analysis cited above can be circumvented by a numerical orbit calculation for mirror-confined ions. Thus, by following ions through one bounce period in the exact magnetic field, $\Delta\mu$ can be obtained and adiabatic limits estimated. This method has been used in the design of mirror experiments.

II.D MHD Stability

The stability of plasma to the interchange of adjacent flux tubes presents a basic problem for mirror confinement schemes. This problem was first pointed out by Teller [1954]. In the subsequent analysis of Rosenbluth and Longmire [1958], it was seen that such an interchange would result in an increase in the potential energy of the plasma when

$$\frac{dP}{dr}\frac{d}{dr}\oint d\ell/B > 0, \tag{19}$$

with P the plasma pressure and r the radius of the field line. (This condition can also be derived from an energy principle analysis [Bernstein *et al.*, 1958].) Thus, Eq. 19 presents a necessary condition for stability.

Noting that $\int d\ell/B$ is proportional to the flux tube volume, Eq. (19) can be interpreted as indicating that stability requires a radial decrease of the volume of the flux tubes being exchanged. This stability criterion can also be cast as a line integral of field line curvature (see Sec. III.C). This condition then states that stability requires that the confining fields are convex, either locally or on the average, toward the plasma interior. In this form the explicit dependence on B in the integrand is seen to be B^{-2}, and the resulting stability criterion presents a beta-weighted integral of curvature.

For a mirror-confined plasma the pressure tends to peak near the midplane where B is a minimum and thus beta tends to peak at this point. If the midplane normal curvature is unfavorable, as in a simple "maximum B" mirror (see Fig. I.A.1), instability will result.

An MHD stable single mirror cell can be obtained by superimposing a cusp and mirror field as shown in Fig. II.A.1, as was first proposed by H. Grad [in Berkowitz *et al.*, 1958] and subsequently demonstrated experimentally [Gott *et al.*, 1961]. The cusp can be obtained from either a quadruple or a higher order field. (The most efficient coil has been shown to be quadruple as higher order cusps require more current due to field cancellation near to the magnetic axis). The flux tube created by this arrangement is elliptic at one mirror throat, circular at the midplane and elliptic in the perpendicular sense at the other mirror throat. The field strength ($|B|$) varies along a field line in the same way it does in a simple mirror but now the midplane has good curvature and, in fact, the entire mirror cell can exhibit good curvature. Noting that in the vacuum the radius of curvature R is given by $R^{-1} = \partial \ln B/\partial r$, it is seen that good curvature implies a magnetic field that increases radially as well as axially in moving away from the mirror midplane and thus the constant modulus B surfaces form nested ellipsoids. This arrangement has been termed a minimum-B mirror and is shown in Fig. II.A.2. The minimum-B mirror has been shown to be stable to all MHD perturbations [J.B. Taylor, 1963] and so presents a particularly desirable configuration.

In a tandem mirror or a multiple mirror device in which several mirror cells must be linked together, the beta-weighted curvature criterion generally presents an upper limit to the pressure that can be supported in bad curvature regions and has been used as a figure of merit in tandem mirror designs. The minimum-B cell has been termed the MHD "anchor." However, the more good curvature present in the anchor, the higher the ellipticity of the flux tube at the mirror

throat and the more the bad curvature in the transition region (adjoining the anchor). Tandem mirror design therefore requires coil elements to be optimized with extreme care.

II.E Microstability

A plasma confined in a mirror is not in thermodynamic equilibrium. In addition to deviations from equilibrium in configurational space, there additionally exist deviations from equilibrium in velocity space. Loss processes can be described as driven by the free energy sources within the plasma. The free energy is the difference between the internal (kinetic) energy of the plasma and the lowest internal energy state consistent with Liouville's theorem. Liouville's theorem follows directly from the Vlasov equation and states that $f(\underline{x}, \underline{v}, t)$ is constant along phase space trajectories, so that f behaves like an incompressible fluid in phase space. Thus, for example, a distribution function that has constant amplitude outside of the loss cone, as illustrated in Fig. II.E.1.a, is in a higher energy state than that illustrated in Fig. II.E.1.b which has the same amplitude and area and is thus accessible by Liouville's theorem. Of course in tapping the free energy, the energy difference will necessarily end up in wave fields.

There are two sources of free energy that drive ion microinstabilities in mirrors. The presence of the loss cone associated with mirror confinement adds a pitch angle dependence to the confined distribution functions. Thus, equilibrium distribution functions for mirror-confined plasmas can never be isotropic. A measure of anisotropy that is useful in stability calculations is the ratio of

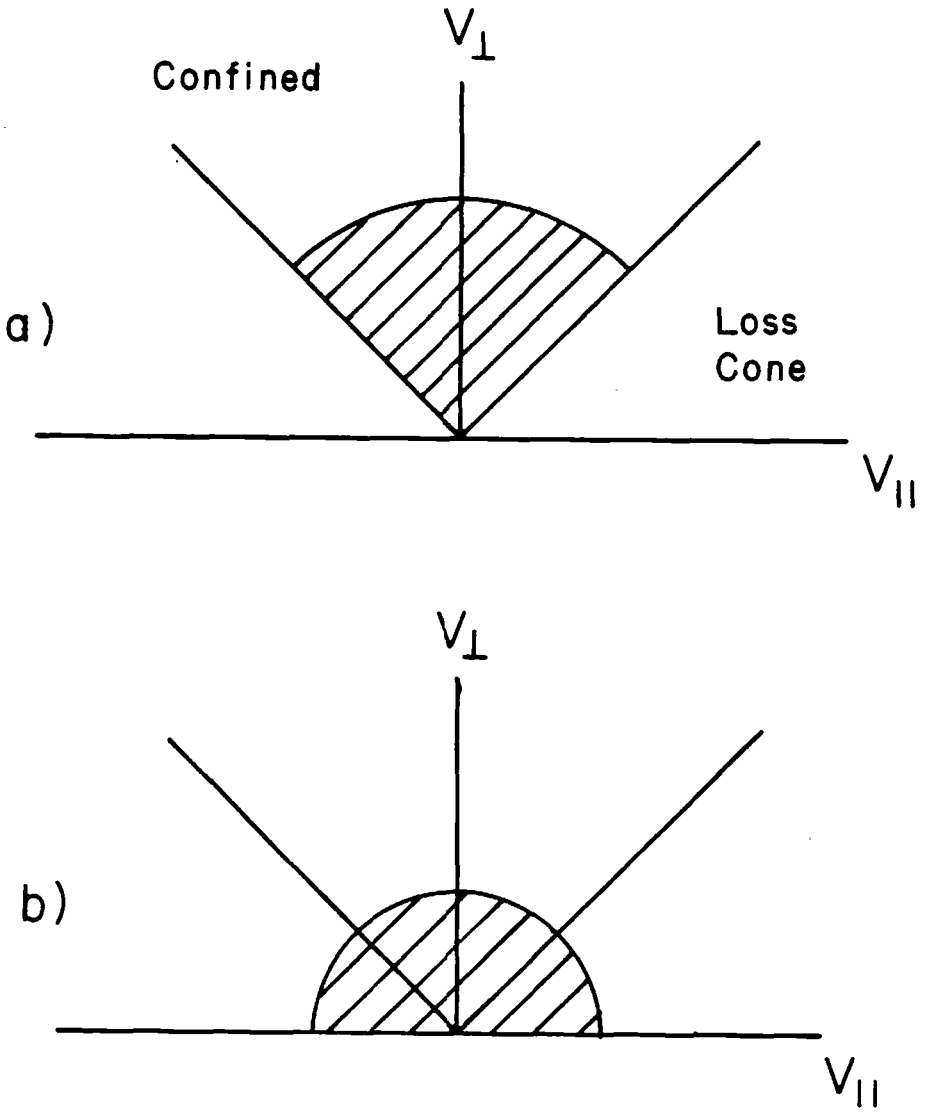

Figure II.E.1: Schematic distribution functions illustrating the free-energy drive of microinstabilities: a) idealized loss cone distribution function; b) lower free-energy state consistent with Liouville's theorem.

perpendicular to parallel pressure. In high beta plasmas anisotropy can prevent equilibrium, resulting in the so-called mirror mode. Furthermore, anisotropy can drive high-frequency microinstabilities such as the Alfven ion cyclotron mode, which tends to diffuse ions in pitch angle so as to decrease the anisotropy, resulting in a degradation of confinement. These modes which limit anisotropy may be controlled by injection schemes which create sufficient parallel pressure.

The second source of ion microinstability in mirrors derives from a "hole" in velocity space which results from the expulsion of cold ions by the positive "ambipolar potential" discussed above. Thus the ion distribution function cannot be monotonic in energy and is susceptible to cyclotron frequency instabilities which can diffuse hot ions into the low energy hole. The most virulent of these modes are believed to be the drift cyclotron loss cone (DCLC) and the axial loss cone (ALC) modes. The theory of these instabilities is reviewed in Ch. III.E.

Axial injection of warm plasma as a means of stabilization of loss cone modes was first proposed by Post [1967] and verified experimentally [Baiborodov *et al.*, 1973; Ioffe *et al.*, 1974; Coensgen *et al.*, 1975; Kanaev, 1979]. If the perpendicular distribution function is defined as

$$f_\perp(v_\perp) = \int_{-\infty}^{\infty} f(v_\perp, v_\parallel) dv_\parallel$$

it is observed that the instability drive occurs when $\partial f_\perp / \partial v_\perp > 0$ for resonant ions ($v_\perp = \omega / k_\perp$). Reversing the sign of the perpendicular distribution function gradient will stabilize these modes.

It is important to notice that this condition is considerably less restrictive than totally filling the hole. Stability generally is seen to require the ratio of

warm to hot density to be $\lesssim 5\%$. When the warm plasma is not warm enough to resonate with the wave, one might expect development of a turbulence level that can heat the warm plasma to obtain marginal stability. This turbulence will serve to degrade hot ion confinement but the level of deterioration of confinement can be much reduced below the level that results in the absence of warm plasma.

Stabilization of this type has been observed by streaming warm plasma through a mirror as demonstrated on the 2XIIB experiment in LLNL. However, this technique also tends to cool electrons and cannot be extrapolated to the reactor regime. A second approach to stabilization would invoke the creation of an ion distribution that can self trap warm plasma and thereby stabilize these modes (see Section IV.B). This approach has been termed "sloshing ions." Importantly, since sloshing ion distributions peak in velocity space at a pitch-angle near to the loss cone, some degradation in the classical confinement will necessarily occur with respect to distribution functions that peak in the direction perpendicular to the field. Thus, use of sloshing ions requires high mirror ratio mirror cells typically requiring $R > 4$. Such mirror ratios permit injection at a pitch angle which can create a sufficient midplane potential depression for self trapping of warm plasma and still maintain adequate mirror confinement.

References Sections II.A and II.B

1. Alfven, H., 1950, *Cosmical Electrodynamics*, (Oxford Univ. Press, Oxford).

2. Baldwin, D.E., 1977, Rev. Mod. Phys. **49**, 317.

3. Baldwin, D.E. and B.G. Logan, 1977, TMX Major Project Proposal, Lawrence Livermore National Laboratory Report LL-PROP-148, Appendix A1, 37.

4. Baldwin, D.E. and B.G. Logan, 1979, Phys. Rev. Lett. **43**, 1318.

5. Budker, G.I., 1958, "Thermonuclear Reaction in Systems with Magnetic Plugs," AN SSSR, Fizica Plazmy; Problema Upravkiaemykh Thermo. Reaktsii, **1**, 3.

6. Carlson, G.A. and R.W. Moir, 1975, Mirror Fusion Reactor Study, Lawrence Livermore National Laboratory Report UCRL-76985.

7. Catto, P.J. and I.B. Bernstein, 1981, Phys. Fluids, **24**, 1900.

8. Chandrasekhar, S., 1943, Rev. Mod. Phys. **15**, 1.

9.. Cohen, B.I., 1980, "Status of Mirror Fusion Research." Lawrence Livermore National Laboratory Report UCAR 10049-80-Rev. 1.

10.. Dimov, G.I., V.V. Zakaidakov and M.E. Kishinevskii, 1976, Sov. J. Plasma Phys. **2**, 362 [Fiz. Plazmy, **2**. 597].

11. Fowler, T.K. (1981) in *Fusion* (E. Teller, ed.), *Vol. 1*, Part A, (Academic Press: New York) p. 241.

12. Fowler, T.K. and B.G. Logan, 1977, Comments Plasma Phys. and Controlled Fusion Research **2**, 167.

13. Futch, A.H., Jr., J.P. Holdren, J. Killeen and A.A. Mirin, 1972, Plasma Phys. **14**, 211.

14. Galbraith, D.L. and T. Kammash, 1978, Plasma Phys. **20**, 959.

15. Gerich, C.A., editor, 1982, The Nuclear Mirror Fusion Program Plan, UCAR-10042-82, p. 106.

16. Gott, V.B. *et al.*, 1961, Proc. Conf. on Plasma Physics and Contr. Fus. Res., Salzburg, Part 3, p. 1045.

17.. Ioffe, M.S., B.I. Kanaev, V.P. Pastukhov and E.E. Yushmanov, 1974, Zh. Elesp. Theor. Fiz. **67**, 2145 [Trans. Sov. Phys. JETP **40**, 1064].

18. Kaufman, A., 1956, AEC Rept. TID-7520 (Part 2).

19. Landau, L., 1936, Phys. Z. Sowjetunion **10**, 154.

20. Pastukhov, V.P., 1974, Nuclear Fusion **14**, 3.

21. Post, R.F., 1954, "Sixteen Lectures on Controlled Thermonuclear Reactions" LLL Rept. 4231.

22. Post, R.F., 1982, *Int. Conf. on Plasma Physics*, Goteborg, Sweden.

23. Rensink, M.E. *et al.*, 1975, *Proc. Conf. Plasma Phys. Controlled Nucl. Fusion Res.* (IAEA: Vienna), *Vol. I*, 311.

24. Rensink, M.E. and T.A. Cutler, 1976, *Proc. Ann. Meeting Theoret. Aspects CTR*, (Madison, Wisc.)

25. Rosenbluth, M.N. and C.L. Longmire, 1958, Ann. Phys. **1**, 120.

26. Rosenbluth, M.N., W.M. McDonald and D.L. Judd, 1957, Phys. Rev. **107**, 1.

27. Spitzer, L., 1962,*Physics of Fully Ionized Gases* (Interscience: New York).

28. Taylor, J.B., 1963, Phys. Fluids **6**, 1529.

29. Teller, E., 1954, "Comments on Plasma Stability," Sherwood Conf., 6.

References Section II.C

1. Alfven, H., 1950, *Cosmical Electrodynamics*, (Oxford Univ. Press, Oxford).

2. Chirakov, B.V., 1978, Fiz. Plazmy 4, 521 [Translation (1978) Sov. J. Plasma Phys. 4, 289].

3. Cohen, R.H., M.E. Rensink, T.A. Cutler and A.A. Mirin, 1978, Nuclear Fusion **18**, 1229.

4. Hastie, R.J., G.D. Hobbs and J.B. Taylor, 1968 Proc. 3rd Int. Conf. on Plasma Phys. and Contained Fus. Res., Novosibirsk, (IAEA), V. I, 39.

5. Howard, J.E., 1971, Phys. Fluids *14*, 2378.

References Section II.D

1. Baldwin, D.B. and R.H. Bulmer, 1982, "A Physics Conceptual Design for the MFTF-B Transition Coil."

2. Berk, H.L., M.N. Rosenbluth, H.V. Wong, T.M. Antonsen and D.E. Baldwin, 1982, Institute for Fusion Studies Report IFST-59.

3. Berkowitz, J., H. Grad and H. Rubin, 1958, Proc. 2nd Int. Conf. on Peaceful Uses of Atomic Energy, U.N., Geneva, p. 177 or Vol. 3, p. 171.

4. Bernstein, I.B., E.A. Frieman, M.D. Kruskal, R.M. Kulsrud, 1958, Proc. R. Soc. London Ser. A244, 17.

5. Bulmer, R.H., T.B. Kaiser, W.M. Nevins, W.A. Newcomb, L.D. Pearlstein, H.R. Strauss, S. Wollman and M. Wakatani, 1982, presented at the 9th International Conference on Plasma Physics and Controlled Nuclear Fusion Research, Baltimore, USA, paper CN-41/G-2.

6. D'Ippolito, D.A., G.L. Francis, J.R. Myra and W.M. Tang, 1981, Phys. Fluids **24**, 2270.

7. D'Ippolito, D.A. and J.P. Freidberg, 1982, Phys. Fluids **25**, 1617.

8. D'Ippolito, D.A. and J.P. Freidberg, 1982, presented at the Sherwood Meeting on Theoretical Aspects of Controlled Thermonuclear Fusion, Santa Fe, New Mexico, paper 1C12.

9. D'Ippolito, D.A. and B. Hafizi, 1981, Phys. Fluids **24**, 2274.

10. D'Ippolito, D.A., J.R. Myra and J.M. Ogden, 1982, Plasma Physics **24**, 707.

11. Freidberg, J.P. and L.D. Pearlstein, 1978, Phys. Fluids **21**, 1207.

12. Gott, V.B. *et al.*, 1961, Proc. Conf. on Plasma Phys. and Contr. Fus. Res., Salzburg, Part 3, p. 1045.

13. Hall, L.S. and B. McNamara, 1975, Phys. Fluids **18**, 552.

14. Kaiser, T.B. and L.D. Pearlstein, 1982, Lawrence Livermore National Laboratory Report UCRL-87659.

15. Kanaev, B.I., 1979, Nucl. Fusion **19**, 347.

16. Lee, X.S., P.J. Catto and R.E. Aamodt, 1982, Phys. Fluids **25**, 1491.

17. Logan, B.G., 1981, Comments Plasma Phys. Controlled Fusion **6**, 199.

18. Myra, J.R., D.A. D'Ippolito and P.J. Catto, 1982, SAI Report SAI-254-82-174-LJ/PRI-44.

19. Nevins, W.M. and L.D. Pearlstein, 1981, Bull. Am. Phys. Soc. **26**, 984.

20. Newcomb, W.A., 1982, presented at the Sherwood Meeting on Theoretical Aspects of Controlled Thermonuclear Fusion, Santa Fe, New Mexico, paper 3A1.

21. Newcomb, W.A., 1981, J. Plasma Phys. **26**, part 3, 529.

22. Pearlstein, L.D., T.B. Kaiser and W.A. Newcomb, 1981, Phys. Fluids, **24**, 1326.

23. Rosenbluth, M.N., in Plasma Phys. and Cont. Nuc. Fus. (IAEA, Vienna, 1965), p. 485.

24. Rosenbluth, M.N. and C.L. Longmire, 1957, Annals of Phys. **1**, 120.

25. Ryutov, D.D. and G.V. Stupakov, 1981, in *Plasma Physics and Controlled Nuclear Fusion Research* (International Atomic Energy Agency: Vienna, Austria), *Vol. I*, 119.

26. Strauss, H.R., S. Wollman and M. Wakatani, 1982.

27. Stupakov, G.V., 1979, Fiz. Plazmy **5**, 871 [1979, Sov. J. Plasma Phys. **5**, 489].

28. Tang, W.M. and P.J. Catto, 1981, Phys. Fluids 24, 1314; Lee, X.S. and P.J. Catto, 1981, Phys. Fluids 24, 2010.

29. Taylor, J.B., 1963, Phys. Fluids **6**, 215.

30. Thompson, W.B., 1961, Rep. Prog. Phys. **24**, 363.

31. Turner, W.C., J.F. Clauser, F.H. Coensgen, D.L. Correll, W.F. Cummins *et al.*, 1979, Nucl. Fusion **19**, 1011.

References Section II.E

1. Baiborodov, T., V.B. Gott, M.S. Ioffe, B.I. Kanaev, E.E. Yushmanov, 1973, 6th Europ. Conf. on Cont. Fusion and Plasma Physics, Moscow, Vol. 2, p. 122.

2. Coensgen, F.H. *et al.*, Phys. Rev. Lett. **35**, 1501.

3. Ioffe, M.S., B.I. Kanaev, V.P. Pastukhov, E.E. Yushmanov, 1974, Sov. Phys. JETP **40**, 1064.

4. Kanaev, B.I., 1979, Nucl. Fusion **19**, 347.

III. TANDEM MIRROR PHYSICS

III.A. Introduction

The tandem mirror, which was proposed independently in the Soviet Union and the United States [Dimov, *et al.*, 1976; Fowler and Logan, 1977], provides a means for significantly-enhanced ion confinement over the pitch angle scatter limitation of a single cell mirror. In this scheme, confinement along field lines in the "central cell" mirror is increased by plugging the loss cone with electrostatic barriers. The electrostatic barriers are localized in two high density mirror cells termed "plugs" that are positioned at both ends of the central cell. If the plugs are minimum-B cells they can additionally provide overall MHD stability for the configuration; they are, therefore, also termed "anchors." Advantage is taken of the enhanced central cell confinement by extending its length so that the central cell volume greatly exceeds the combined plug volumes. Typical magnetic field and potential profiles are shown in Fig. III.A.1. (A similar arrangement had been explored earlier by Kelley [1967]. In the Kelley approach the end plug and central cell densities were set equal, which eliminates the low energy hole in velocity space. This arrangement would improve confinement and microstability, but would not yield the strongly enhanced central cell confinement that results from electrostatic plugging (Eq. 1).)

In terms of their particle and energy balance, the plugs function much as single mirror cells do. The central cell ions, however, experience an enhanced confinement deriving from a rise of potential, ϕ_c, which accompanies the density

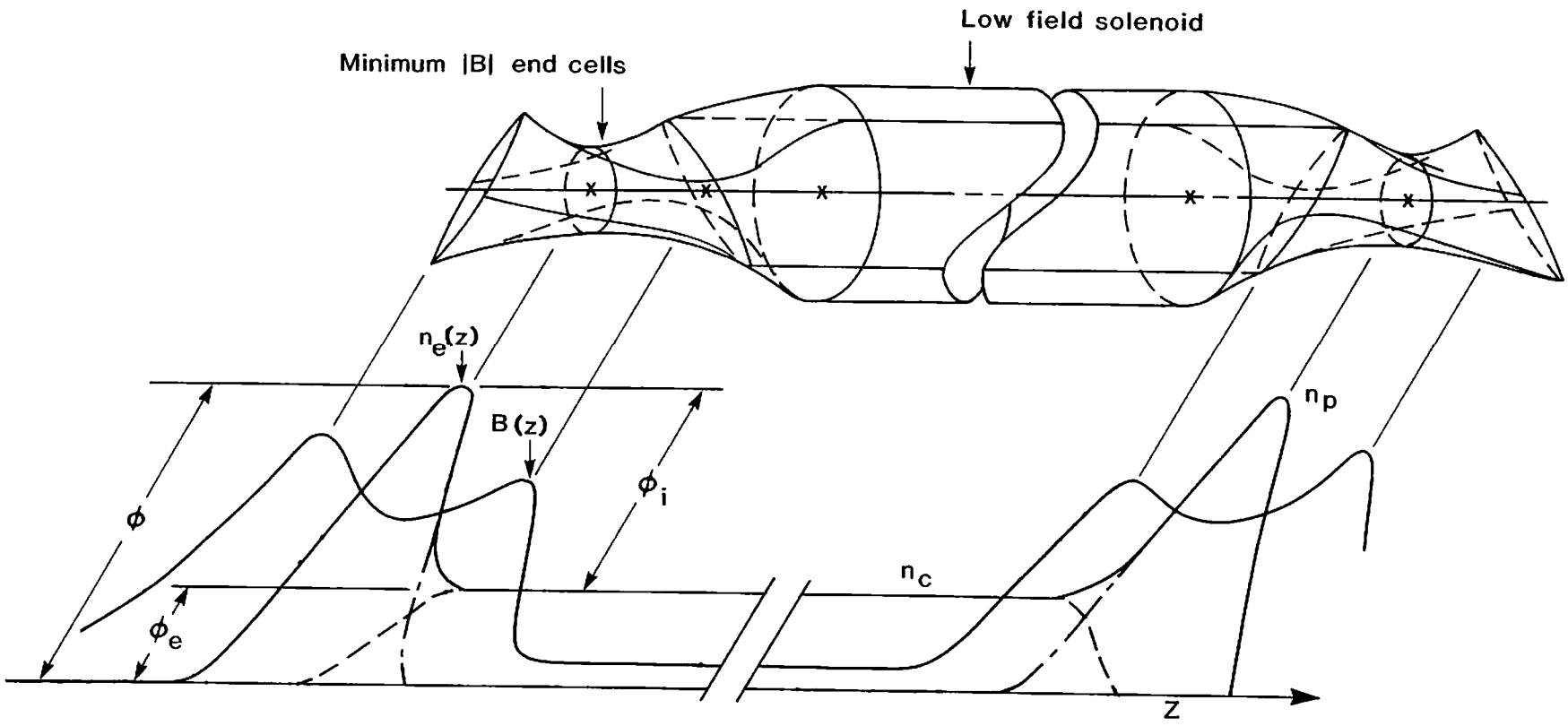

Figure III.A.1 Tandem mirror with ambipolar barriers at the ends

rise in the plugs. Central cell ion confinement can thus be approximated by the Pastukhov time [Pastukhov, 1974], namely

$$n\tau_c = n\tau_{ii} g(R) \left(\frac{e\phi}{T_i}\right) \exp(e\phi_c/T_{ic}), \tag{1}$$

where $g(R)$ is a weak function of mirror ratio and T_{ic} is the central cell ion temperature. This is essentially the result obtained by Pastukhov [1974] for electron confinement in a combined electrostatic and magnetic trap. (For electrons, a factor of 2 enters the equation [R. Cohen *et al.*, 1978] because collisions on both electron and ion species can scatter the electrons). The exponential term in Eq. (1) comes from the phase space density reduction at the high energies near the loss boundary and the linear term reflects a decrease in collisionality for these energetic ions. Typically $e\phi_c/T_{ic} \sim 2$ to 3 is expected which gives an enhancement of confinement above the collisional scatter time, $n\tau_{ii}$, of 20 to 60.

Electrons, being more collisional than ions, can be treated as having a Maxwell–Boltzmann distribution along field lines. Therefore, the Maxwell–Boltzmann relation between plug and central cell densities can be used to obtain the potential rise in the plugs,

$$e\phi_c = T_e \ln(n_p/n_c). \tag{2}$$

Here n_p and n_c represent the plug and central cell densities respectively. The electron temperature, T_e, is constant throughout the device. Thus, the plugging potential results from either a significant plug-to-central cell density ratio or a high electron temperature. Unfortunately, the weak (logarithmic) dependence on

density ratio requires that this ratio be large. To obtain $e\phi_c/T_e > 2$, typically would require $n_p/n_c \sim 10$. It is observed, however, that if the plug electron temperature could exceed the central cell value, there would result a considerably relaxed restriction on plug density. This observation led to the concept of a thermal barrier, which will be discussed in Section IV.A.

In order to complete the description of the ambipolar operation of a tandem mirror, recall that the electrons are confined electrostatically by a potential ϕ_e (see Fig. II.A.1). Therefore the confinement time of the electrons trapped by the barrier ϕ_e is given by Eq.(1) with the mirror ratio R given by B_p/B_c. The ion losses from the plug ($\sim 2n_pV_p/\tau_i$) may be neglected as small compared to the central cell ion losses ($\approx n_cV_c/\tau_c$), provided $V_c/V_p \gg 2n_p\tau_c/n_c\tau_i$ where V_p and V_c are defined as the plug and central cell volume respectively. As a result, an estimate of the self–consistent electron barrier height ϕ_e is obtained by demanding that the loss of central–cell ions equals the electron loss ($\approx n_cV_c/\tau_e$). Consequently [Baldwin and Logan, 1977],

$$\frac{e\phi_e}{T_e}\exp\left(\frac{e\phi_e}{T_e}\right) \approx \left(\frac{\tau_{ii}}{\tau_{ee}}\right)\left(\frac{e\phi_c}{T_i}\right)\exp\left(\frac{e\phi_c}{T_i}\right), \tag{3}$$

with ϕ_c given by Eq. (2). For $n_p/n_c \approx 10$ and $T_e \approx T_i$, Eqs. (2) and (3) yield $e\phi_e/T_e \approx 4$.

The kinetic energy of the neutral beam injected ions used to fuel the plugs must be high enough that the ions are not expelled by a potential drop within the outer half of the mirror cell. For perpendicular injection at the plug midplane, this implies

$$E_0 > \frac{e(\phi_e + \phi_c)}{R_p - 1}, \tag{4}$$

with R_p the plug mirror ratio. When $n_p/n_c = 10$, this inequality yields the approximate requirement, $E_0 > 6T_e/(R_p - 1)$. (Recall that for $E_0 > 15$ T_e electron drag becomes the dominant collisional effect on the energetic ions).

The problems of single cell mirror equilibrium, confinement and stability are directly applicable to the plugs of a tandem mirror. In addition, several new areas of physics arise that are unique to the tandem mirror.

One class of problems that arises relates to the possibility of enhanced radial transport in a long central cell. It was realized early [Lao *et al.*, 1978] that, assuming conservation of J [Eq. (6), Sec. II], drift equilibrium required that the end plugs be rotated with respect to one another so as to produce overall quadrupole symmetry. This result follows because on reflection from a nonaxisymmetric region, charged particles will suffer a drift off the flux tube (the flux tubes are defined by the constant pressure surfaces). These drifts, which occur at each bounce point, can be made to cancel between both ends of the orbit by imposing an overall quadrupole (or higher order) symmetry on the central cell.

It was also observed, however, that in a tandem mirror a residual form of this effect can still be significant resulting from the noncancellation of the bounce point drifts off the flux tube that occurs for a class of ions termed resonant ions [Ryutov, Stupa' ov, 1978]. Resonant ions are those ions with similar drift and bounce frequencies such that during one traversal of the central cell they drift azimuthally $(2n + 1)\pi/2$ for n an integer. This class of ions will not see the quadrupole symmetry of the central cell and the cancellation referred to above will not occur. These ions exist in significant numbers in a tandem mirror because

the long central cell length serves to reduce the bounce frequency. Resonant transport thus results from a coupling of drift and bounce resonances and can be viewed as a consequence of the breakdown of conservation of J [Sec. II, Eq. (6)]. By the same consideration, electrons will not see significant resonant transport because their bounce frequencies always greatly exceed their drift frequencies.

Since tandem mirrors are designed to possess overall quadrupole symmetry, equilibrium considerations are formally quite similar to those studied in ordinary quadrupole plugs. However, the length of the central cell can impose important equilibrium restrictions on tandem mirror designs. One important such consideration is the production of the Stupakov current [Stupakov, 1979]. In an ordinary quadrupole mirror cell, high–beta equilibrium will generate a quadrupole current pattern exhibiting internal currents that flow in a pattern similar to the seam of a baseball. These currents form the return paths for guiding center drifts off of the flux tube and tend to create a quadrupole flux tube distortion. The distortion is proportional to the length of the current path and in the long central cell of a tandem mirror can be severe, leading to enhanced transport and ultimately to unconfined field lines.

Since, in an axisymmetric mirror, all drifts remain in the flux surface, the Stupakov current can be generated only within the nonaxisymmetric end regions of the tandem mirror. To minimize this current one clearly needs to reflect most ions within axisymmetric regions and to minimize the average drift off of the flux tube in the nonaxisymmetric regions.

A second important difference between a tandem mirror and a minimum–B cell is the possibility of low frequency unstable modes. In an absolute minimum–

B mirror well the confined plasma sees only good curvature. Such a system is stable to all low-frequency low-beta curvature driven modes [Taylor, 1963] and has been shown to be quite stable to high-beta MHD and rotationally-driven modes.

A tandem mirror represents a retreat from absolute minimum-B. In the region of transition between the central solenoid and the minimum-B cell there is necessarily bad curvature. In fact, increasing the good curvature in the anchor engenders more bad curvature in the transition. Thus a tandem mirror can only be an average minimum-B system, *i.e.*, the pressure-weighted good curvature outweighs the bad curvature [Eq. (22)] on all field lines. (This is, in fact, the criterion for interchange stability). In addition to interchange instability, such a system can be unstable to modes which localize in the bad curvature regions such as electrostatic "trapped-particle" modes and at high-beta MHD ballooning modes.

Interchange modes are unstable modes that exhibit fluctuations independent of position along the field lines. Interchange stability provides a necessary condition for stability of the tandem mirror system and determines a ratio of confinable central cell to plug pressure. If the central cell consists of a uniform magnetic field cylinder bounded by a transition region which maps the flux tube into the minimum-B plugs, it is clear that lengthening the central cell by adding a neutral curvature region does not change the size of the bad curvature region and thus does not change the instability drive.

There are other physical processes, however, that do scale with central cell length and can obtain dominance in a long central cell. One such mechanism

is the Finite Larmor Radius (FLR) stabilization [Rosenbluth, Krall, Rostoker, 1962; Rosenbluth and Simon, 1965]. This stabilization results because ions see a smaller fluctuating field than do electrons, due to the averaging that occurs along ion gyro-orbits. FLR stabilization will be operative for modes having an azimuthal mode number, m, larger than 1 ($m = 1$ modes can be thought of as a rigid displacement of the plasma cross section so that ions cannot average the perturbation). It has been found that for a sufficiently long tandem mirror central cell only $m = 1$ MHD modes are potentially unstable.

Other processes that scale with central cell length are the radial centrifugal forces and azimuthal Coriolis forces experienced by the plasma due to plasma rotation which results from a radial equilibrium electric field. The rotational drive is proportional to the square of the rotation speed and is independent of the sign of the electric field, whereas the Coriolis term scales with the product of the rotational velocity and the radial pressure gradient. For inward directed electric fields the Coriolis term can become stabilizing. Otherwise both of these terms are destabilizing and present a limitation to the tolerable radial electric fields which again become more severe for long central cell lengths.

Assuming interchange stability, an average minimum-B system is subject to modes that can localize themselves in the bad curvature regions, *e.g.*, the tandem mirror c ntral cell. For modes with long parallel wavelengths the plasma conductivity along field lines will be large and the parallel electric field ($E_{||}$) will be driven to zero. This validates the infinite conductivity assumption of ideal MHD, and MHD theory provides a self-consistent theory of stability for such modes. In this formalism the plasma can be considered to be frozen to the

field lines and the magnetic field must distort as the plasma moves. Therefore, localization of perturbations always leads to bending of field lines, which in turn is only possible when the plasma pressure is comparable to the magnetic field pressure, that is, at finite beta. At finite beta MHD ballooning will determine the maximum pressure that can be sustained in the central cell for a given anchor pressure; this limitation is always more restrictive than that set by interchange stability. Similar to the interchange case, FLR effects will tend to stabilize all but $m = 1$ modes and rotation will be destabilizing. Optimizing tandem mirror designs with respect to MHD ballooning thus requires diminishing the central cell curvature drive (which can be accomplished, for example, by tapering the central cell fields).

The high conductivity assumption of MHD breaks down for modes which balloon over sufficiently short distances [Berk *et al.*, 1982]. These modes tend to be electrostatic ($E_{\|} \sim -\nabla\phi$) and have been termed trapped particle modes. Since electrostatic fluctuations do not bend field lines, trapped particle ballooning modes can grow in low–beta plasmas. They generally exhibit lower growth rates than the MHD modes just described, although in some situations they can exhibit MHD–like growth rates.

Reactor Implications

If the total number of ions in the central cell divided by the total number in both plugs is made substantially larger than the density ratio required to create the electrostatic end plugs, the tandem mirror fusion power gain, Q_t, can

be increased to much more attractive values than those attainable in a single cell device. To verify this we follow Fowler [Fowler, 1981] and note that Q_t is the ratio of the fusion power produced in the volume V_c of the central cell, $\frac{1}{4}n_c^2\langle\sigma v\rangle E_n V_c$, divided by the power injected into the volume, $2V_p$, of both plugs, $2V_p E_0 n_p^2/(n\tau_i)_p$, so that

$$Q_t = \left[\frac{1}{4}(n\tau_i)_p\langle\sigma v\rangle\frac{E_n}{E_0}\right]\left(\frac{V_c n_c^2}{2V_p n_p^2}\right), \tag{5}$$

with n_c and n_p the densities in the central cell and plugs, respectively. Because the first term in Eq. (5) is, to good approximation, the single cell fusion power gain, $Q_s \sim 1$, the tandem mirror reactor fusion power gain can be enhanced over the single cell value by $V_c n_c^2/2V_p n_p^2$ and typically can be in the range of 5 to 10.

Although this improvement in Q above that which is attainable in a single mirror cell is substantial, the tandem mirror as presented here entails significant engineering constraints. In reactor applications obtaining desirable fusion power densities sets the central cell plasma parameters (density and temperature). However, since sufficient plugging of central cell ions requires an order of magnitude density rise between the central cell and plugs, high plug densities are required. Reasonable confinement times for the plug ions then require very high energies for the neutral beam systems that fuel the plugs, typically in excess of one MeV. Additionally, confinement of this high pressure plug plasma requires high magnetic fields, typically reaching above 15 T. This field level is particularly difficult to achieve in minimum-B type plug coil sets. Thus one reactor design created at LLNL [Moir, R.W. *et al.*, 1977], which produced $Q =$

5 with 2 MW/m^2 neutron wall loading required 2 MeV neutral beams and 16 T quadrupole plugs, a formidable task.

Finally, the basic tandem mirror scheme showed difficulty in achieving both high neutron wall loading and acceptable Q. The interrelation of Q and wall loading follows from constraints on the central cell parameters (density, n_c, and temperature, T_c), the total power produced (and thus the central cell volume) and the magnet parameters (central cell field, B_c, plug field, B_p, and plug length, L_p). Eq. (5) may be recast in terms of these parameters to obtain the following form:

$$Q \approx \left[\frac{(n_c\langle\sigma v\rangle/4)^3}{n_p^2 E_L} \frac{V_c}{2\pi L_p} \frac{B_c}{B_p} \right] p_n^{-2}, \tag{6}$$

with p_n the central cell wall loading (power per unit area). Clearly high wall loading results in low Q and vice versa. The LLNL reactor study [Moir *et al.*, 1977] was designed to have a $Q = 5$ and a neutron wall loading of ~ 2 MW/m^2. The implication of the above scaling indicates that doubling Q would require a drop in wall loading to about $\frac{1}{2}$ MW/m^2. Thus, although it was seen that the tandem mirror scheme led to a reactor that proved to be a significant improvement over a single cell mirror, Q (or wall loading) was nevertheless marginal and required difficult technology development.

These concerns precipitated the invention, in 1978, of the thermal barrier which will be discussed in Section IV.A.

III.B Radial Transport

The axial variation of the electrostatic potential in a tandem mirror is used to confine both electrons and ions so that the end loss rate is substantially smaller than in the single mirror counterpart. Because of this improvement in axial confinement, radial losses in tandem mirrors can be significant compared with axial losses. In conventional single cell mirrors radial losses were always negligible compared to the large axial losses.

The neoclassical mechanism which leads to the radial loss in a tandem mirror is a result of radial particle drifts, or more precisely, of drifts across magnetic flux surfaces. These occur when particles pass through a region of nonaxisymmetric magnetic fields [Ryutov and Stupakov, 1978; Cohen, 1979], unless those fields are precisely tailored [Catto and Hazeltine, 1981; Myra et al., 1983].

III.B.1 Magnetics

In its original and simplest embodiment, a tandem mirror, as described earlier, is an axisymmetric solenoid terminated by two end plugs. In order to maintain stability (see Section III.C), however, the magnetic fields of the plug are made to curve away from the plasma by the introduction of a quadrupole magnetic field. In this way the plugs can also be employed to stabilize or "anchor" the axisymmetric central cell, as well as the transition region which is needed to connect it to the plugs. In cylindrical r, θ, z variables, only the sign of a magnetic field possessing quadrupole symmetry is changed by the *two* rotations;

$\theta \to \pi/2 \pm \theta$ and $z \to -z$.

As will become evident, the introduction of the nonaxisymmetric quadrupole fields causes the flux and drift surfaces to separate; this is, therefore, the source of radial transport in tandem mirrors. Because of the long, axisymmetric central cell in tandem mirrors, these radial losses (which are negligible in single cell mirrors) can become substantial unless care is taken to limit them.

In attaching the tandem mirror plugs to the central cell, the quadrupole fields of the plug are aligned in such a way that the tandem mirror possesses an overall quadrupole symmetry [Lao *et al.*, 1978]. In cylindrical r, θ, z variables, a long-thin or paraxial magnetic field configuration is obtained by assuming $L^{-1} \sim |\partial/\partial z| \ll |\nabla_\perp| \sim r^{-1}$ and results in, [Furth and Rosenbluth, 1964; Cordey and Watson, 1970],

$$\underline{B} = B(z)\hat{\underline{z}} + \nabla\psi \tag{7}$$

with

$$\psi = \frac{1}{4}r^2[-B'(z) + B(z)f'(z)\cos 2\theta], \tag{8}$$

where a prime denotes d/dz. A symmetric magnetic well, $B(z) = B(-z)$, is said to possess quadrupole symmetry when the fanning of the two ends differs by 90° so that $f(-z) = -f(z)$. For long, thin vacuum mirror fields the radius of curvature is of order L^2/r.

In the absence of closed magnetic surfaces (as in a tokamak), flux surfaces are defined by surfaces of constant pressure. In the central cell of a tandem

the anisotropy of the ion and electron pressures is small and such a definition is appropriate. Assuming that the constant pressure surfaces are circular at $z = 0$, the magnetic flux, $2\pi\alpha$, for the quadrupole magnetic field of Eqs. (7) and (8) is found from $\underline{B} \cdot \nabla\alpha = 0$ to be

$$\alpha = \frac{1}{2} r^2 B(\cosh(f) - \sinh(f)\cos 2\theta). \tag{9}$$

As can be seen from Eq. (9), the departure of the odd function $f(z)$ from zero causes the flux surfaces to distort or "fan" beyond the axisymmetric central cell region of the tandem [where $f'(z)$ in Eq. (9) no longer vanishes]. In these fanned regions the flux and drift surfaces are no longer aligned in general, so that collisions cause neoclassical radial steps in the drift orbits relative to the flux surfaces. If $\underline{B}$ is written as

$$\underline{B} = \nabla\alpha \times \nabla\beta, \tag{10}$$

with $2\pi\alpha$ the flux and β an angle variable, then the field line curvature $\underline{\kappa} \equiv \underline{b} \cdot \nabla\underline{b}$, where $\underline{b} = \underline{B}/B$, may be written as

$$\underline{\kappa} = \kappa_\alpha \nabla\alpha + \kappa_\beta \nabla\beta. \tag{11}$$

The neoclassical transport coefficients for a scalar pressure plasma may be written in terms of the geodesic curvature κ_β,

$$\kappa_\beta = -|\underline{B}|^{-2} \nabla\alpha \cdot \underline{B} \times \underline{\kappa}, \tag{12}$$

and neoclassical transport occurs only because of regions with $\kappa_\beta \neq 0$. The normal curvature κ_α, where

$$\kappa_\alpha = |\underline{B}|^{-2} \nabla\beta \cdot \underline{B} \times \underline{\kappa}, \tag{13}$$

does not enter transport calculations, but is crucial in determining the stability of the plasma, as will be discussed in a later section.

III.B.2. Nonresonant Losses

Provided that the azimuthal drift of a particle is small during one parallel transit of the device, it will move so as to maintain constancy of the adiabatic invariant

$$J = \oint ds v_{\|}, \tag{14}$$

where the integral is over one complete bounce, s is arc length along the magnetic field and $v_{\|}$ is the velocity component along the magnetic field. The constant J or drift surfaces project shapes onto the midplane of the central cell which, in general, depart from the circular projection of the flux surfaces. (See Fig. III.B.1.) In extreme cases, drift surfaces may not even be confined for all particles, leading to a direct loss of plasma to the side wall limiters. Collisions can also change J and cause particles to wander from one drift surface to another. The "step" size for this neoclassical process is characterized by the departure of the drift surfaces from circles [Baldwin, 1978; Ryutov and Stupakov, 1978]. Enhanced transport which conserves J can occur for both electrons and ions.

In the limit where a bounce–averaged description of particle drifts given by Eq. (14) is adequate, symmetry can be exploited to zero out the net radial step. This occurs when the quadrupole fanning of the flux surfaces has an odd parity, which may be accomplished in a tandem mirror by a proper orientation of the end cells so that the flux tube fans orthogonally at either end of the central cell [Lao, *et al.*, 1978], as shown in Fig. III.B.2. Such a device is referred to as having quadrupole symmetry. Then J is rendered independent of azimuthal angle

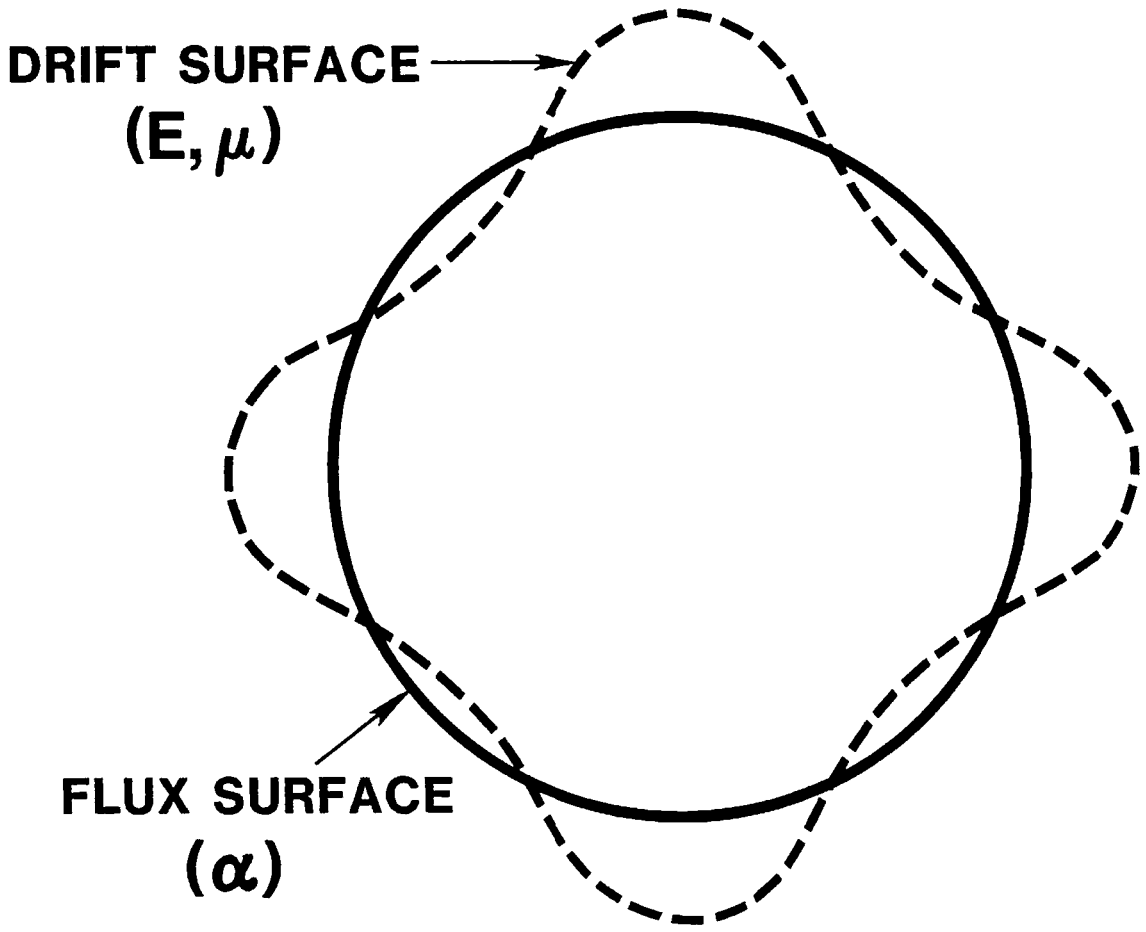

Figure III.B.1: Intersection of an ion drift surface, for a particular E and μ, with the midplane of the confinement system. The flux surfaces are chosen to be circles at the midplane. Neoclassical "steps" result from the departure of flux and drift surfaces in the presence of collisions. A particle with a different E and μ will in general have a different drift surface.

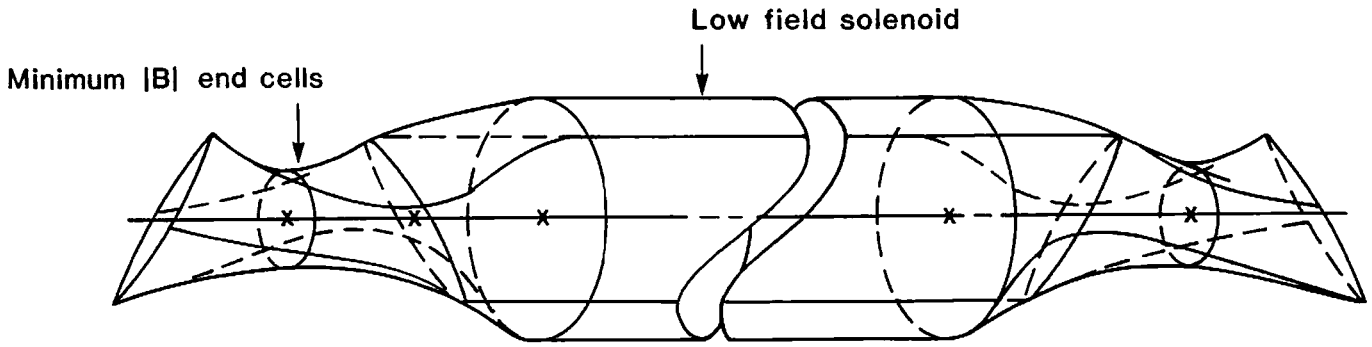

Figure III.B.2 Schematic diagram shows a flux surface for a quadrupole symmetric tandem mirror.

through the second order in a paraxial expansion (*i.e.*, for magnetic field lines close to the magnetic axis) by virtue of a cancellation in the integral of Eq. (14). Thus the drift surfaces retain approximate circularity. Such devices have been termed "omnigenous" in the literature [Hall and McNamara, 1975]. Here, the term omnigenous is reserved to describe those magnetic field configurations with $\kappa_\beta \equiv 0$ [see Eqs. (11)-(12)], in which the radial drift vanishes locally. Configurations with finite local drifts which exploit symmetry to eliminate bounce-averaged radial drift will be described as possessing average or global omnigenity as opposed to local omnigenity.

In spite of this exploitation of cancellations in the bounce-averaged drift, neoclassical transport is still an issue in quadrupole symmetric devices. Drift surfaces have a noncircularity when higher order corrections in the plasma beta and the long-thin parameter are retained. Additionally, in a tandem mirror, particles can be trapped in segments of the machine where they do not "see" the quadrupole symmetry of the entire machine [Byers, 1982]. The *Yushmanov* particles reflected by Φ at one bounce point, and by B at the other, are an example. More importantly, J is not a good invariant for many ions so that "resonant" transport can occur.

III.B.3. Resonant and Stochastic Transport

The assumption of small azimuthal drifts per transit, inherent in the bounce-averaged description of Eq. (14), is difficult to satisfy for the ions in a tandem mirror because of the length of the central cell. (The much larger electron bounce frequency makes this assumption always valid for electrons). If an ion can undergo an azimuthal drift of $\pi/2$ (or an odd multiple thereof) in half a bounce, it will experience successive additive rather than cancelling radial drifts. This is because an azimuthal drift of $\pi/2$ is enough to undo the cancellation, due to the quadrupole symmetry, which occurs for radial drifts on a *given* field line. Ions with E and μ causing them to drift in this manner are referred to as resonant [Ryutov and Stupakov, 1977, 1978b]. The resonance condition may be expressed as

$$\int \frac{ds}{v_{||}} \Omega_d = (2k+1)\pi/2, \qquad k = 0, \pm 1, \cdots \tag{15}$$

where Ω_d is the azimuthal drift frequency and the integral extends between the turning points of the ion's axial motion so that the left-hand-side of Eq. (15) is approximately $L_c \Omega_d / v_{||}$ with L_c the length of the central cell. Figure III.B.3 shows the drift orbit for a resonant ion with $k = 5$.

When resonant ions exist in a tandem mirror, the resulting transport is expected to dominate over nonresonant neoclassical loss mechanisms. Thus there has been considerable theoretical effort expended in calculating the magnitude and scalings of resonant transport, as well as in attempting to find ways to reduce its impact [Ryutov and Stupakov, 1977, 1978; Cohen, 1979; Myra and Catto,

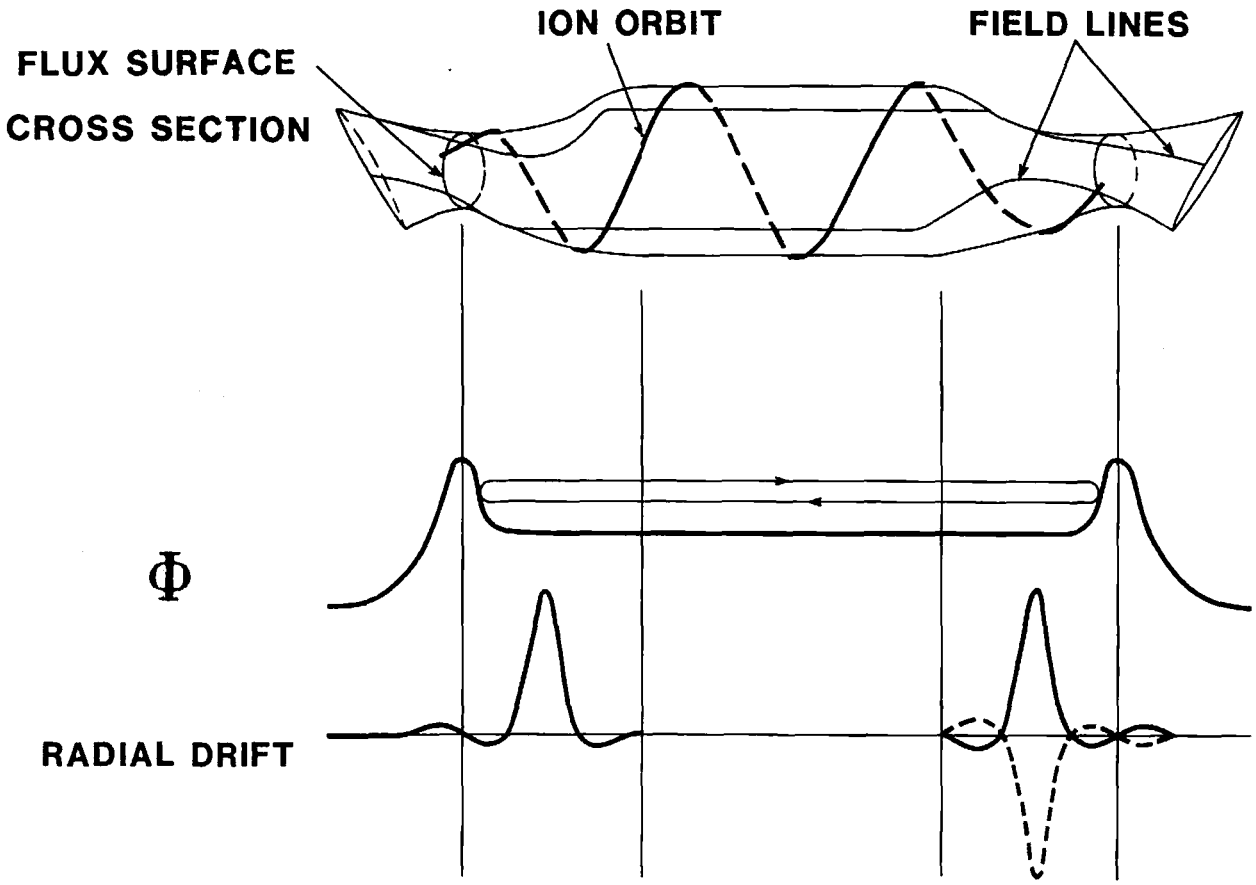

Figure III.B.3: Schematic diagram illustrating the drift orbit for a resonant ion which undergoes an azimuthal drift of $11\pi/2$ per half bounce. Also sketched are the confining electrostatic potential and the radial drift velocity. The solid curve in the lowermost plot shows the radial drift which a resonant ion experiences on its orbit. The dotted curve is the cancelling radial drift which an ion would have experienced if it stayed on the same field line for the complete transit.

1983].

The precise form of the resonant diffusion coefficients depends not only on details of the geometry but also on the regime of collisionality and the degree to which the resonant curves in phase space remain sharply defined and isolated from each other. To obtain an estimate of the diffusion coefficient it is adequate to estimate the radial step size and combine it with an appropriate correlation time.

The ion radial step across a flux surface per half bounce, denoted by δ, is given by a trajectory integral of the form

$$\delta = \frac{1}{rB} \int \frac{ds}{v_{\|}} \underline{v}_d \cdot \nabla \alpha, \tag{16}$$

where the $(rB)^{-1}$ factor converts a step in flux units to one in the radius variable r, and $\underline{v}_d$ is the guiding center drift velocity. Radial $\underline{E} \times \underline{B}$ drifts are usually neglected so that the $\nabla \alpha$ component of the remaining magnetic drift is proportional to the geodesic curvature κ_β defined in Eq. (12). For most tandem designs, the dominant contribution to δ comes from the quadrupole fields in the transition region, since the radial drift is zero in the axisymmetric central cell. Unless special efforts are taken to make the magnetic field locally omnigenous or nearly so (*i.e.*, $\kappa_\beta \simeq 0$ everywhere), the step per half bounce typically scales as

$$\delta \sim \frac{r\rho_i}{L_t}, \tag{17}$$

where ρ_i is the ion gyroradius and L_t is the length of the transition region. In obtaining Eq. (17) the estimates $\int ds/v_{\|} \sim L_t/v_{\|}$ have been employed

where v_i is the ion thermal velocity, together with $v_i\rho_i/R_\beta$ as the estimate of the radial component of the drift velocity. Here R_β is the radius of geodesic curvature. Unless the fields are especially tailored, the radii of geodesic and normal curvatures are comparable, and of order L_t^2/r in the transition region, yielding Eq. (17) for δ. (In the omnigenous case, $R_\beta \to \infty$.) Thus the ions undergo a radial step of magnitude δ at each end of the device.

For resonant–plateau transport to occur [Ryutov and Stupakov, 1977; Cohen, 1979; Myra and Catto, 1983], the coulomb collision frequency, ν, must be in an intermediate regime which allows the ion to complete several transits of the device before suffering a 90° scattering. In this regime the ion motion remains correlated for a time ν^{-1} and the number of half–bounces, j, completed during this time is,

$$j \sim \frac{1}{\nu t_\parallel}, \tag{18}$$

where $t_\parallel = v_\parallel/L_c$ is the parallel transit time. The net mean square step per j half bounces is therefore $j\delta^2$, *not* $j^2\delta^2$, since it is a diffusive process. Finally, an estimate of the resonant–plateau diffusion coefficient is obtained from the mean square step $j\delta^2$ over the correlation time $jt_\parallel$, yielding

$$D_{rp} \sim \delta^2/t_\parallel. \tag{19}$$

This result for D_{rp} is independent of collisionality, and hence termed resonant–plateau.

Equation (19) typically implies significant radial losses. In TMX, for example, radial diffusion of this order of magnitude is observed and competes with

end loss [Drake *et al.*, 1981].

When the collision frequency drops below a critical value ν_c (*i.e.*, j becomes sufficiently large),

$$\nu < \nu_c \ll t_{\|}^{-1},$$

and $j\delta^2$ overestimates the mean square step per j half bounces because the radial drift detunes the resonance. The diffusion coefficient is then reduced below the level of Eq. (19) and is found to scale linearly with ν. This is generally called the resonant–banana regime [Cohen and Rowlands, 1981]. Because D scales with ν in this regime, extrapolation of radial losses to the fairly collisionless conditions of a reactor can be quite favorable *if* resonant–banana diffusion can be achieved. Unfortunately, another diffusion mode, stochastic diffusion, which has less favorable scalings, intervenes.

Equations (16) or (17) show that the radial step is, in general, a function of the flux or radius variable, *i.e.*, $\delta = \delta(r)$, where $\delta(r)$ is an increasing function, which depends on the magnetic geometry. If δ is allowed to exceed a critical value, known as the stochastic threshold,

$$\delta > \delta_{st} \sim \frac{v_{\|} r_c}{L_c \Omega_d}, \tag{20}$$

where r_c is the central cell radius, successive radial displacements become effectively decorrelated due to the onset of intrinsic stochasticity in the (collisionless) particle orbits. This may be understood in terms of the familiar resonance–overlap criterion. The resonance condition given by Eq. (15) has radial dependence. That is to say, the K^{th} resonance occurs at a specific radius with a radial gap

between it and the K + 1 resonance. When $\delta < \delta_{st}$, radial motion causes the ion to detune from the resonance, whereas when $\delta > \delta_{st}$, the radial motion of the ions causes them to jump from one resonance to another. In the fully stochastic limit, resonances are no longer well defined. The correlation time becomes the parallel transit time $t_{\|}$, and the mean square step per correlation time is just δ^2. Thus the diffusion coefficient is approximately

$$D_{st} \sim \delta^2 / t_{\|} \quad \text{for} \quad \delta > \delta_{st} \tag{21}$$

which yields the same estimate as that obtained for D_{rp}. Because the stochastic process is viable in the total absence of classical collisions it may render the favorable resonant–banana scaling inappropriate for reactors, unless $\delta < \delta_{st}$ can be ensured over most of the plasma column.

Since δ is primarily set by the magnetic geometry, a careful design of magnetic field coils to reduce the radial step [Catto and Hazeltine, 1981; Myra *et al.*, 1983; Baldwin and Bulmer, 1982] can have a large payoff, especially in the more collisionless regimes. Tandem designs free of resonant and stochastic ion transport are possible if ions are confined within an entirely axisymmetric region [Kesner, 1980; Kesner *et al.*, 1982] and if the stability of such a configuration can be ensured to be unsusceptible to ballooning and trapped particle modes. In systems with nonaxisymmetric plugs, bounding the central cell with an axisymmetric high-field "throttle-coil" can reduce resonant transport significantly.

III.B.4 Ambipolarity Considerations

The radial structure of the ambipolar potential is coupled to the radial transport problem. Thus radial transport ultimately affects end loss through its effect on the ambipolar potential barrier heights Φ_i and Φ_e. One-dimensional radial transport models have been employed to study the self-consistent density and potential profiles [Rensink *et al.*, 1980; Myra and Catto, 1982]. Because radial potential gradients (together with density and temperature gradients) drive the ion flux, control of external boundary conditions on the ambipolar potential, possibly through manipulation of plasma sheaths, may offer another avenue for reducing radial transport [Myra and Catto, 1982; Myra and Catto, 1983; Mirin *et al.*, 1983] and improving the equilibrium [Bulmer *et al.*, 1982].

III.C MHD Equilibrium And Stability

III.C.1 Basic Theory

A mirror plasma can be unstable to a variety of low-frequency, global modes. The most important sources of free energy for MHD instabilities in mirror geometry are pressure gradients, pressure anisotropy, and plasma $\underline{E} \times \underline{B}$ rotation. (Low frequency instabilities driven by $E_{||}$ are outside the scope of MHD and will be discussed in Sec. III.D.)

There are four parameters which characterize confinement and stability in mirror geometry. The first is $\lambda = L_{\perp}/L_{||}$, the ratio of the perpendicular to parallel scale lengths. The vacuum magnetic field is usually characterized by two parameters, which measure the strength of the mirror and quadrupole field components, respectively. For example, one might choose $R_m = B_{max}/B_{min}$ and $f_{max} = \ell n(a/b)$ where R_m is the mirror ratio, f_{max} is the fanning function maximum, and b/a is the maximal elongation of the vacuum flux surface. Finally, the plasma pressure p is usually given in terms of the parameter $\beta = 2p/B^2_{min}$. With the development of the tandem mirror concept, the mirror program has evolved toward large-aspect-ratio devices ($\lambda \ll 1$) for which the paraxial or long-thin expansion [Newcomb, 1981] is appropriate. This has greatly facilitated the theoretical treatment of the equilibrium and stability problems.

Before considering the tandem mirror in its present form, it is useful to review briefly the influence of MHD considerations on the development of the mirror program. The first mirror experiments were simple (or axisymmetric) mirrors, in which the magnetic field strength, B, increases with axial distance

from a plane of symmetry and there is no quadrupole field. The simple mirror is unstable at all values of β to pressure-driven interchange modes [Rosenbluth and Longmire, 1957], because the field lines bow away from the plasma near the midplane, and the average curvature is therefore in the wrong direction. (Fig. III.C.1).

To correct this shortcoming, the minimum-B mirror was proposed. In this device the surfaces of constant B are closed, and B increases outward from the center of the plasma. To achieve this, a highly nonaxisymmetric field configuration is required (Fig. III.C.2) in which the superposition of a stabilizing quadrupole ($\cos 2\theta$) magnetic field on the simple mirror field yields a configuration with average good curvature on each field line. The minimum-B mirror is therefore stable at low β to all MHD modes [Taylor, 1963]. However, if β is of order unity, various instabilities can occur. First, the pressure anisotropy ($p_\perp > p_\parallel$) can lead to the onset of the mirror mode [Thompson, 1961]. Second, the plasma diamagnetism expels the magnetic flux and thereby reduces the favorable curvature. Plasma diamagnetism will produce a seemingly stabilizing grad-B drift. However, the parallel component of the perturbed magnetic field will enter in such a way as to cancel this effect. Thus the self-dug well of a plasma will not affect MHD stability. Recent analytic and numerical calculations indicate that interchange stability can be lost in this way when β is of the order of the vacuum magnetic well depth [Hall and McNamara, 1975; D'Ippolito and Freidberg, 1982a; Strauss *et al.*, 1982]. Good theoretical estimates of these β limits for specific configurations await the completion of numerical work now in progress [Bulmer *et al.*, 1982], but the experimental results in 2XIIB (a small-

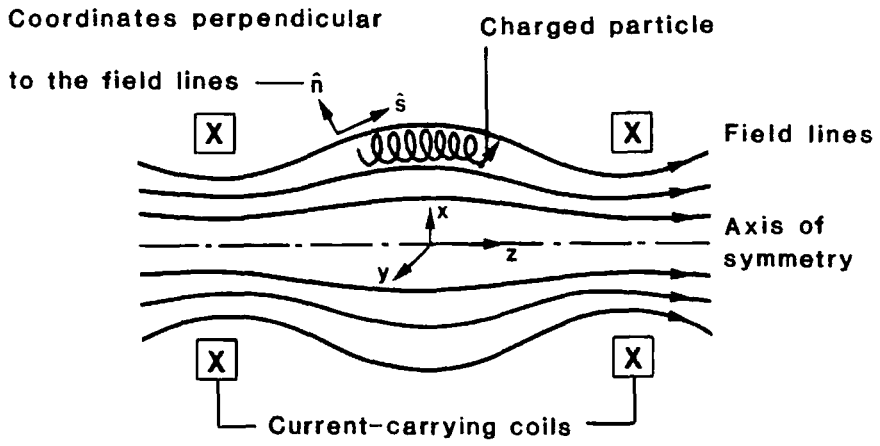

Figure III.C.1: Magnetic configuration of a *simple mirror* device with circular coils.

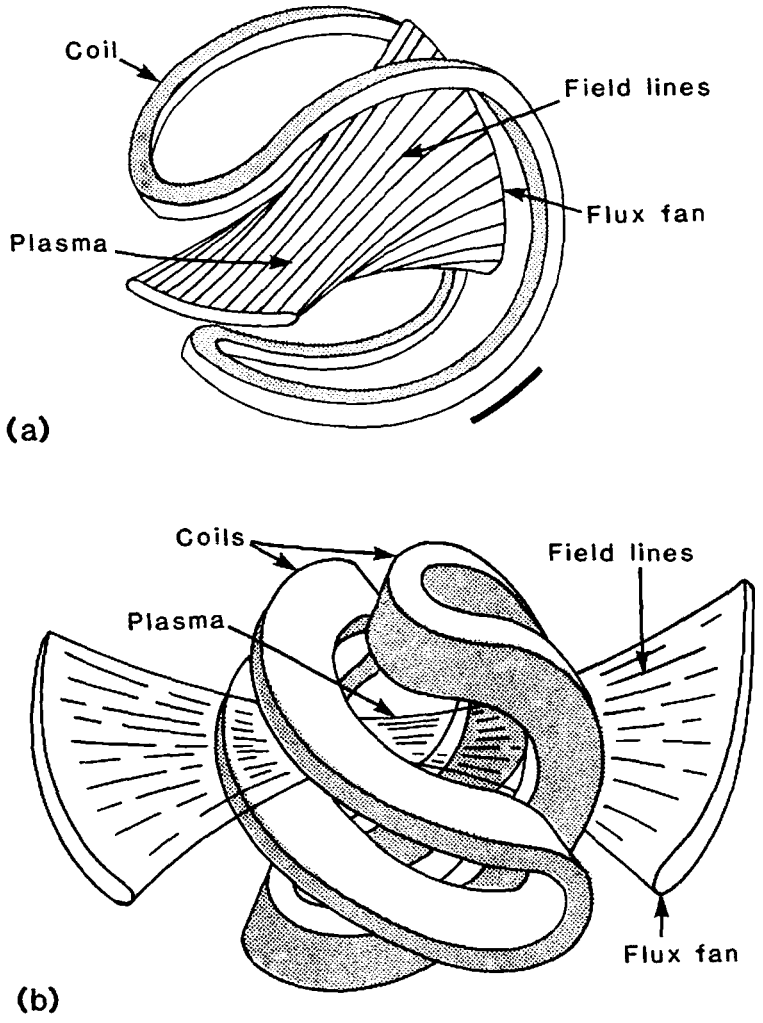

Figure III.C.2: Sketch of magnet systems that create *magnetic well* geometries, showing (a) baseball coil (so-called because the winding is in the shape of a baseball seam) and (b) yin-yang coils.

radius device) indicate that β of order unity is achievable without loss of MHD stability [Turner *et al.*, 1979]. In spite of these excellent equilibrium and low frequency stability properties, the isolated minimum–B mirror was abandoned as a fusion reactor concept for reasons outside the scope of MHD theory (specifically in poor confinement and the resulting low power amplification).

The development of the quadrupole–stabilized tandem mirror concept reopened the question of MHD stability as an important issue in reactor designs. In its simplest form the tandem mirror consists of a long solenoidal mirror connected at both ends to minimum–B mirror cells, which serve as end plugs and as MHD anchors (Fig. III.C.3). It is impossible to make the connection from the axisymmetric central cell to the very elliptical mirror throats of the quadrupole anchors without introducing a region of unfavorable curvature. The competition between the destabilizing "transition region" and the stabilizing anchor determines the MHD stability of the tandem mirror. In the paraxial limit, this competition can be expressed quantitatively by the following field line integral,

$$\Gamma \equiv \int ds \frac{(p_\perp + p_\parallel)}{B^2}(B\kappa_\alpha), \tag{22}$$

where κ_α is the normal component of the curvature (defined in Sec. III.B.1) and the Rosenbluth–Longmire condition for stability to pressure–driven interchange modes is $\Gamma > 0$. In the paraxial limit $B\kappa_\alpha$ is approximately independent of B, so the correct weighting of the geometric factor in Eq. (22) is the local plasma beta. Typically, a large pressure weighting of the anchor relative to the transition region is required for interchange stability. This is illustrated in Fig. III.C.4, in which the integrand in Γ and the normalized weighting function $(P_\perp + P_\parallel)/B^2$

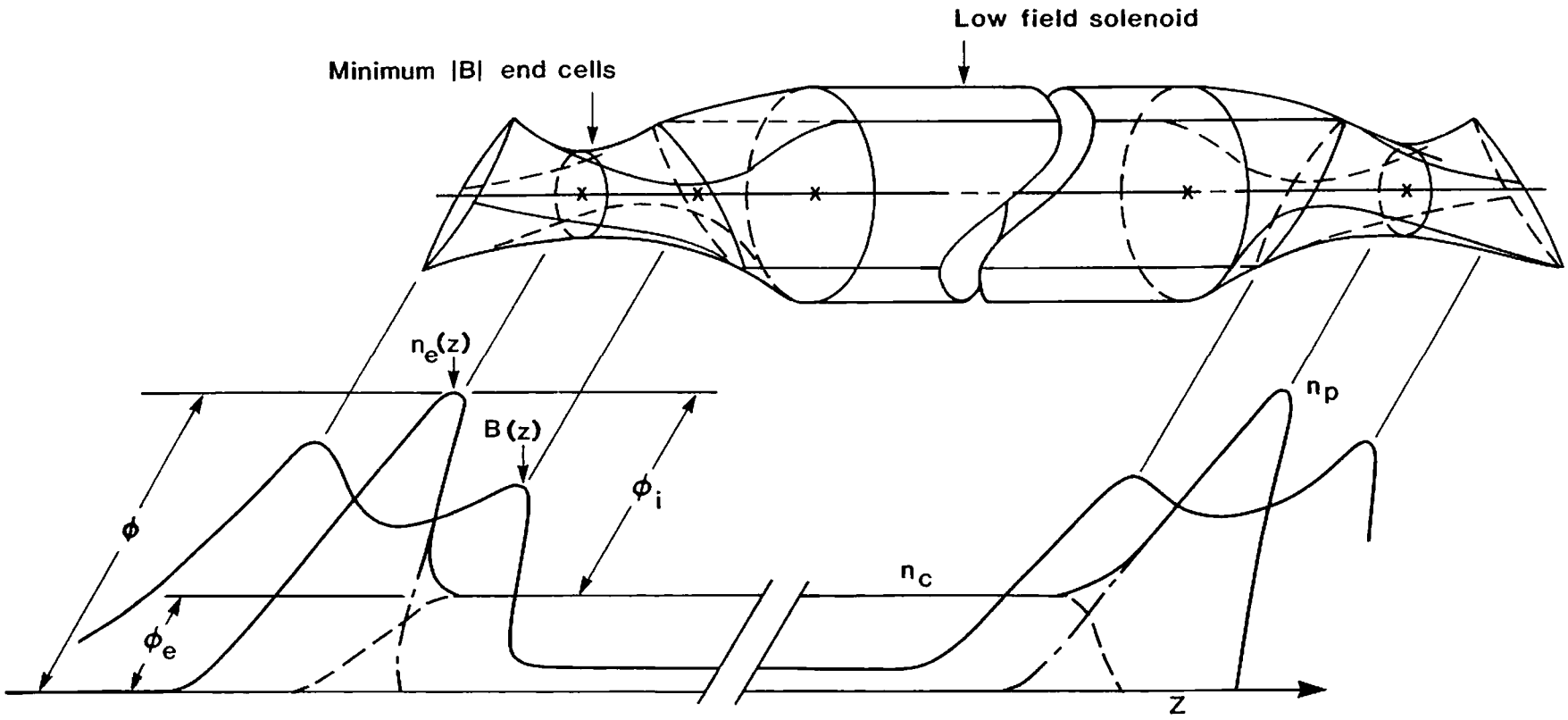

Figure III.C.3 Tandem mirror with ambipolar barriers at the ends.

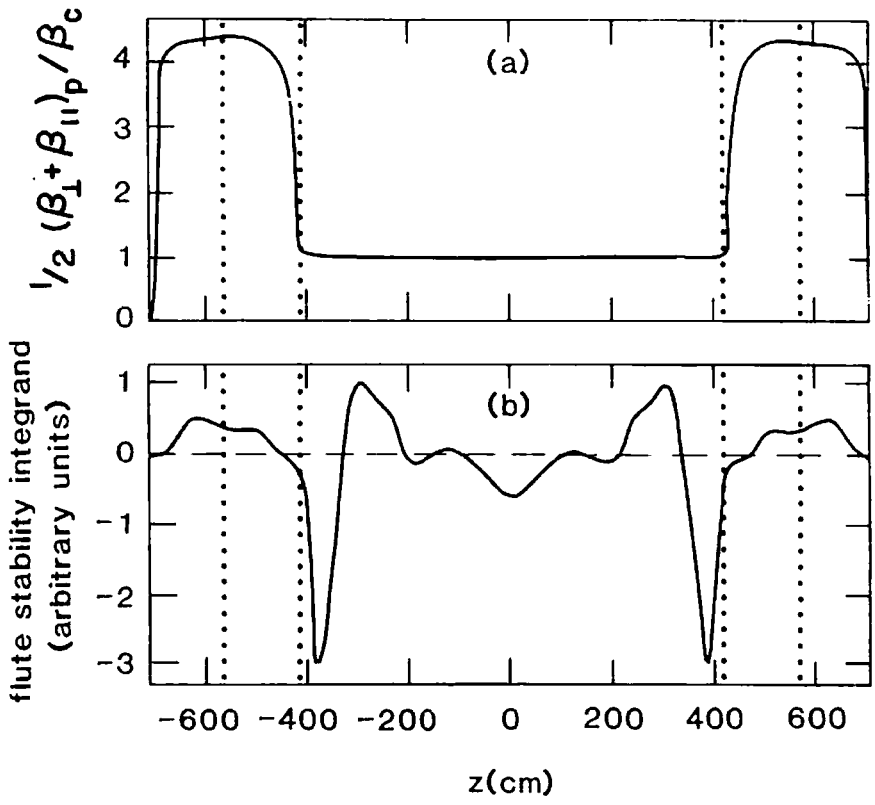

Figure III.C.4: Plots of the pressure weighting function $\frac{1}{2}(\beta_\perp + \beta_\parallel)_p/\beta_c$ normalized to the central cell beta, and the stability integrand for TMX-Upgrade parameters.

are plotted for typical TMX–Upgrade parameters.

A more detailed discussion of the MHD stability of the tandem mirror can be separated conveniently into two issues: (1) the properties of the minimum–B anchors must be calculated to determine the maximum achievable anchor beta, β_a; (2) given an anchor, the maximum value of beta in the central cell, β_c, for stability to MHD modes must be determined.

The question of anchor stability is complicated by the three-dimensional nature of the equilibrium. Recent low-β analytical studies [Pearlstein *et al.*, 1981] and numerical simulations [Strauss *et al.*, 1982 and references therein] have made some progress in calculating the equilibria of quadrupole anchors. The stability studies are not yet complete, but the results of 2XIIB indicate that high values of β_a should be achievable without loss of anchor stability.

Turning to the central cell, pressure-driven modes are considered for which the instability drive is the bad curvature in the transition region. At low β_c, the mode amplitude $X \equiv rB\xi$ is constant along the field line (the flute or interchange limit), where ξ is the component of the plasma displacement normal to the flux surface. As discussed above, interchange stability is ensured by means of a high pressure weighting in the anchor. At high β_c, it becomes energetically favorable for the mode to avoid the anchor, even at the cost of bending magnetic field lines, and the most unstable perturbation has a "ballooning" character. The destabilizing curvature term $\sim a\beta_c/R_c$ and the stabilizing line bending term $\sim \delta B_\perp^2 \sim (B\xi/L_\parallel)^2$, where R_c is the radius of curvature and $L_\parallel$ is the axial scale length of the perturbation, tend to balance at some critical value of β_c at which the ballooning mode goes unstable. The value of $L_\parallel$ is determined

by the detailed properties of the anchor. A strong anchor (deep magnetic well) effectively excludes the eigenfunction so that $L_{||}$ is of the order of the length of the transition region. The weaker the anchor, the larger the value of $L_{||}$ and $L_{||} \rightarrow \infty$ as $\beta_c \rightarrow 0$.

The detailed axial dependence of the ballooning eigenmode is complicated by the fact that a field line on the flat side of the elliptical flux surface bends differently than one at the tip of the ellipse. Also, the two quadrupole anchors are rotated 90° with respect to one another in order that particle drifts at opposite ends of the machine cancel to lowest order (to reduce radial transport). The result is that a given field line has a different curvature at each end of the tandem mirror and is therefore anchored differently at each end [Kaiser and Pearlstein, 1982]. This is illustrated in Fig. III.C.5 for typical TARA design parameters ($\beta_a = 0.5, \beta_c = 0.27$). Shown are the radius of a field line in the symmetry plane and the corresponding marginally-stable eigenfunction in the $k_\perp \rightarrow \infty$ limit, obtained by solving the ballooning differential equation using Kaiser's code. The eigenfunction is essentially line tied (zero) in the left-hand anchor, rises sharply in the left-hand transition region (since bending energy is minimal in the flat part of the fan) and peaks in the left-hand bad curvature region of the central cell. The eigenfunction then decreases slowly through the central cell and is constant through the right-hand transition region, since the field line passes through the tip of the fan where the bending energy is high. Thus, the eigenfunction tends to maximize the instability drive by peaking in the bad curvature regions and avoiding the stabilizing anchors, subject to the constraint of minimizing the bending energy.

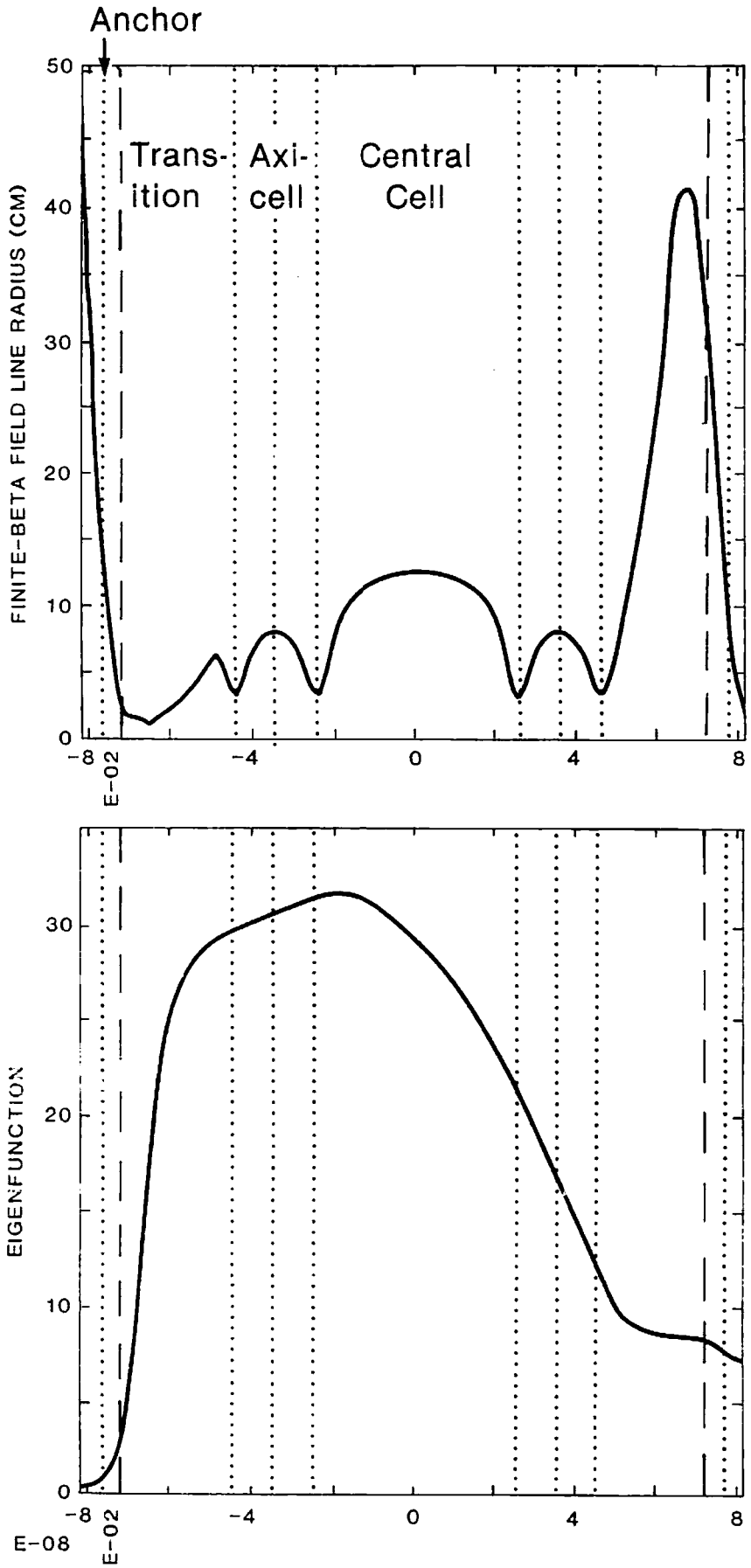

Figure III.C.5: Field Line Radius and Eigenfunctions for TARA.

A great deal of theoretical work has been devoted recently to calculating the critical β_c for ballooning modes, and the results can be classified according to the radial structure of the eigenfunction. Defining an "azimuthal mode number" m by $k_\perp \sim m/r$ (an exact relation for axisymmetric geometry), it can be shown that the eigenfunction becomes more sharply peaked in the radial direction as m increases. In ideal MHD theory, the worst mode has infinite m. The stability of this mode in tandem mirror geometry with quadrupole anchors [Ryutov and Stupakov, 1981; Kaiser and Pearlstein, 1982; Nevins and Pearlstein, 1981] and axisymmetric anchors [D'Ippolito *et al.*, 1982] has been extensively explored. However, it was also shown that finite ion Larmor radius (FLR) effects [Tang and Catto, 1981; Lee and Catto, 1981] strongly stabilize the higher m modes in the tandem mirror [Nevins and Pearlstein, 1981; D'Ippolito *et al.*, 1981]. FLR stabilization is much more effective in a tandem mirror than in a toroidal device such as the tokamak because the FLR terms act along the whole length of the machine, whereas the curvature drive for the instability is localized in the relatively short transition region. Thus, the ballooning limit on β_c will be determined by the low-m modes, particularly by $m = 1$, for which FLR stabilization is ineffective. In the absence of FLR effects, the critical beta scales as [D'Ippolito and Hafizi, 1981; Nevins and Pearlstein, 1981]

$$\beta_c \sim \left(C_1 + \frac{1}{m} C_2\right) \frac{R_c}{L_\parallel}, \tag{23}$$

where C_1, C_2 and $L_\parallel$ must be determined by solving for the radial and axial structure of the eigenfunction. Detailed stability analyses have been carried out for the quadrupole-stabilized tandem in the eikonal ($m \to \infty$) and rigid shift

($m = 1$) limits [Bulmer *et al.*, 1982; and references therein]. The results of all these studies indicate that critical central cell betas in excess of 50% should be easily achievable in the tandem mirror. When wall stabilization of the $m = 1$ or rigid shift mode is taken into account, the limit on β_c is raised even higher [D'Ippolito and Hafizi, 1981; Bulmer *et al.*, 1982].

Another MHD instability which may limit β_c is the rotational instability driven by the $\underline{E} \times \underline{B}$ plasma rotation [Freidberg and Pearlstein, 1978]. Since a large electrostatic potential is needed to confine the central cell ions axially, it is expected that a radial electric field will be present throughout the central cell of the tandem mirror. Simple estimates of the critical beta scaling for the rotational instability give

$$\beta_c \sim C\left(\frac{\pi a^2}{\rho_i L_{\|}}\right)^2, \tag{24}$$

where ρ_i is the ion gyroradius. Numerical studies in θ–pinch geometry have been carried out to determine the numerical coefficient C in Eq. (24) and it was shown that $m = 1$ has the lowest instability threshold [Freidberg and Pearlstein, 1978]. The conclusion drawn in this work is that low–m modes are stable for typical tandem mirror parameters. However, this conclusion may be modified by the destabilizing effect of mirror curvature [D'Ippolito and Freidberg, 1982b].

The extension of the tandem mirror design to include additional mirror cells to act as plugs or thermal barriers does not change the qualitative MHD picture given here, although it influences the numerical computations. When the effect of $E_{\|} \neq 0$ is taken into account, of course, the end–plug/thermal barrier plays a crucial role.

In summary, the main MHD limitation on the quadrupole–stabilized tandem mirror is that the central cell β must be less than a critical value to avoid onset of a rigid shift ($m = 1$) ballooning mode. The critical beta for this mode can be raised to acceptable values by proper shaping of a lateral conducting wall near the plasma. More localized (higher m) ballooning modes tend to be stabilized by FLR effects, and rotational modes also appear to be stable.

III.C.2. Advanced Theory

While the basic MHD equilibrium and stability picture for the quadrupole tandem mirror is rather favorable at the present time, there are a number of related physics issues which remain to be addressed.

A better treatment of the finite–β three–dimensional equilibrium problem is needed for a number of reasons. First, there is the need for a self–consistent finite–β treatment of the global ballooning modes, particularly of the rigid–shift mode. Present treatments use either vacuum fields or the finite–β axisymmetric central cell approximation. Second, the influence of the finite–β equilibrium fields on the particle drift orbits is an important area for future work. Present studies of transport–minimizing vacuum fields [Baldwin and Bulmer, 1982; Myra et al., 1982] must be extended to include the finite–β fields when an accurate three–dimensional equilibrium solver becomes available. Recent numerical attempts to solve the paraxial equilibrium equation [Newcomb, 1981] are beginning to show promising results [Strauss et al., 1982; Bulmer *et al.*, 1982].

There are two areas in which MHD equilibrium theory seems inadequate

at the present time and needs to be extended. The first area concerns the Stupakov effect [Stupakov, 1979], which is a finite-β octupole distortion of the equilibrium flux surfaces in the central cell due to parallel currents flowing out of the quadrupole anchors. The distortion can lead to enhanced radial transport and is therefore undesirable. According to ideal MHD theory, the flux surface distortion grows linearly with the length of the central cell [Stupakov, 1979; Pearlstein *et al.*, 1981], whereas when FLR terms are included in the mode the distortion seems to saturate at a finite level [Newcomb, 1982]. Both of these results were obtained by using low-β expansions, and therefore need to be verified at finite β.

The second area in which MHD theory needs to be extended concerns the effect of $E_{\|}$, which is substantial in a tandem mirror. Recent work has shown that electrostatic trapping of particles in regions of bad curvature [Berk *et al.*, 1982] and axial shear in the $\underline{E} \times \underline{B}$ drift velocity [Lee *et al.*, 1982] are both significant destabilizing effects.

Finally, in the long term it may be useful to consider other MHD anchor designs in addition to quadrupole minimum-B mirrors. For example, axisymmetric anchor designs involving magnetic cusps [Logan, 1981] or hot electron rings, as in the EBT experiment, [D'Ippolito *et al.*, 1982, and references therein] may be of future interest.

III.D Trapped Particle Modes

The design of tandem mirrors has been influenced largely by considerations of stability to MHD perturbations, in particular, interchange and ballooning modes. In both these modes the drive is due to the free energy of the plasma expanding against a convex confining magnetic field.

In MHD theory it is assumed that $\overline{E} + \frac{\overline{V} \times \overline{B}}{c} = 0$. Together with Faraday's law this implies that the plasma is frozen to the field lines. Thus, as the plasma expands, it carries the field lines with it. If the plasma displacement is localized, the field lines will bend, creating a perturbed magnetic field at the expense of the kinetic energy of the plasma perturbation. The stability of the modes is determined by the balance of energy gained by the plasma expansion to the energy lost to bending the field. Tandem mirror designs make use of this stabilizing effect of field line bending by placing a minimum-B cell at each end of the central maximum-B cell. The plasma in the minimum-B cells is confined by field configurations which are concave towards the plasma. In order to avoid expending energy to bend the field lines, the plasma displacement is forced to be constant along a field line. But the energy gained by the plasma as it expands in the central cell where the curvature is unfavorable is more than offset by the cost in energy to the expanding plasma in the minimum-B anchors where the curvature is favorable.

This stabilization mechanism could be defeated if a mode could concentrate in the central cell, vanish in the anchors, yet not pay the penalty of creating perturbed magnetic fields. Such is the case for trapped particle modes. Although trapped particle instabilities have long been studied in tokamaks [Kadomtsev and

Pogutse, 1970], the occurrence of such unstable modes has only recently been predicted in tandem mirrors [Berk, *et al.*, 1982]. Since, unlike tokamaks, all confined mirror particles are trapped (*i.e.*, there is no equivalent of the tokamak circulating particle species) and furthermore since most central cell confined particles do not enter the stabilizing anchor cells, the predicted growth rates can be large, approaching the MHD growth rate.

Because trapped particle modes are primarily electrostatic ($\underline{E} \approx -\nabla\phi$), the stabilizing effect of field line bending disappears. For electrostatic modes the conductivity along field lines is too small for the parallel electric fields to generate sufficient currents to perturb the field. The plasma motion can then be thought of as motion across field lines without any concomitant field distortion.

To see how this behavior comes about, the warm plasma conductivity is first considered:

$$\sigma_{\|} \equiv E_{\|}/J_{\|} = 4\pi i v_e^2 k_{\|}^2/\omega_{pe}\omega Z'(\omega/k_{\|}v_e). \tag{25}$$

Here, Z' is the derivative of the plasma dispersion function.

For typical tandem mirror parameters $v_e^2 \gg \omega_{pe}^2 k_{\|}^2$ and it is found that $\sigma \approx -2\pi i v_e^2/\omega_{pe}^2\omega$. Combining this result with Ampere's law

$$-k^2 A_{\|} = (4\pi/c)J_{\|}$$

and taking $E_{\|} = -\nabla\phi + i\omega/cA_{\|}$, the following result is obtained:

$$E_{\|} = \frac{-\nabla\phi}{1 - 2\left(\frac{\omega_{pe}^2}{k^2c^2}\right)\left(\frac{\omega^2}{v_e^2 k_{\|}^2}\right)}. \tag{26}$$

Generally, ω_{pe}^2/k^2c^2 is a large number proportional to density while $(\omega^2/v_e^2k_{\|}^2)$ can be small, depending on parallel wavelength and electron temperature. For high density and small $k_{\|}$ the MHD limit $E_{\|} \sim 0$ is obtained. (If the cold plasma limit of the Z function $(\omega/k_{\|}v_e \to \infty)$ had been taken, Eq. (26) would becomes $E_{\|} = -\nabla\phi/(1 + \omega_{pe}^2/k^2c^2)$, which again gives $E_{\|} \sim 0$ for sufficiently high density).

In the opposite limit of low density and large $k_{\|}$, Eq. (26) yields the electrostatic results $E_{\|} = -\nabla\phi$. If the tandem mirror magnetic geometry picture in Fig. III.D.1 is considered, the unstable trapped particle eigenmode would tend to be flute–like throughout the central cell and roll off in a distance Δ so as to have near–zero amplitude within the tandem mirror anchor. The correct conductivity calculation can be shown to yield a form similar to Eq. (26), with $k_{\|}^2$ replaced by $(L_a\Delta)^{-1}$ where Δ is the distance over which the eigenmode falls off and L_a is the distance between eigenmode fall off and the bounce point for passing particles. Thus, for a sufficiently narrow Δ, the m mode will always be seen to be electrostatic.

In a tandem mirror most central cell ions reflect from the mirror fields bounding the central cell. When the trapped particle eigenmode sheath forms at the peak mirror field points ($Z = L_c$ only those "passing" particles which transit the sheath contribute to a reduction of the growth rate. Ignoring FLR stabilization and assuming that the transiting ions and electrons bounce at the same location, one can show that the instability growth rate, γ^2, is

$$\gamma^2 = \gamma^2_{MHD} / \left(1 + \frac{L_a}{L_c} \frac{n_p}{n_c} \frac{1}{(k_\perp \rho_i)^2} \right), \tag{27}$$

where n_p/n_c is the ratio of passing to central cell density, L_a/L_c the ratio of anchor length to central cell half length and ρ_i the ion gyroradius, γ^2_{MHD} the MHD growth rate defined by

$$\gamma^2_{MHD} = \omega_* \overline{\omega}_D / (k_\perp \rho)^2,$$

in which ω_* is the diamagnetic drift frequency $[\omega_* = (k_\perp T/M\Omega)(d \ln n/dr)]$ and $\overline{\omega_D}$ the central cell trapped particle bounce-averaged curvature drift ($\overline{\omega}_D = k_\perp T \overline{R_c^{-1}}/M\Omega$) with R_c the average central cell normal field line radius of curvature. Thus, for a sufficiently small passing density fraction, the growth rate for this mode can approach the MHD growth rate.

In the above discussion several important stabilizing effects were ignored. FLR will cause ions to average the fluctuating field and this decreases their response to a perturbation with respect to the electron response leading to a charge separation term. The FLR charge separation term is, however, only present for modes exhibiting an azimuthal mode number, m, greater than one.

A second charge separation effect arises because in a tandem mirror electrostatically-confined ions and electrons do not normally bounce at the same location. Thus the passing ions and electrons will see a different bounce-averaged fluctuating potential. For example, in a simple tandem mirror as pictured in Fig. III.D.1, passing ions will reflect before the anchor midplane ($z = z_c + z_a/2$) whereas passing electrons will reflect close to the outer mirror throat (located at $z = z_c + z_a$). In the trapped particle mode perturbed fields are localized to the

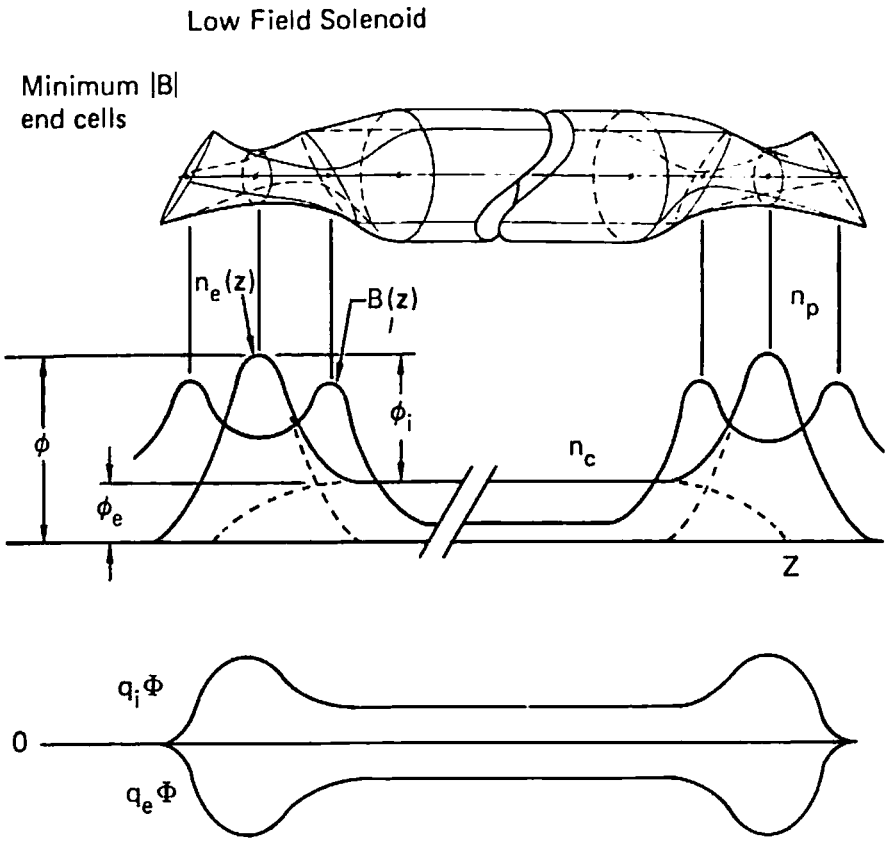

Figure III.D.1: Tandem mirror with ambipolar barriers at the ends.

central cell, and when the passing ions bounce beyond the electrons, the bounce and FLR charge separation terms are additive. In this arrangement trapped particle modes can be stabilized for all azimuthal mode numbers. Such an arrangement could be achieved for thermal barrier confinement and in fact forms the basis for the expected stability of the MFTF-B experiment to trapped particle modes.

Including charge separation terms, the trapped particle dispersion relation will take the approximate form

$$\omega^2(1 + A_1/m^2) + \omega\omega_*(1 - 1/m + A_2/m^2) + \gamma^2_{MHD} = 0 \qquad (28)$$

with

$$A_1 = \frac{n_p(L_i - L_c)}{n_c L_c (k\rho_i)^2}$$

and

$$A_2 = \frac{n_p(L_i - L_e)}{n_c L_c (k\rho_i)^2}.$$

Here L_i and L_e represent, respectively, the passing ion and electron bounce points and L_c is the half-width of the flute-like portion of the eigenmode. For the quadratic dispersion relation given by Eq. (28), stability for the $m = 1$ mode is obtained when

$$\frac{(L_i - L_e)}{L_c} > 4\left(\frac{\gamma_{MHD}}{\omega_*}\right)^2 (k\rho)^2 \left(\frac{n_p}{n_c}\right), \qquad (29)$$

a condition that is not difficult to satisfy.

When the passing electrons bounce beyond the passing ions the bounce average charge separation term will subtract from the FLR term. For a device that has sufficient passing density for $m = 1$ stabilization, instability will occur at a sufficiently high mode number for the FLR term to cancel against the bounce average charge separation term.

A second stabilization scheme that has been suggested recently [Kesner and Lane, 1983] would require an inward-pointing equilibrium radial electric field. This arrangement produces a stabilizing Coriolis force for $m > 1$ modes. The $m = 1$ mode is also seen to have enhanced stability in this scenario since it is shown in this work that this mode is rigid and thus cannot localize radially in regions of maximum drive.

III.E Microstability

III.E.1 Ion Microinstabilities

While the physics principles of longitudinal electrostatic confinement allow substantial enhancement of axial containment properties of tandems over those of simple mirrors, generating and sustaining this electrostatic mechanism relies heavily on the assumption of classical or near–classical containment properties of the simple mirror traps, which are used as end plugs in the tandem configuration. The laboratory experiences in the mirror program, and those theoretical explanations consistent with observations always require that ion microinstabilities must be controlled strictly or suppressed entirely in order to achieve classical confinement. In the sense of this critical issue, ion microinstabilities can be defined as those modes driven unstable by the nonmaxwellian nature of the ion distribution function in phase space. The modes are thereby classified according to their source of available ion energies and include those driven by the free energy associated with the loss cone (as in the case of the drift cyclotron loss cone (DCLC) instability [Post and Rosenbluth, 1966; Mikhailovskii, 1965, 1967] and axial loss cone (ALC) instability [Berk, Pearlstein and Cordey, 1972; Gerver, 1979a, 1979b, 1980]), or by the ion anisotropy (as in the case of the Alfven ion cyclotron (AIC) instability [Cordey and Hastie, 1972; Davidson and Ogden, 1975]). Additionally, even when the ion distribution function is locally maxwellian, there may be instabilities driven by the radial density gradient (*e.g.*, the lower hybrid drift instability, the drift cyclotron instability, the universal drift instability, the drift Alfven instability), which can cause enhanced radial transport.

The basic problem with ion microinstabilities is that the nonlinear consequence of these modes is to redistribute the ions in phase space, reducing the associated free energies. Unfortunately, this phase space redistribution usually means ion velocity space transport into regions with weaker axial containment (such as the loss cone region) and therefore can cause substantial nonclassical end losses. Furthermore, the rate of velocity space transport depends only on the strength of the unstable mode, not explicitly on the axial length so that length scaling to reduce the ion loss rate here is not possible except in the instances when the mode stability properties are sensitive to the mirror cell length. In some important parameter regimes some of the ion microinstabilities are flute-like and therefore are basically insensitive to mirror cell length, leaving the stabilizing control features to be a careful velocity space tailoring including use of large mirror ratios (closing the loss cone) and the injection of warm plasma streams with the proper density and temperature. These tailoring methods may not always be practically viable in a tandem scenario or may provide additional energy loss channels which will degrade the classical bare Q factor. For all these reasons then, it is critically important for a tandem mirror design to be as close to ion microstable as possible.

Because of both their historical significance in the mirror program and their potential future threat, the remainder of this section is devoted to discussing ion modes in considerable detail.

(1) Loss Cone Instabilities

Instabilities driven unstable by the loss cone are considered first. For these modes $k_\perp v_i > \omega$, so $k_\parallel v_A \gg \omega$, and (in contrast to anisotropy-driven modes

such as AIC) the ion response is electrostatic. If the electrons are cold ($k_{\|} v_e \ll \omega$ and $k_{\perp} v_e \ll \omega_{ce}$), then the infinite medium dispersion relation is [Tang, *et al.*, 1972; Callen and Guest, 1971, 1973; Gerver, 1979b]

$$1 + \frac{\omega_{pe}^2}{\omega_{ce}^2} + \frac{\omega_{pe}^4}{k_{\perp}^2 c^2 \omega_{ce}^2} - \frac{\omega_{pe}^2 k_{\|}^2}{\omega^2 k^2}\left(1 + \frac{\omega_{pe}^2}{k_{\perp}^2 c^2}\right)^{-1}$$

$$- \frac{\omega_{pe}^2 \hat{B} \cdot (\mathbf{k} \times \nabla n_e)}{k_{\perp}^2 \omega \omega_{ce} n_e} + \hat{k}_{\perp} \cdot \underline{\underline{\epsilon}}_{ion} \cdot \hat{k}_{\perp} = 0, \qquad (30)$$

where $\underline{\underline{\epsilon}}_{ion}$ is the ion dielectric tensor.

In Eq. (30) the 1 is the vacuum term, the $\omega_{pe}^2/\omega_{ce}^2$ is the electron polarization drift term, and $\omega_{pe}^4/k_{\perp}^2 c^2 \omega_{ce}^2$ represents the compressibility of magnetic field lines (a finite β effect), terms which are not usually very important. The term $\omega_{pe}^2 k_{\|}^2/\omega^2 k^2$ is due to the motion of electrons along the magnetic field lines in response to the parallel electric field of the wave; this is the term which (together with the vacuum term) gives Langmuir waves. At finite β, when $\omega_{pe}^2 > k_{\perp}^2 c^2$, the $k_{\|}^2$ term becomes $k_{\|}^2 c^2/\omega^2$, since the motion of electrons along field lines is less important than the restoring force from the bending of field lines; this term (together with cold ions) would give shear Alfven waves. The term $\omega_{pe}^2 \hat{B} \cdot (\mathbf{k} \times \nabla n_e)/k_{\perp}^2 \omega \omega_{ce} n_e$ is due to the $E \times B$ motion of the electrons (in the azimuthal electric field of the wave) back and forth in the radial direction, which (because of the radial density gradient) causes the electron density to fluctuate at the wave frequency; this term (together with hot ions) gives rise to a drift wave propagating in the ion diamagnetic drift direction.

At low growth rates, $\gamma \ll \omega_{ci}$, the ion term $\hat{k}_{\perp} \cdot \underline{\underline{\epsilon}}_{ion} \cdot \hat{k}_{\perp}$ gives rise to

Bernstein waves, which have negative energy (due to the ion loss cone) when $\omega/k_\perp \lesssim v_i$. Loss cone instabilities occur because these negative energy Bernstein waves can interact with positive energy waves, either a drift wave (in the case of DCLC), a Langmuir wave (in the case of ALC at low β) or a kinetic shear Alfven wave (in the case of ALC at high β). At higher growth rates, $\gamma \gg \omega_{ci}$, the ion cyclotron harmonics are no longer important, and the ions are effectively unmagnetized, as far as their response to the wave is concerned. In this regime, instead of considering the instabilities as due to interaction between a positive energy wave and a negative energy Bernstein wave, one may consider the instabilities as due to inverse ion Landau damping of a positive energy wave (a drift wave, a Langmuir wave, or a kinetic shear Alfven wave), which occurs when the ion distribution has a positive slope (due to the loss cone) at the phase velocity of the wave, $v_\perp = \omega/k_\perp$. In either regime, $\gamma > \omega_{ci}$ or $\gamma < \omega_{ci}$, loss cone instabilities can occur if $\omega/k_\perp \lesssim v_i$, and this requires $k_\perp \gg k_\parallel$; these modes propagate nearly perpendicular to the magnetic field. The DCLC mode, because it is a destabilized drift wave, propagates in the ion diamagnetic direction; the ALC mode may propagate in either the ion or electron diamagnetic direction. In infinite medium, the ALC mode is only convectively unstable, and is known as the convective loss cone (CLC) mode, but it becomes absolutely unstable when the finite length of the plasma is taken into account.

To estimate the conditions needed for stability of DCLC and ALC the straight-line orbit approximation (which is valid when $\gamma \gtrsim \omega_{ci}$) can be used for the ion term $\hat{k}_\perp \cdot \underline{\underline{\epsilon}} \cdot \hat{k}_\perp$ in Eq. (30). In this approximation, the ion term depends only on $F_{ion}(u)$, the one-dimensional ion velocity distribution in the $k_\perp$

direction. If $\partial F_{ion}/\partial u|_{u=\omega/k_\perp} > 0$, *i.e.*, if $\omega/k_\perp$ is in the loss cone, then the ion term has a positive imaginary part, and the mode is unstable. A mode will be stable if it has $\omega/k_\perp$ such that $\partial F_{ion}/\partial u|_{u=\omega/k_\perp} < 0$, either because $\omega/k_\perp$ is outside the loss cone, or because there is warm plasma of sufficient density partially filling the loss cone, with $v_{warm} \gtrsim \omega/k_\perp$ [Berk *et al.*, 1969; Gerver, 1976; Berk and Gerver, 1976].

Thus the instability may be viewed as analogous to a laser with the condition $\partial f_{ion}/\partial u > 0$ indicating an inverted population (a source of free energy). When a natural mode is present that is resonant with the unstable energy reservoir, that is, $\omega/k_\perp = u$, instability will occur. Alternately, if there are no normal modes that can resonate with the distribution function in the unstable region, or if the presence of warm plasma removes the free energy source, then the distribution function will be stable. (In the absence of warm plasma the instability will tend to diffuse "hot" ions down into the hole in $v_\perp$ space, and a marginally stable state, characterized by plasma turbulence, can result.)

Taking an ion perpendicular velocity distribution proportional to $v_\perp^2 \exp(-v_\perp^2/2v_i^2)$, the ion term in Eq. (30) becomes

$$\hat{k}_\perp \cdot \underline{\underline{\epsilon}} \cdot \hat{k}_\perp \simeq i\sqrt{\pi/2}\frac{\omega_{pi}^2\omega}{k_\perp^3 v_i^3} \tag{31}$$

Assuming $k_\perp \lambda_D \ll 1$, (certainly true for the most dangerous modes), the vacuum and electron polarization drift terms may be neglected in Eq. (30). For DCLC, the $k_\parallel^2$ term may be neglected. Then, in Eq. (30), the ∇n_e term must balance the ion term, which is given by Eq. (31). If the ion Larmor radius is small compared to the radial density gradient, it follows that the phase velocity

of the wave $\omega/k_\perp$ is much lower than the ion thermal velocity. This means that in order to stabilize DCLC it is only necessary to introduce a small amount of warm plasma at a low temperature, just enough to give the ion distribution function a negative slope ($\partial F_{ion}/\partial u < 0$) at $u \leq \omega/k_\perp$; it is not necessary to make $\partial F_{ion}/\partial u \leq 0$ at all u by filling in the entire loss cone with warm plasma.

In a real mirror cell when finite geometry is taken into account, the amplitude of the DCLC or ALC modes may vary with the axial position along the magnetic field lines. In order to stabilize these modes with warm plasma, the stability condition ($\partial F_{ion}/\partial u|_{u=\omega/k_\perp} < 0$) must be satisfied in some average sense along the field line, weighted according to the amplitude of the mode. The DCLC mode is usually fairly flute–like, (*i.e.*, its amplitude is nearly constant along field lines) for reasonably short plasmas and reasonably low β (the criterion for DCLC to be flute–like is roughly $L \lesssim \max[5R_p, 12\beta_i^{-1}R_p^{3/4}\rho_i^{1/4}]$, where ρ_i is the ion Larmor radius, R_p is the radial scale length, and L is the axial length). Thus, the DCLC mode can be stabilized even if the warm plasma is localized axially (in the inner half of the end cell, for example); all that matters is the average warm plasma density over the length of the mirror cell.

For ALC, and also for DCLC when it is not flute–like, the mode can localize axially away from the region where there is warm plasma. One way to stabilize these modes would be to have an unconfined stream of warm plasma pass through the entire length of the machine, as was done in the 2XIIB experiment [Coensgen *et al*, 1975], but this would not be tolerable in a reactor. Thus it is necessary in a tandem mirror reactor, and desirable in an experiment, to have L, the length over which there is no warm plasma, be sufficiently short that $\omega/k_\perp > v_i$ when

$k_{\|}L \gtrsim 1$. From Eq. (30), neglecting the ∇n_e term,

$$k_{\|}^2 \simeq \frac{\omega_{pi}^2}{c^2}\left(1+\frac{k_{\perp}^2 c^2}{\omega_{pe}^2}\right)\left(\frac{\omega}{k_{\perp}v_i}\right)^3. \tag{32}$$

If loss-cone modes are stable for $\omega/k_{\perp}v_i > 0.3$, and if $k_{\|}L > 1$ is the condition for a mode to be axially localized, then, from Eq. (32), unstable loss-cone modes will exist only if the region without warm plasma is longer than the critical length [Gerver, 1980],

$$\begin{aligned} L_c &\simeq \frac{6c}{\omega_{pi}}\left(1+\frac{k_{\perp}^2 c^2}{\omega_{pe}^2}\right)^{-1/2} \\ &= 6\beta_i^{-1/2}\rho_i\left(1+\frac{k_{\perp}^2\rho_i^2}{\beta_i}\frac{m_e}{m_i}\right)^{-1/2} \end{aligned} \tag{33}$$

For most tandem mirror experiments and reactor designs, the outer half of the outermost cell, where there is no confined warm plasma, has a length comparable to the critical length, L_c, given by Eq. (33). In order to determine whether such equilibria would be stable to loss cone modes, it is not enough to use the infinite medium expression for $k_{\|}$ and to make the crude approximation that modes will exist if $k_{\|}L > 1$. Instead, it is necessary to solve an axial eigenmode equation [Gerver, 1980], *viz.*, Eq. (30) with the $k_{\|}^2$ term replaced by a second-order-differential operator, subject to appropriate boundary conditions (usually outgoing waves at the mirror throat), and to see if there are any eigenmodes with $Im\omega > 0$. In general, $k_{\perp}$ will vary with axial position due to the axial dependence of magnetic field strength and the fanning of field lines.

In the eigenmode equation the ion term $(\hat{k}_\perp \cdot \underline{\epsilon} \cdot \hat{k}_\perp)$ is an integral operator, since it depends on the perturbed electric field experienced by ions throughout their orbits back and forth along the magnetic field. However, since the ion bounce frequency is always small compared to ω_{ci} (otherwise the ions would not be adiabatic), the infinite medium expression is always valid if the straight-line orbit approximation is valid ($Im\omega \gtrsim \omega_{ci}$). In this case, the critical length for stability determined by finding the axial eigenmodes tends to be fairly close (within a factor of 2) to the estimate given by Eq. (33), with some minor dependence on the details of the equilibrium. If the ion cyclotron harmonics are kept, then the usual infinite medium expression involving sums of Bessel functions [Krall, 1968; Mikhailovskii, 1967a] can still be used except close to the cyclotron harmonic resonance points, *i.e.*, close to those values of z for which $\omega = n\omega_{ci}(z)$. At these points the ion term is not singular, as it would be in infinite medium; there is a finite resonance width due to the fact that the ion cyclotron motion gets out of phase with the wave as the ion moves into a region with a different ω_{ci} [Pearlstein, Smith and Nevins, 1980]. This resonance width is roughly

$$\Delta_n = \left[0.5nv_\parallel \left|\frac{d\omega_{ci}}{dz}\right| + \left(0.022nv_\parallel^2 \left|\frac{d^2\omega_{ci}}{dz^2}\right|\right)^{2/3}\right]^{1/2}. \tag{34}$$

If $\Delta_n \gtrsim |\omega - n\omega_{ci}(z)|$ over much of the orbit of a typical ion, then the ion term $\hat{k}_\perp \cdot \underline{\epsilon}_{ion} \cdot \hat{k}_\perp$ must be treated as an integral operator. If $\Delta_n \ll |\omega - n\omega_{ci}(z)|$ almost everywhere, then the ion term just depends on the local $\phi(z)$ and is given by the usual infinite medium expression, but with the resonant denominators $(\omega - n\omega_{ci})^{-1}$ replaced by resonance functions of width Δ_n, whose exact shape

depends on the ion distribution function and on $B(z)$.

If ω is close to, but slightly less than $n\omega_{ci}$ at the midplane, then $\omega(\partial/\partial\omega)(\hat{k}_\perp \cdot \underline{\epsilon}_{ion} \cdot \hat{k}_\perp) < 0$ if ω/k is inside the loss cone, and in infinite medium there would be a stable wave with negative energy. When the eigenmode equation is solved with outgoing wave boundary conditions, an unstable mode is found, since the outgoing waves at the mirror throats (which are positive energy Langmuir waves) provide positive dissipation of the negative energy wave at the midplane [Berk, Pearlstein and Cordey, 1972]. This negative energy wave can also be driven unstable by any other form of positive dissipation, *e.g.*, damping by warm ions near the inner mirror throat, or electron Landau damping, or some nonlinear damping process. The negative energy wave instability is stabilized if there is enough warm plasma at the midplane. Also, if the parallel ion temperature is great enough, then the resonance width Δ_n becomes large [see Eq. (34)], and negative dissipation (due to resonant interaction with ions in the loss cone) will stabilize the negative energy wave.

When the ion cyclotron harmonics are included, numerical studies [Pearlstein, 1982; Gerver, 1983] show that the critical length is more sensitive to the details of the equilibrium and tends to be somewhat shorter than the critical length given by Eq. (33). These studies show that there is a minor improvement in loss cone stability w' en sloshing ions are used, because the distance over which there are no axially confined warm ions is shorter. However, complete stability to loss cone modes is much easier to achieve (for reasonable β_i and L) when there are at least a few percent of warm ions at almost all axial positions, due either to an unconfined stream or to a negative potential near the outer mirror throat.

The dispersion relations discussed so far are valid only for cold electrons, that is, for $\omega/k_{\|} \gg v_e$ and $\beta_e \ll 1$. These assumptions are only moderately good for advanced tandem mirrors which make use of ECRH. If $\omega/k_{\|} \lesssim v_e$ but $\omega \gg \omega_{be}$, where ω_{be} is the electron bounce frequency (this implies $k_{\|}L \gg 1$), then the $k_{\|}^2$ term in Eq. (30) must be replaced by a term calculated from the Vlasov equation, which has an imaginary part associated with electron Landau damping. Electron Landau damping can only be important at rather low β_i or high $k_{\perp}\rho_i$ (*viz.* $\beta_i \lesssim (m_e/m_i)k_{\perp}^2\rho_i^2$, which means $\omega_{pe}/k_{\perp}^2c^2 \lesssim 1$), otherwise the $k_{\|}^2$ term reduces to $k_{\|}^2c^2/\omega^2$ independent of $\omega/k_{\|}v_e$.

At high β_e, another process, electron damping due to transit time magnetic pumping (TTMP), can occur when $\omega \simeq k_{\|}v_e$ [Stix, 1962]. This process is similar to electron Landau damping, but the force on the resonant electrons is $\mu dB_z/dz$ instead of eE_z. If also, $\omega \lesssim \omega_{be}$, then integral operators, involving integrals over the bounce orbits of the electrons, occur and this makes it much more difficult to find the axial eigenmodes. Numerical solutions have not been done in this case.

At the high β_e necessary for TTMP to be important, the electron thermal velocity is usually much greater than $\omega/k_{\|}$, so very little damping occurs. For these hot ECRH electrons, however, damping may also occur by electrons whose ∇B–drift frequency $\mathbf{k}_{\perp}\cdot\mathbf{v}_d$ is resonant with the wave [Davidson *et al.*, 1977]. This resonance may lead to either damping or growth, depending on the signs of $\mathbf{k}_{\perp}\cdot\mathbf{v}_v/\omega$ and $\partial f_e/\partial v_{\perp}^2$. Recent numerical solutions of the axial eigenmode equation for ion loss-cone instabilities in MFTF-B, including the ∇B–drift resonance, have shown that in practice ∇B–drift damping is not very important [Pearlstein,

1982].

Another mechanism that may sometimes affect ion loss-cone instabilities is a damping or growth caused by the ponderomotive force of Langmuir waves whose group velocity perpendicular to the magnetic field is resonant with $\omega/k_\perp$ of the ion loss cone mode [Avinash and Varma, 1983]. Either this process or electron Landau damping could account for the stabilizing effect on DCLC of an axially-injected electron beam (which excited Langmuir waves) in the Constance single-cell mirror experiment [Klinkowstein, 1978], and it may be applicable to tandem mirrors as well if a great enough energy density of Langmuir waves can be excited.

Nonlinear couplings of loss cone instabilities do not always increase stability, but under some conditions can be strongly nonlinearly destabilizing, particularly if they couple to lower frequency modes [Aamodt *et al.*, 1979a; Rosenbluth, Coppi and Sudan, 1969]. There is experimental evidence in the OGRA of low frequency MHD-like modes. Axial confinement properties were dramatically degraded only when both the high and low frequency waves were allowed to coexist.

The stability of a given equilibrium to loss-cone modes does not really depend on whether unstable axial eigenmodes exist locally at each field-line at each value of $\mathbf{k}_\perp$, but rather on whether any unstable three-dimensional eigenmodes exist. A locally-unstable axial eigenmode may be stabilized (or destabilized if it has negative energy) by wave energy convecting away radially. Also, the corrections of order $(k_\perp R_p)^{-1}$ to the wave frequency (where R_p is the radial scale size of the plasma), due to mode structure perpendicular to the magnetic field, may change the stability of locally-defined axial eigenmodes. If

WKB is valid ($k_\perp R_p \gg 1$), then the three-dimensional normal modes can be found by ray-tracing of local axial eigenmodes from one field line to another, radially and azimuthally; a modified ray-tracing method, valid for complex group velocities, must be used [Gerver, 1983]. Although the perpendicular mode structure is not expected to change conclusions about the requirements for stabilizing loss-cone modes qualitatively, it will probably have to be taken into account if detailed stability thresholds are to be found for a particular experiment.

(2) Alfven Ion Cyclotron Instability

For $\omega/k_\perp > v_i$, instabilities cannot be driven by the ion loss cone, but at still greater perpendicular phase velocities, $\omega/k_\perp > v_A$, the ion response is no longer electrostatic, and there is an instability (the Alfven ion cyclotron, or AIC, instability) driven unstable by the ion anisotropy [Cordey and Hastie, 1972; Davidson and Ogden, 1975]. The AIC mode is most simply considered for $k_\perp = 0$. In this case there is no mixing between left circularly-polarized transverse modes, right circularly-polarized transverse modes, and longitudinal modes. The AIC mode is on the left circularly-polarized branch (*i.e.*, the wave electric field rotates in the same direction as the ions orbit around field lines), which has the dispersion relation

$$1 - \frac{k_\parallel^2 c^2}{\omega^2} + \epsilon_{LL} = 0, \tag{36}$$

where ϵ_{LL} is the left-left component of the dielectric tensor.

For $\omega \ll \omega_{ce}$ and $k_{\|} v_e \ll \omega_{ce}$, the electron term of ϵ_{LL} is $\omega_{pe}^2/\omega\omega_{ce}$. The vacuum term may be neglected if $\omega_{pi} \gg \omega_{ci}$. In the limit $T_{\|} \to 0$, Eq. (36) becomes

$$\frac{-k_{\|}^2 c^2}{\omega^2} + \frac{\omega_{pe}^2}{\omega\omega_{ce}} + \frac{\omega_{pi}^2}{\omega(\omega_{ci} - \omega)} - \frac{1}{2}\beta_{i\perp}\frac{k_{\|}^2 c^2 \omega_{ci}^2}{\omega^2(\omega - \omega_{ci})^2} = 0, \qquad (37)$$

where use has been made of $\beta_{i\perp} \equiv \omega_{pi}^2 v_{i\perp}^2/\omega_{ci}^2$. If $\beta_{i\perp} = 0$, Eq. (37) is the usual dispersion relation for shear Alfven waves and ion cyclotron waves. When finite $\beta_{i\perp}$ is included, Eq. (37) is a cubic equation in ω, which has an unstable root when $k_{\|}^2 c^2/\omega_{pi}^2$ is greater than some critical value which goes down with increasing $\beta_{i\perp}$, and has a maximum growth rate of $(\beta_{i\perp}/2)^{1/2}\omega_{ci}$ at $k_{\|}^2 c^2/\omega_{pi}^2 \gg 1$ and $Re\omega \simeq \omega_{ci}$. When the ion distribution is bimaxwellian, with $T_{\|}$ finite but much less than $T_{i\perp}$, then the mode becomes stable at $k_{\|}^2 c^2/\omega_{pi}^2 > T_{i\perp}/T_{i\|}$, with the maximum growth rate occurring at $k_{\|}^2 c^2/\omega_{pi}^2 \sim 1$ and $Re\omega$ somewhat less than ω_{ci}; the mode is unstable to all $k_{\|}^2 c^2/\omega_{pi}^2 < T_{i\perp}/T_{i\|}$, but with exponentially small growth rate when $k_{\|} c/\omega_{pi} \ll 1$. When $\beta_{i\perp}$ is small, or $T_{\|}$ is nearly equal to $T_{\perp}$, then the maximum growth rate is not harmful to plasma confinement.

In an infinite medium, the AIC mode is only convectively unstable, and a crude estimate can be made of when it is likely to be harmful by requiring than the convective growth rate be greater than about $10v_g/L$, where v_g is the group velocity along the magnetic field and L is the plasma length. A more accurate determination of the stability criteria may be made by solving the axial eigenmode problem in a finite length equilibrium. Numerical studies of the AIC axial eigenmodes show that when the length is short enough the AIC mode is completely stable [Watson, 1980]. Critical lengths are typically several ion

Larmor radii for moderate $\beta_{i\perp}$ and $T_{\|}/T_{\perp}$. Since the ion bounce frequency is comparable to the wave frequency for these short lengths, the dispersion relation involves sums over the ion bounce frequency harmonics; this generally does not cause major changes in the stability thresholds. These finite length effects probably explain why the AIC instability was not observed in the 2XIIB experiment (where it might have been expected from infinite medium theory), but was seen in TMX, which has smaller $T_{\|}/T_{\perp}$ [Casper and Smith, 1982].

Finite plasma radius also has a stabilizing effect on the AIC mode, due to the effect of finite $k_{\perp}c/\omega_{pi} \gtrsim 1$. So far, the effect of finite plasma radius has only been estimated by making assumptions such as $k_{\perp} = 1/2R_p^{-1}$, and treating the plasma as an infinite medium in the radial direction. It would be of interest to find the radial eigenmodes for a particular radial plasma profile.

In more advanced tandem mirror designs, sloshing ions are used (*i.e.*, ions whose distribution functions peak at an angle less than 90° to the magnetic field), and the ion distribution is no longer well described as a bimaxwellian. Studies of AIC with a sloshing ion distribution [Smith, 1983] show that it is substantially more stable than with a bimaxwellian, especially if $T_{\|}$ (defined here as the width of each peak of the ion distribution, not as $\langle v_{\|}^2 \rangle$) is not too small. These theoretical studies have been in agreement with observations of the AIC mode in the TMX-U experiment [Casper and Smith, 1983].

On the other hand, with sloshing ions, finite $k_{\perp}$ can be destabilizing, leading to an instability, similar to AIC, which depends not on the anisotropy but on the two-peaked nature of the ion distribution [Foote and Kulsrud, 1981]. This instability, called the electromagnetic two-stream instability, will put limits on

the depth of the midplane density dip which can be obtained by sloshing ions at a given β.

(3) Drift Instabilities

Even when the ion distribution function is locally maxwellian, instabilities can still be driven by the free energy associated with the radial density and temperature gradients. These drift instabilities generally have lower growth rates than the velocity space instabilities discussed previously, but when loss cone and anisotropy driven modes are stable, drift waves can be the most important instabilities remaining. The nonlinear effect of drift waves is to cause enhanced radial transport, rather than enhanced end losses; although enhanced end losses are usually of greater concern, enhanced radial transport can also severely degrade performance if the plasma is not too many ion Larmor radii across. Other constraints (including requirements for avoiding velocity space instabilities) may require plasmas that are only a few ion Larmor radii across, so drift instabilities could be of importance in the central cell as well as in the end cells.

Drift instabilities are of two general types: (1) high frequency drift waves, with $\omega \gtrsim \omega_{ci}$, $k_\perp \rho_i \gg 1$, and $k_\parallel v_e \lesssim \omega$, propagating in the ion diamagnetic direction, and (2) low frequency drift waves, with $\omega \ll \omega_{ci}$, $k_\perp \rho_i \lesssim 1$, and $k_\parallel v_e \gtrsim \omega$, propagating in the electron diamagnetic direction. The high frequency drift waves, which have real frequency $\omega \simeq \omega_{*i} \equiv k_\perp v_i \rho_i \nabla n_e / n_e$, include the drift cyclotron instability [Mikhailovskii and Timofeev, 1963] at the ion cyclotron

frequency and its harmonics, and the lower hybrid drift instability [Davidson *et al.*, 1977], which occurs at frequencies well above the ion cyclotron frequency (up to about $\omega_{\ell h}\rho_i\nabla n_e/n_e$) at very short perpendicular wave lengths (up to $k_\perp\rho_i \simeq (m_i/m_e)^{1/2}$). Although these modes, which are driven by the ion density gradient, can have very high growth rates (comparable to the growth rates of velocity space instabilities in some cases) there are some stabilizing effects. The high frequency drift waves are stable for weak density gradients, $\rho_i/R_p \lesssim (m_e/m_i)^{1/2}$, where R_p is the radial scale length; this condition is usually satisfied in the central cell, although it generally cannot be satisfied in the end cells. The drift cyclotron instability can be stabilized by field line curvature when it is in the good direction (minimum B) [Bhadra, 1967; Krall and Fowler, 1967] or by ∇B when the equilibrium is $P(B)$ (with no explicit dependence on the flux surface ψ), as short fat plasmas tend to be [Pearlstein, 1978]. The lower hybrid drift instability is stabilized by electron convection along the field lines and tends to be stable in both the short plasmas in past mirror experiments and the fat plasmas envisioned in later devices [Aamodt, *et al.*, 1979b; Catto *et al.*, 1980; Pearlstein, 1978]. By contrast, the long thin plasmas of theta pinches tend to be unstable to the lower hybrid drift instability.

The low frequency drift waves [Kadomtsev, 1965; Mikhailovskii, 1971; Krall, 1968] include the universal drift instability [Kadomstev and Timofeev, 1962] and the drift Alfven instability. These modes, unlike the high frequency drift waves, can be driven unstable by arbitrarily small density gradients (the historical reason for the name "universal instability"), and are thus of concern in the central cell. The universal drift instability has real frequency $\omega \simeq \omega_{*_e} \equiv$

$k_\perp v_i \rho_i (T_e/T_i) \nabla n_i/n_i$, and is driven unstable by the electron density gradient, with a maximum growth rate of $\gamma \simeq (v_i/R_p)(T_e/T_i)$ (comparable to the real frequency) at $k_\perp \rho_i \simeq 1$. At finite β ($> m_e/m_i$), the Alfven speed v_A is less than the electron thermal velocity v_e, and the shear Alfven wave, with real frequency $\omega = k_\parallel v_A < k_\parallel v_e$ is also driven unstable by the presence of an electron density and temperature gradient; this is the drift Alfven instability. Low frequency drift waves can be stabilized by forcing them into a regime where they are ion Landau damped ($k_\parallel \gtrsim v_i/\omega$). This can be done either by finite length (so that $k_\parallel$ cannot be less than v_i/ω) or by shear (which makes $k_\parallel$ vary across the field, so that on some flux surface $k_\parallel \gtrsim v_i/\omega$) [Pearlstein and Berk, 1969]. However, neither of these stabilization mechanisms (which are important in toroidal devices) may apply in the long straight central cell of a tandem mirror, and it may be necessary to live with a certain amount of enhanced radial transport in the central cell. Numerical studies of the axial eigenmodes of both the universal drift mode and drift Alfven mode at finite β_i have been done by Hastings, 1980 and by Horton 1981, who also derives expressions for the enhanced radial transport.

III.E.2 Electron Microinstabilities

The specific role or possible performance limitations that high frequency electron instabilities ($\omega \simeq \omega_{ce}$) will induce in a tandem mirror device is a very complicated question. While there is a multitude of experimental evidence [Ard *et al.*, 1966; Ikegami *et al.*, 1968; Perkins, 1968; Blanken and Lazar, 1970; Porkolab *et al.*, 1971; Schwartz and Lichtenberg, 1972] with supporting theoretical explanations of the presence of such waves in hot electron mirror systems, a quantitative understanding of the nonlinear effects of these waves in the context of a tandem configuration is yet to be obtained. The reason is that the stability picture itself is a many-dimensional figure, strongly subject to explicit parameter ranges of densities, temperatures, anisotropies and loss cone sizes, and that the quantitative limits of these ranges and resulting instability growth lengths are extremely sensitive to the assumed electron velocity distribution shapes, including their relativistic nature. Consider these facts in the context of an ECRH-generated thermal barrier, for example, where one expects as many as three coexisting species of electrons, cold, warm, and hot, each having an axially-local distribution function determined in part by the nonlocal effects of the wave-guide-driven electron cyclotron waves, the self-consistent ambipolar potential, and the β_e corrected magnetic field. Typically, in a tandem, while axial variations of these "equilibrium" quantities can be small in a distance of an electron microinstability wavelength, there are important instances where the final convective or absolute nature of an initially-localized disturbance is in fact determined in an axially-localized region where there are rapid magnetic field

strength changes.

Because of this complicated scenario for electron microinstabilities, in this monograph only a simple overview of the problem is presented with details to be found in the quoted references and the rapidly evolving literature with specific applications to tandems.

The class of basic electrostatic waves associated with these electron instabilities are the electron plasma, upper hybrid, and "Bernstein" modes. The transverse or electromagnetic fluctuations are in the nature of whistler or electromagnetic Bernstein modes. The specific modes of concern are listed in Table III.E.1.

Table III.E.1

Mode	Type	Alternate Name	Drive
Upper hybrid loss cone	Electrostatic	Two component double–humped distribution	Loss Cone
Whistler	Electromagnetic	Electron–cyclotron	Anisotropy beta
Harris	Electrostatic	Timofeev	Anisotropy
Electron–cyclotron maser	Electromagnetic	Relativistic	Relativistic bunching mechanism with an inverted distribution

The electron free energies which, in restricted parameter regimes, can drive these modes unstable are: inverted populations, including loss–cone induced and velocity–space driven, double–humped distributions; and temperature anisotropies ($T_{\|} \neq T_{\perp}$) which naturally occur in ECRH–driven systems where $T_{\perp} > T_{\|}$.

These free energy sources can be found in various tandem scenarios including: the all-important thermal barrier region of the standard positive potential tandem; the critical longitudinal confinement driving element of a negative potential tandem; the plug region of electron ring MHD-stabilized symmetric tandems; and the hot β_e (instead of β_i) weighted quadrupole MHD-stabilizing plug regions in ECRH-driven plugs (instead of the usual neutral-beam-driven plugs). These axial regions have considerable potential for exciting electron microinstabilities and this latent potential itself is radically different for a final steady-state tandem scenario where substantial fractions of hot electrons exist as opposed to a startup configuration where the plasma is primarily cold. Each regime must be studied separately.

Characteristically, for ECRH hot electron plasmas $\omega_{pe}^2 \sim \omega_{ce}^2$, and in this regime the electron microinstability wave vectors typically satisfy the order-of-magnitude estimates $k_\parallel c/\omega_{ce} \lesssim 1$, $k_\perp \rho_e \lesssim 1$, and have frequency $\omega \sim \omega_{ce}$. Because these fluctuation spatial scales are typically of the order of centimeters as opposed to the meter scale lengths of the macroscopic plasma in a tandem, stability methods and nonlinear self-modifications of unstable situations usually must rely on local distribution function modifications. However, in the instances of weakly unstable convective waves or in regions of sharp magnetic field gradients, there is the possibility that macroscopic lengths might be chosen so as to minimize the growth of fluctuations. To date all stability calculations for tandem devices have assumed infinite medium wave characteristics or at most simplified local WKB models.

The velocity space free energy source for the electron modes originates from

a combination of the ECRH drive and loss cone containment characteristics. As such, most of the instability calculations applied to tandems have proceeded by modeling electron equilibrium distributions with bimaxwellians, with different perpendicular and parallel temperatures, and when included, loss cone voids by polynomials in perpendicular energies multiplying the maxwellians. For these distributions using nonrelativistic dynamics, maximum growth rates of the order $\gamma \lesssim 10^{-1}\omega_{ce}$ have been calculated. However, the magnitude of the growth factor has been shown to be very sensitive to functional shapes and, in particular using distribution functions from Fokker-Planck solutions of models of the ECRH-supported system [Stallard *et al.*, 1983], have obtained reduced growth rates [Casper *et al.*, 1983; Chen *et al.*, 1982]. Retaining relativistic features can substantially modify these results when $k_{\|}c/\omega \lesssim 1$. For such waves and particularly when $\omega > \omega_{ce}$ and in loss cone systems, the relativistic modification of the resonant electron velocity surface in $v_{\|}$-$v_{\perp}$ space is so large [Wu and Lee, 1979; Hewitt, 1982] even for low energies, that maser-like growth mechanisms are greatly enhanced [Hewitt *et al.*, 1982]. In fact just this relativistic modification of the maser action is believed responsible for the observed planetary, solar and stellar radio emissions [Wu and Lee, 1979; Hewitt *et al.*, 1982; Wu *et al.*, 1982; Melrose *et al.*, 1982]. This same low energy modification of the resonant electron surface can also explain the observed [Gladd, 1983] relativistic reduction in whistler growth rates for velocity space anisotropic non-loss-cone plasmas and drives the fast waves ($\omega/k_{\|} > c$) unstable in loss cone systems [Lau and Chu, 1983; Tsang, 1983]. In any case, within the limits of the present simplified analyses the hot electron populations envisaged for thermal barriers on regular tandems or negatively operating tandems are susceptible to substantial growth

of electron microstabilities [Gladd, 1983; Lau and Chu, 1983; Porkolab, 1983; Guest and Sigmar, 1971; Tsang, 1982 and 1983].

In some tandem parameter regimes with modeled electron equilibrium distribution functions the local, or infinite media calculations have found growth rates in substantial excess of the electron axial bounce frequency in the combined magnetic and ambipolar traps. If indeed such an "equilibrium" is allowed to be created then this local theory analysis is certainly applicable and one could expect substantial nonlinear modifications of the system, e.g., electron loss cone filling or isotropization, and a concomitant degradation of local parameters such as the local ambipolar dip. However, the hot electron component in ECRH plasmas is generated only over many bounce cycles and one might expect that steady state distribution functions close to marginal stability are more likely to occur. In this instance nonlocal stability analyses including electron bounce motion must be used. This is tractable only in special circumstances and at this time there is not a consensus on the relevant new physics issues.

This electron scenario appears at first sight to be similar to the steady-state neutral-beam-driven ion loss cone microinstability picture in mirrors, wherein marginally-stable ion distributions are apparently slowly generated and the plasmas are quiescent except for periods of intense rf activity and associated rapid ion losses. However, under further scrutiny this similarity becomes somewhat artificial because the effect of electron bounce motion on electron microinstabilities is not totally understood especially including the all-important fact that the ion cyclotron modes tend to be flute-like while electron wavelengths are typically 10^{-2} to 10^{-3} of the bounce length. Additionally, different particle species cou-

plings, both nonlinear and linear, are different for the two classes of modes. Nonetheless, the argument for near-marginal stability generation is an appealing one; the questions are: are there such "marginally stable" distributions; if so, what local ambipolar confinement characteristics do they allow; and can the periods of intense oscillations be eliminated or controlled?

Finally, there is some concern over the nonlinear scattering effects of inherent electron waves. In particular there is the possibility of these fluctuations resonantly wave-wave scattering or nonlinear Landau damping with themselves or the ambient ECRH waves and thereby coupling directly to the ions causing increased ion velocity space diffusion. Such a possibility leads directly to a reduction in the bare Q factor for a tandem and thereby is cause for some concern. Since the calculations including realistic models of a tandem are difficult and strongly subject to inappropriate approximations, no good quantitative estimates of this effect have been completed. Therefore, the real significance of electron microinstabilities must await further linear and nonlinear analyses and a definitive ECRH-supported tandem data base.

III.F Power And Particle Balance

III.F.1 Classical Tandem Mirrors

In its simplest form the classical tandem mirror is driven by injecting energetic neutral beams into minimum $|B|$ end plugs which bound the solenoidal central cell. The neutral beams are the sole power source for the configuration and, in addition, provide a particle source for the hot-ion, high-density end plugs. Power input into the lower density, central cell plasma is obtained via the electrons. The plug electrons are heated by collisional drag on the plug hot ions and, in the absence of a thermal barrier, this power is convected quickly to the central cell electrons. The central cell plasma is fueled from ionization of cold neutral gas, and the resulting cold ions tend to thermalize with the warmer central cell electrons. Thus it would be expected that

$$E_i \gg T_e > T_{ic}, \tag{39}$$

with E_i the plug ion mean energy and T_e, T_{ic} the central cell electron and ion temperatures respectively. In practice, a direct coupling between hot plug ions and central cell ions has been observed (in TMX) which can heat central cell ions so that $T_{ic} \gtrsim T_e$. The particle and power flow in a classical tandem mirror is illustrated schematically in Fig. III.F.1.

The power balance is illustrated by reference to the TMX experiment [Simonen *et al.*, 1981]. The hot ion density in the plug is sustained by ionization and charge exchange of the neutral beams on the core plasma. Ionization events provide both a particle and power source, and charge exchange events are a power drain

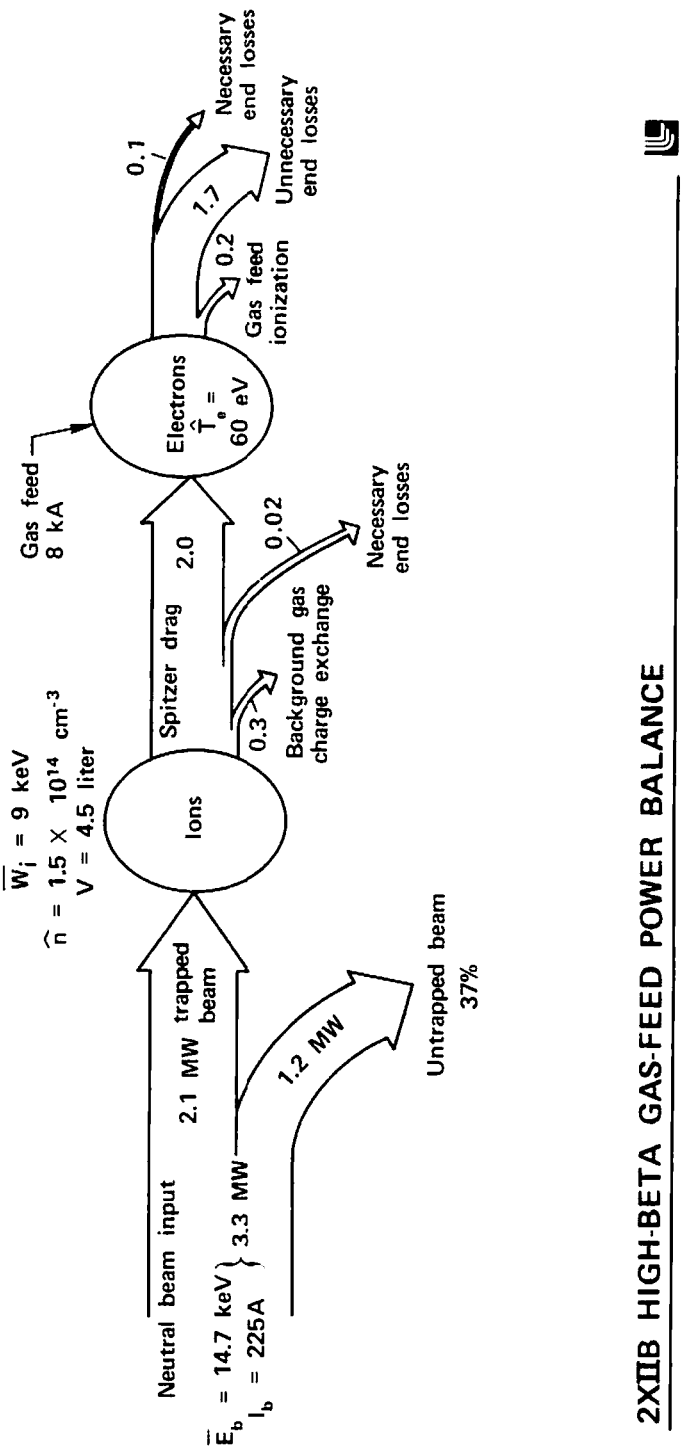

Figure III.F.1 Measurements and calculations used to determine power flow of the 2XIIB mirror plasma. Illustration courtesy of Lawrence Livermore National Laboratory.

or source dependent upon the mean hot ion energy relative to the energy of the injected neutrals. Since the charge exchange rate for typical injection energies is a few times the ionization rate, the mean ion energy tends to approximate the average neutral injection energy. In the TMX experiment, typically 150 A with a mean energy of 10 keV was injected into each end plug corresponding to a total input power of 3 MW. Approximately 5% of the incident flux of neutrals were trapped by impact ionization on the target plasma and 20% of the incident flux was ionized by charge exchange. Most of the injected power, typically 100 kW per plug, was coupled to the electrons by collisional drag. The remaining power loss mechanisms in the plug, in the order of importance, were charge exchange on cold neutral gas, rf fluctuations, and axial particle loss which accounted for only approximately 10 kW out of the total 3 MW incident. The presence of a cold gas blanket surrounding the hotter core is thought to play an important role in limiting neutral gas penetration and thus limiting the associated charge–exchange power loss.

Nearly all of the input power to the plug electrons is convected to the central cell electrons. The primary power loss mechanism for the central cell electrons is axial confinement loss. TMX electron temperatures were obtained in the range of 50 to 200 eV. Ionization loss and impurity radiation accounted for approximately one third of the central cell electron loss, and only 5 kW out of 200 were attributed to ion drag. To balance the axial loss from the central cell, the plasma is replenished via ionization of cold neutral gas. On TMX, the central cell cold gas current was varied from 300 to 3000 equivalent amperes. End loss appeared not to be ambipolar with a net electron current near the axis and

ion current at large radius. This result is interpreted as indicative of resonant transport.

In the absence of plug instability, the central cell ions are heated via drag on the warmer central cell electrons. Since these ions are electrostatically confined, any power input to the ions will elevate the ion temperature and reduce ion confinement. The additional loss of ions boiling out of the potential well balances the power input. The end plugs of TMX, however, were believed to exhibit the Alfven ion cyclotron instability [Smith *et al.*, 1983], and as the plug to central cell density ratio was increased, ion cyclotron fluctuations became the dominant heating mechanism for the central cell ions. The fluctuations degraded central cell confinement such that the end loss stream was sufficient to reduce the anisotropy of the plug hot ion distribution function providing a marginally stable state. In TMX, the neutral beams were injected perpendicular to the magnetic field. On TMX-U, and other mirror machines, sloshing ions are planned for the end plugs. The sloshing ions provide a distribution that is less susceptible to microinstability. A second important loss mechanism for central cell ions is radial transport. The central cell of a tandem is not axisymmetric due to the mapping of a solenoidal flux tube into the minimum-|B| end plugs and this can lead to radial transport. On the outer field lines in the TMX experiment, ions were preferentially lost radially with electrons leaving the machine axially. The total volumetric fractional loss of ions was approximately half in the radial direction. In TMX-U, ion radial loss is an important factor in the central cell power balance, and the new axisymmetric tandem mirror is designed to avoid the excessive radial loss predicted in scaling to a reactor.

An alternative to the neutral-beam-sustained tandem is the use of ion cyclotron resonance frequency (ICRF) heating in the end plugs [Kesner, 1978]. This has been demonstrated on the Phaedrus tandem mirror as described in Sec. V.C. Unlike neutral beams, rf is normally a power but not a particle source. However, since rf will diffuse particles in velocity space, it can move central cell trapped ions into the plug-trapped region of velocity space.

The trapping process can occur in two ways. When central cell ions pass through the region of resonance with the wave (located in the plug) they will become trapped if they receive a large enough single-pass acceleration. Recall that ion confinement in the plugs requires that $E_\perp > \phi_p/(R-1)$ with ϕ_p the potential drop from the plug midplane to the magnetic field maximum. This is the process that is believed to be operative in Phaedrus [Breun *et al.*, 1979]. Since typically $\phi_p \sim 5$ Te, this fueling scheme is severely limited at high electron temperatures. With single-pass trapping the rf resonance can be located on either side of the plug midplane.

A second rf-fueling scheme would involve an rf-driven diffusion of central cell trapped ions [Kesner, 1979]. In this scenario the rf-resonance zone would be located between the inner mirror peak and plug midplane. Rf would first drive ions into the Yushmanov region where they are trapped between the inner mirror peak and midplane potential maximum and finally into the magnetically-trapped region.

For rf-sustained plug operation the power and particle sources are intimately related. Recent Monte-Carlo studies [Todd, 1982] have provided detailed modeling of the process. These calculations generally agree with Phaedrus results and

corroborate the assertion that ICRF–sustained operation does not extrapolate well to reactor conditions although it may figure importantly in start–up.

III.G Role Of Neutral Beams in Tandem Mirrors

Neutral beams play a key role in mirror experimental physics in that they provide a means of maintaining a hot ion mirror plasma. In conventional mirror cells, *i.e.*, single mirror cells or the end plugs of tandem mirrors, the ions are magnetically confined and neutral beams supply both the particle and the power source. This is in contrast with the tandem mirror central cell (in which confinement is electrostatic) or with toroidal devices in which neutral beams function primarily as a power source. The requirement that injected ions have high energy follows from the tendency of mirror cells to develop a positive potential, ejecting low energy ions. This eliminates the possibility of fueling mirror plugs by gas puffing or pellets. Under limited circumstances ICRF has been seen to fuel tandem mirror plugs (Sec. IV.F), but this method of fueling is limited by the requirement that the ion cyclotron wave must heat untrapped ions to sufficient energy for confinement in one traversal of the rf resonance region.

In present day neutral beam sources ions are produced in a low field plasma source, accelerated through a grid structure up to a high energy and then passed through a neutralizer cell where the energetic ions are neutralized by charge exchange on a background gas. The resulting "currents" of neutrals are then directed into the plasma region. The current density of neutral beams is limited by space–charge effects in the acceleration grid structure to values of $\lesssim 0.5$ A/cm^2. The dominant neutral species emerging from the system is atomic hydrogen (H) or deuterium (D), although significant fractions of H_2 (D_2) and H_3 (D_3) molecules are also produced in present day sources. Neutral beam systems have been developed which can produce beams of up to 120 keV energy.

Upon entering the plasma the neutral particles ionize by both impact ionization (primarily on electrons) and by charge exchange. The diatomic and triatomic molecules break apart to produce half and one-third energy components. At moderate energy (less than 50 keV for hydrogen) charge exchange provides the dominant ionization process, whereas above 100 keV the charge exchange cross section diminishes rapidly. These cross sections are proportional to the relative velocities of the colliding particles and thus the charge exchange cross section for hydrogen at a given energy is comparable to that of deuterium at the square-root of the mass ratio ($\sqrt{2}$) higher energy.

Ion fueling results from impact ionization of the beam neutrals in the target plasma. Charge exchange will replace an existing ion with an ion at the beam energy and pitch angle and strictly speaking is not a fueling source. However, charge exchange on a cold ion will replace the cold ion by a hot one, effectively acting as an additional fueling source.

Neutral beam buildup has been shown to occur most efficiently for a dense plasma target. The target serves several functions: it provides a scattering source for impact ionization of the energetic beam neutrals as well as for charge exchange on the cold target ions. Furthermore, it will shield the hot plasma from cold neutral gas which would otherwise charge exchange away the hot ions.

Plasma buildup follows an approximate relationship

$$\frac{dn_h}{dt} = \left[(\langle\sigma v\rangle_i + \langle\sigma v\rangle_{cx})\frac{n_t L_e}{V_b}\frac{I_b}{ev_b}\right] + \langle\sigma v\rangle_i \frac{n_h L_e}{V_b}\frac{I_b}{ev_b}$$

$$- \frac{n_h^2}{\langle n\tau\rangle} - n_h[n_0^{H_2}\langle\sigma v\rangle_{cx}^{H_2} + n_0^H\langle\sigma v\rangle_{cx}^H], \qquad (40)$$

with n_h and n_t, the hot and target densities respectively; $\langle\sigma v\rangle_i$ and $\langle\sigma v\rangle_{cx}$, the maxwellian averaged ionization and charge–exchange cross sections; I_b, v_b, the beam current and velocity; L_e, the effective axial extent of the ionized particle trajectory; V_b, the volume through which the beam penetrates within the plasma; $\langle n\tau\rangle$, the hot ion confinement parameter; and n_0, the local neutral gas density, made up of atomic and diatomic hydrogen. Notice that the ionization source due to the cold target is independent of the hot ion density. On the other hand, both the ionization source on hot ions and the neutral gas charge–exchange loss terms are linearly proportional to the hot ion density. Therefore, the hot plasma will build up to a level dictated by the cold target density, and buildup beyond this level is determined by the linear terms and requires a sufficiently low cold gas density that the ionization source outweighs the neutral gas charge exchange loss term. Thus it is required that

$$n_0 < \frac{I_b L_e}{eV_b v_b}\left[\langle\sigma v\rangle_i / \left(\langle\sigma v\rangle_{cx}^H + \frac{n_0^{H_2}}{n_0^H}\langle\sigma v\rangle_{cx}^{H_2}\right)\right].$$

When this condition is met, buildup will continue up to a level at which the coulomb loss term $(n_h^2/\langle n\tau\rangle)$ will balance the source. Thus it is of fundamental importance that the neutral gas density within the plasma not exceed a level determined by the available neutral beam current.

This requirement is interrelated with the neutral beam technology since an important source of cold gas is that which streams into the confinement chamber

from the neutral beam sources. A second source of cold gas is that released from the vacuum chamber under bombardment by the energetic charge-exchanged neutralized ions. This gas release can be controlled by wall pumping techniques such as gettering. A third gas source is backstreaming from the beam dump. This is particularly important in present day mirror plasmas in which the plasma is "thin" to the beams so that only a small fraction of the beam current is ionized within the plasma.

It is believed that the penetration of cold gas into the plasma is controlled by the production of a cold plasma halo that surrounds the hot core. To be effective, this halo must contain a sufficient line density ($\int n_{halo} ds$) to attenuate the cold gas significantly. It is particularly important to attenuate the molecular species which has a temperature determined by the wall temperature ($\sim$ 0.02 eV) and a relatively high charge exchange cross section. The atomic hydrogen which is produced within the halo by Frank–Condon processes on the molecular species is more penetrant since it is characterized by an energy of typically 2 to 5 eV.

Because of the poor confinement of hot ions in a mirror (which is limited by the pitch–angle scatter time) the mean hot ion energy tends to be close to the beam injection energy. The hot ions will transfer some energy to electrons before they pitch angle scatter and are lost. The electrons produced during ionization are cold and can heat up to only a small fraction of the ion temperature during their confinement. (The electron confinement time is constrained to equal the ion confinement time by requirements of neutrality.) The exact distribution function of hot ions can be determined by solutions of the Fokker–

Planck equations [Killeen *et al.*, 1976; Cutler *et al.*, 1977]. In addition, excellent analytic approximations for confinement time and hot ion mean energy have been obtained [Logan *et al.*, 1980].

Charge–exchange ionization of neutral beams on the hot trapped target does not provide a particle source. It does provide an energy source proportional to the difference of beam and mean hot ion energies. More importantly, it serves to maintain a peaking of the distribution function near the beam energy and pitch angle. (This effect will naturally diminish at the high energies at which the charge–exchange cross section becomes small ($E_b \geq 100$ keV).) Maintenance of a peaked distribution function will enhance confinement although it will also degrade stability [see Sec. III.E].

The stability problem associated with an anisotropic ion distribution can, in principle, be ameliorated by injecting neutral beams either at a near–to–loss–cone pitch angle at the midplane or perpendicularly at an off–midplane location. The resulting ion distribution has been termed "sloshing–ions" and is discussed in Sec. IV.B. It is important that, even though ion stability is improved by this process, collisional confinement will degrade because the source ions start out closer to the loss cone (this effect can be diminished through use of high mirror ratio cells). Furthermore, the resulting equilibrium ion distribution will fill out a larger effective volume within the mirror cell and thus will require higher beam current to sustain a given peak density and $n\tau$.

A second application for neutral beams in a tandem mirror is as a means for "pumping" a thermal barrier (Sec. IV.A). For this application the neutral beams would be aimed at an angle within the mirror cell loss cone so as to produce

unconfined ions. Charge exchange thus will replace confined with unconfined ions and effectively depress ion density within the mirror cell. It should be noted that due to the declining charge-exchange cross section at high energies the usefulness of this pumping technique is limited in reactor grade tandem mirrors.

Finally, it is observed that for production of very high energy ($E_i \gtrsim 150$ keV) positive neutral beam sources become impractical because of the reduction in the efficiency of the source neutralizer cell (resulting from the declining charge-exchange cross section). In principle this problem can be solved through the use of negative ion sources for the neutral beams. Of course the charge-exchange-related ionization phenomena discussed above will also become inoperative at these high beam energies.

III.H The Role of Resonant Frequency (rf) Heating

III.H.1 Electron Cyclotron Resonance Frequency Heating in Tandem Mirrors

ECRH is the acronym for electron cyclotron resonance heating. At positions where the local electron frequency of gyration(f_{ce}) is equal to wave frequency, the electron observes a nearly constant electric field and can be resonantly accelerated. The electron cyclotron frequency is determined by the following formula: f_{ce} = 28 GHz $\times$B(tesla). For magnetic field strengths in the range of 0.3 to 4 tesla, f_{ce} ranges from 8 to 112 GHz. Thus, ECRH falls into the microwave band of frequencies. A second important parameter in ECRH is the plasma frequency(ω_{pe}) which determines accessibility of the microwave field. Microwaves are reflected at the plasma periphery when the core density is such that the local plasma frequency exceeds the microwave frequency. A simple formula for cutoff density is given by $N(\mathrm{cm}^{-3}) = 1.24 \times 10^{10} F^2$ (GHz) where F is the wave frequency. The maximum density for ECRH accessibility scales as the square of the frequency.

The availability of high power, long pulse length, microwave sources in the ECRH frequency range has limited the experimental data base acquisition. Prior to the development of the gyrotron, klystrons in the range of 5–20 GHz were used in ECRH experiments. Nearly all of the ECRH experimental data base for mirrors is in this frequency range. The lower frequency limits the plasma density to 1 to 3 $\cdot 10^{12}$ particles cm^{-3}. In the last few years, gyrotrons operating at 28 GHz have been delivered to a number of laboratories. The cutoff density for 28 GHz is 10^{13} cm^{-3} which provides sufficient overall line density to sustain a neutral beam injected plasma. TMX-Upgrade will be the first mirror

experiment to incorporate both ECRH and neutral beam injection, both of which are elements in the operation of a thermal barrier.

ECRH physics can be divided into two areas; (1) wave propagation and damping, and (2) wave–particle interaction physics. These areas are not mutually exclusive in that the wave particle interaction determines the damping. However, the division is useful in discussing ECRH physics. To determine the wave propagation characteristics in any rf heating experiment, the parameter of interest is the ratio of the rf wavelength to the characteristic scale length of the plasma parameters such as density. For microwave frequencies above 10 GHz, the wavelength is less than 3 cm and is usually much smaller than the plasma scale length. Thus, ECRH wave propagation can be analyzed by using the ray tracing technique. Ray tracing assumes that wave propagation is determined by the local plasma parameters, and equiphase fronts can be calculated from the accumulated phase change along the ray trajectory (the phase memory concept). The ray trajectory is then the path of power flow which is everywhere normal to the equiphase fronts. Ray tracing can then be used to determine the radiation pattern from a waveguide antenna which imposes a boundary condition on the initial equiphase surfaces. For mirror experiments in the low density range, the plasma is transparent to microwaves. In this regime, the ray trajectories bounce off the vacuum chamber walls and generate a field pattern similar to an overmoded cavity. As the density and temperature increase, the plasma becomes opaque to microwaves. In this case, ray tracing can be used to determine the absorption along a ray trajectory, and rays are usually absorbed in a single pass. The calculation is linear so that the absorption is dependent upon the assumed

equilibrium distribution for the electrons. The detailed wave–particle interaction then determines the evolution of the equilibrium distribution function (*i.e.*, the heating).

The dominant wave–particle interaction in the cold plasma limit is the single particle resonance at the cyclotron frequency ($\omega = \omega_{ce}$). As the plasma temperature increases, such that the electron gyroradius is comparable to the rf wavelength, the electron observes a spatially–modulated electric field. This results in resonant wave particle interactions at the harmonics of the cyclotron frequency. In particular, second harmonic heating ($\omega = 2\omega_{ce}$) has been used to generate hot electron rings ($\sim$ 500 keV) in both simple and toroidally–linked mirrors such as the Elmo Bumpy Torus experiment (EBT–1).

In EBT devices, the rings form on field lines that have a mirror ratio larger than two with the second harmonic resonance zone located at some radius at the midplane. Thus, both fundamental and second harmonic heating take place on these field lines, and the magnetic field configuration is similar to that in tandem mirror plugs which incorporate thermal barriers. For thermal barriers, fundamental frequency heating provides energy transfer to the bulk of the electron distribution in the outer potential peak of the plug. Fundamental heating also provides a source of higher energy electrons (*i.e.*, with finite gyroradius) that may be heated efficiently at the midplane second harmonic location to create the thermal barrier. Thus, generation of hot electrons for both the EBT ring application and thermal barrier applications involves heating at both fundamental and second harmonic resonances.

The numerical methods used to calculate the evolution of the electron dis-

tribution function are Monte-Carlo methods and Fokker-Planck calculations. Only Monte-Carlo methods are described since they are more intuitive. In Monte-Carlo calculations one follows an ensemble of test particles in a magnetic field configuration retaining information such as the velocity of each electron as it transits a given position in space. One can then reconstruct the distribution function at that point. Coulomb collisions may be included by altering a test particle's velocity coordinates after a specified time interval according to a specified collision operator. ECRH may be modeled by calculating the single particle motion through the resonance zone, and altering the test particle's energy accordingly. In these calculations, the test particle distributions evolve, and one can obtain an estimate of the equilibrium electron distribution function. Once the time evolution of the equilibrium distribution function is known, one can couple this information back to the ray tracing code which uses the equilibrium distribution to calculate the wave damping.

Although much of the analysis of ECRH heating in tandem mirrors has assumed cyclotron damping to be the dominant absorption process, other nonlinear processes can intercede. Recent experimental observations [Smatlack, 1982] and analysis [Nicholson, 1983] indicate the possibility of parametric decay processes for a sufficient wave field amplitude. The proposed process would take place at the half critical density surface ($\omega^2 = \omega_{pe}^2/2$) and could result in power absorption near the plasma edge.

III.H.2 Ion Cyclotron Range of Frequency (ICRF) Heating in Tandem Mirrors

Rf heating near the ion cyclotron frequency is generally referred to as ion cyclotron range of frequencies (ICRF) heating. The primary cold plasma wave-particle resonance occurs at the ion cyclotron frequency ($\omega = \omega_{ci}$). When thermal effects are included and a second ion species introduced, a number of other absorbing wave–wave and wave–particle resonances appear. Among these are heating at the harmonics of the cyclotron frequency, mode conversion at the two–ion hybrid resonance, and direct electron heating via Landau damping. Experiments have observed all of the above physical effects, and hence heating in this frequency range is labeled ICRF, evolving from ICRH (ion cyclotron resonance heating). For magnetic field strengths of ongoing mirror experiments (2–30 kG), the hydrogen ion cyclotron frequency ranges from 3–45 MHz. The lower end of this frequency range is the HF band where high power rf sources at the megawatt level are available.

The ICRF plasma waves can be divided into two groups; fast modes with wavelengths comparable to or greater than the plasma scale length, and slow modes with wavelengths comparable to an ion gyroradius. Among the long wavelength modes are the fast magnetosonic wave, and the electromagnetic ion cyclotron wave [Stix, 1962]. The identity of the slow modes is dependent upon the frequency and direction of propagation. Among these modes we have the ion Bernstein wave [Bernstein, 1958], the electrostatic ion cyclotron wave [Hirose *et al.*, 1970], the kinetic Alfven wave [Hasegawa, 1975], and the ordinary slow wave. The fast magnetosonic wave is primarily right–hand polarized, E_- (E rotating

counter to the ion gyromotion) near $\omega = \omega_{ci}$. The wavelength of the fast wave is defined by the simple formula $k_\perp = (\omega_{pi}/c)\ \ (\omega/\omega_{ci})$. For plasma densities such that the wavelength is comparable to the plasma radius, there is an onset of fast wave propagation when the plasma density is sufficiently high for radial eigenmodes to exist within the plasma. The eigenmode condition is generally of the form $na^2 > 10^{15}$ with a the plasma radius (cm) and n a mean density (cm^{-3}). The Phaedrus ICRF experiments (Sec. V.C) were below the cut-off frequency of the fast wave. In this case, the near fields of the antenna provide the power transfer to the plasma. These fields are predominantly right-hand polarized near $\omega = \omega_{ci}$ [McVey *et al.*, 1982], and the antenna can be thought of as coupling to evanescent fast waves. In a cold plasma, $|E_+|$ of the fast wave is identically zero at the fundamental frequency ($\omega = \omega_{ci}$). However, in a warm plasma, Doppler shift of the wave field, and finite transit-time of the ions through the resonance zone [Perkins, 1980] result in a finite value of $|E_+|$, and hence ion heating. For fast wave propagation at the second harmonic ($\omega = 2\omega_{ci}$) in a cold plasma, the wave field is left-hand polarized and ion heating can occur due to finite gyroradius effects. The electromagnetic ion cyclotron wave propagates below ω_{ci}, and excitation is restricted to a narrow band of the parallel wave number (k_z). For a given plasma radius, the optimum excitation frequency approaches ω_{ci} as the plasma density decreases [Hosea *et al.*, 1970]. There is no density cut-off, but efficient excitation of the ion cyclotron wave generally requires a uniform magnetic field and a coil with a narrow k_z spectrum [Stix, 1962].

Short wavelength modes such as the ion Bernstein wave and a slow ordinary mode are important in determining the overall dissipation of the antenna fields.

Near the second harmonic frequency, the fast wave couples with an ion Bernstein wave [Swanson *et al.*, 1975]. The near fields of an inductive antenna excite an evanescent fast wave at $2\omega_{ci}$. The fast wave has mixed inductive and electrostatic components that couple to an ion Bernstein wave in a density gradient [Golovato *et al.*, 1982; McVey, 1983; Ono, 1983]. Near the fundamental cyclotron frequency, a slow ordinary mode (polarization identical to the ordinary wave near ω_{ce}) is directed excited at the surface of the plasma [McVey *et al.*, 1982]. This mode is a surface wave that is dissipated via Landau damping leading to direct electron heating by the near fields of the antenna.

Phaedrus Experiment

The Phaedrus tandem mirror was specifically constructed to test rf heating in tandem mirrors. In a general description of the operational mode of the Phaedrus tandem mirror, (Sec. V.C) the relevant ICRF physics will be discussed. Phaedrus is a tandem mirror with a magnetic field geometry similar to that of the TMX experiment. The central solenoid is bounded by two minimum-B end plugs. The central cell magnetic field strength is typically 400 G, and the plug–midplane field is nominally adjusted to 3 kG. ICRF heating is applied to the central cell at 700 kHz, and separately to each plug at 4.5 MHz. Stream gun injection generates a start–up plasma for a duration of 1 ms, and after gun turn off, gas puffing in the central cell provides the sole particle source. A steady state equilibrium results with pulse lengths only limited by the duration of rf power, which is typically 10 to 20 ms. The equilibrium plasma parameters are typically as follows: the central and plug densities are comparable and in the range of $0.5 - 1 \times 10^{13}$ particles $\cdot$ cm^{-3}, the electron temperature $\sim$ 30 eV,

the central cell ion temperature $\sim$ 40 eV, and the plug ion temperature 0.5 — 1 keV.

Two elements are key in the rf-sustained operational mode of the Phaedrus tandem mirror. First, ICRF heating has been observed to heat the electrons directly. The electron temperature must be sustained in order to ionize the neutral gas efficiently. Second, ICRF heating at the ion cyclotron resonance maintains pressure-weighted end plugs which provide MHD stability for the overall tandem. Thus, ICRF replaces neutral beams in the rf-sustained mode of operation generating a magnetically-confined hot ion plasma in the plugs. The central cell loss provides the fueling source for the magnetically- trapped ions. In a single transit through the plugs, ICRF heating must project ions from the loss region of velocity space (below the ambipolar potential) into the trapped region. As the ambipolar potential becomes larger, single pass heating of ions into the confined region of velocity space becomes more difficult. Phaedrus results verify the difficulty of plug fueling from the central cell stream. With only central cell gas puffing, the plug densities were comparable to the central cell density.

On the Phaedrus experiment, various ICRF antenna configurations were tested. In the plugs, the optimal antenna was a single straight rod located off-midplane, outside the neutral beam footprint [Smith, 1980]. The rod antenna was oriented parallel to the elliptical fan of the minimum |B| geometry optimizing the near field coupling of the antenna. In the central cell, a half-turn loop (shielded only with axial limiters) was found to be an efficient antenna [McVey *et al.*, 1982]. In general, the observed heating was attributed to the near fields of the antenna. No evidence of coupling to a fast wave or ion cyclotron wave

was observed in the loading resistance. Wave coupling efficiencies were generally in the range of 70-95%, and the ion heating efficiencies ranged from 20-50% [Smith, 1980; Golovato *et al.*, 1982; McVey *et al.*, 1982].

Applications in Tandem Mirrors

Rf heating in the ion cyclotron range of frequencies has a number of potential applications in tandem mirrors:

During start-up, ICRF can be used as a power source to sustain the central cell and to generate a target plasma in the plugs for neutral beam injection [Kesner *et al.*, 1982].

In the Phaedrus experiment, plasmas have been sustained in the central cell alone using ICRF heating with no auxiliary heating in the plugs [Ferron *et al.*, 1982]. MHD stability is believed to derive from rf ponderomotive effects. Such experiments eliminate the need for stream guns to generate a target plasma for the neutral beams.

ICRF heating in the central cell can provide bulk ion heating at low plasma densities. During start-up, preheating of the central cell ions appears necessary in order to minimize collisional filling of the thermal barrier [Molvik *et al.*, 1982].

It has been observed that ICRF heating can modify the radial potential profile [Hershkowitz, 1982]. Radial potential control is an important factor in determining the radial transport in the central cell and the overall plasma equilibrium.

ICRF heating is being investigated as both an ion and electron pumping mechanism. In the thermal barrier, heating of the trapped ions in the perpendicular direction may be a useful barrier pump mechanism. Calculations of ICRF pumping of the transition region of an axicell or throttled tandem-mirror design indicates that Rf pumping can replace most of the CX pump beams [Cummins and Rensink, 1983].

ICRF can be used to heat electrons along the field lines via Landau damping. If the frequency is adjusted to the electron bounce frequency, the ICRF can preferentially pump electrons in a positive potential plug [Smith and McVey, 1982]. The rf-induced parallel diffusion of electrons forces the plug potential to rise above a Boltzmann factor which enhances the central cell ion confinement.

References Section III.A

1. Baldwin, D.E., 1977, Rev. Mod. Phys. 49, 317.

2. Baldwin, D.E. and B.G. Logan, 1977 TMX Major Project Proposal, Lawrence Livermore National Laboratory Report LL-PROP-148, Appendix A1, 37.

3. Baldwin, D.E. and B.G. Logan, 1979, Phys. Rev. Lett. 43, 1318.

4. Berk, H.L., M.N. Rosenbluth, H.V. Wong, T.M. Antonsen and D.E. Baldwin, 1982, Proc. 9^{th} Int. Conf. Plasma Phys. and Controlled Fusion, Baltimore.

5. Carlson, G.A. and R.W. Moir, 1975, Mirror Fusion Reactor Study, Lawrence Livermore National Laboratory Report UCRL-76985.

6. Catto, P.J. and I.B. Bernstein, 1981, Phys. Fluids 24, 1900.

7. Cohen, B.I., 1980, Status of Mirror Fusion Research, Lawrence Livermore National Laboratory Report UCAT 10049-80-Rev. 1.

8. Cohen, R. *et al.*, 1978, Nucl. Fusion 18, 1229.

9. Dimov, G.I., V.V. Zakaidakov and M.E. Kishinevskii, 1976, Sov. J. Plasma Phys. 2, 362 [1976, Fiz. Plazmy 2, 596].

10. Fowler, T.K., 1981, In *Fusion* (E. Teller, ed.) (Academic Press: New York) **Vol.** 1, Part A, 241.

11. Fowler, T.K. and B.G. Logan, 1977, Comments Plasma Phys. and Controlled Fusion Research 2, 167.

12. Futch, A.H., Jr., J.P. Holdren, J. Killeen and A.A. Mirin, 1972, Plasma Phys. 14, 211.

13. Galbraith, D.L. and T. Kammash, 1978, Plasma Phys. **20**, 959.

14. Kelley, G.G., 1967, Plasma Phys. **9**, 503.

15. Lao, L.L., R.W. Conn and J. Kesner, 1978, Nucl. Fusion **18**, 1308.

16. Moir, R.W. *et al.*, 1977, Preliminary Design Study of the Tandem Mirror Reactor, Lawrence Livermore National Laboratory Report UCRL-53202.

17. Pastukhov, K.P., 1974, Nucl. Fusion **14**, 3.

18. Post, R.F. 1982, Int. Conf. on Plasma Phys.Controlled Nucl. Fusion Res. 5^{th} Tokyo, Nov. 11-15, 1974, (IAEA: Vienna), **Vol. 1**, 311.

19. Rensink, M.E. and T.A. Cutler, 1976, Proc. Ann. Meeting Theoret. Aspects CTR, Madison, Wisconsin.

20. Rosenbluth, M.N., M.A. Krall and N. Rostoker, 1962, Nucl. Fusion Suppl. Pt. 1, 143.

21. Rosenbluth, M.N., and A. Simon, 1965, Phys. Fluids **8**, 1300.

22. Ryutov, D.D. and G.V. Stupakov, 1977, JETP Lett. **26**, 174; 1978 Fiz. Plazmy **4**, 501; 1978, Dukl. Akad. Nauk. SSSR **240**, 1086.

23. Stupakov, G.V., 1979, Fiz. Plazmy **5**, 958; 1979, Fiz. Plazmy **5**, 871.

24. Taylor, J.B., 1963, Phys. Fluids **6**, 1529.

References Section III.B

1. Baldwin, D.E., 1978, Lawrence Livermore Laboratory Internal report No. UCID-17926 (unpublished).

2. Baldwin, D.E.and R.H. Bulmer, 1982, Lawrence Livermore National Laboratory Report UCID-19562.

3. Breun, R., S.N. Golovato, L. Yujiri *et al.*, 1981, Phys. Rev. Lett. **47**, 1833.

4. Bulmer, R.H., T.B. Kaiser, W.M. Nevins, W.A. Newcomb, L.D. Pearlstein, H.R. Strauss, S. Wollman, M. Wakatani, 1982, Int. Conf. on Plasma Phys. Controlled Nucl. Fusion Res. 9th Baltimore, Sept. 1-8, paper IAEA-CN-41/G-2.

5. Byers, J.A., 1982, Nucl. Fusion **22**, 49.

6. Catto, P. and I.B. Bernstein, 1981, Phys. Fluids **24**, 1900.

7. Catto, P.J. and R.D. Hazeltine, 1981, Phys. Rev. Lett. **46**, 1002; and 1981, Phys. Fluids **24**, 1663.

8. Coensgen, F.H., C.A. Anderson, T.A. Casper *et al*, 1980, Phys. Rev. Lett. **44**, 1132.

9. Cohen *et al*, 1978.

10. Cohen, R.H., 1979, Nucl. Fusion **19**, 1579.

11. Cohen, R.H. and G. Rowlands, 1981, Phys. Fluids **24**, 2295.

12. Cohen, R.H., M.E. Rensink, T.A. Cutler and A.A. Mirin, 1978, Nucl. Fusion **18**, 1229.

13. Cordey, J.G. and C.J.H. Watson, 1970, in Proceedings of the British Nuclear Energy Society Nuclear Fusion Reactor Conference, ed. by J.H. Hall and J.H.C. Maple (British Nuclear Energy Society: Culham), 122.

14. Correll, D.L. *et al.*, 1982, Nucl. Fusion **22**, 223.

15. Dimov, G.I., V.V. Zakaidakov and M.E. Kishinevskii, 1976, Fiz. Plazmy **2**, 597; 1976 Sov. J. Plasma Phys. **2**, 326.

16. Drake, R.P., E.B. Hooper, C.V. Karmendy, S.L. Allen, T.A. Casper, J.F. Clauser, F.H. Coensgen, R.H. Cohen, D.L. Correll, J.C. Davis, J.H. Foote, A.H. Futch, R.K. Goodman, D.P. Grubb, G.E. Gryzkowski, G.A. Hallock, A.L. Hunt, W.E. Nexson, W.L. Pickles, A.E. Pontau, P. Poulsen, T.C. Simonen, O.T. Strand and W.R. Wampler, 1981, Lawrence Livermore National Laboratory Report No. UCRL-85872 (to be published).

17. Fowler, T.K. and B.G. Logan, 1977, Controlled Fusion **2**, 167.

18. Furth, H.P. and M.N. Rosenbluth, 1964, Phys. Fluids **7**, 764.

19. Galbraith, D.L. and T. Kammash, 1978, Plasma Phys. **20**, 59.

20. Hall, L.S. and B. McNamara, 1975, Phys.Fluids **18**, 552.

21. Kesner, J., 1980, Nucl. Fusion **20**, 557.

22. Kesner, J., R.S. Post, D.B. McVey and D.K. Smith, 1982, Nucl. Fusion **22**, 549.

23. Lao, L.L., R.W. Conn, J. Kesner, 1978, Nucl. Fusion **18**, 1308.

24. Mirin, A.A., S.P. Auerbach, R.H. Cohen, J.M. Gilmore, L.D. Pearlstein, M.E. Rensink, 1983, Nucl. Fusion **23**, 703.

25. Myra, J.R., D.A. D'Ippolito, P.J. Catto, 1983, Phys. Fluids **26**, 1028.

26. Myra, J.R., P.J. Catto, 1983, Phys. Fluids **26**, 1836.

27. Pastukhov, V.P., 1974, Nucl. Fusion **14**, 3.

28. Ryutov, D.D. and G.V. Stupakov, 1978, Fiz. Plazmy 4, 501 [Sov. J. Plasma Phys. 4, 278 (1978)].

29. Ryutov, D.D. and G.V. Stupakov, 1978b, Dokl. Akad. Nauk. SSSR **240**, 1086 [Sov. Phys.-Dokl. 23, 412 (1978)].

30. Ryutov, D.D. and G.V. Stopakov, 1977, Pis'ma Zh. Eksp. Teor. Fiz. **26**, 186 [JETP Lett. 26, 174 (1977)].

References Section III.C

1. Baldwin, D.E. and R.H. Bulmer, 1982, "A Physics Conceptual Design for the MFTF-B Transition Coil".

2. Berk, H.L., M.N. Rosenbluth, H.V. Wong, T.M. Antonsen and D.E. Baldwin, 1982, Institute for Fusion Studies Report IFSF-59.

3. Bulmer, R.H., T.B. Kaiser, W.M. Nevins, W.A. Newcomb, L.D. Pearlstein, H.R. Strauss, S. Wollman, M. Wakatani, 1982, presented at the 9^{th} International Conference on Plasma Physics and Controlled Nuclear Fusion Research, Baltimore, paper CN-41/G-2.

4. D'Ippolito, D.A., G.L. Francis, J.R. Myra and W.M. Tang, 1981, Phys. Fluids **24**, 2270.

5. D'Ippolito, D.A. and J.P. Freidberg, 1982, Phys. Fluids **25**, 1617.

6. D'Ippolito, D.A. and J.P. Freidberg, 1982, presented at the Sherwood Meeting on Theoretical Aspects on Controlled Thermonuclear Fusion, Santa Fe, New Mexico, paper 1C12.

7. D'Ippolito, D.A. and B. Hafizi, 1981, Phys. Fluids **24**, 2274.

8. D'Ippolito, D.A., J.A. Myra and J.M. Ogden, 1982, Plasma Physics **24**, 707.

9.. Freidberg, J.P. and L.D. Pearlstein, 1978, Phys. Fluids **21**, 1207.

10. Hall, L.S. and B. McNamara, 1975, Phys. Fluids **18**, 552.

11. Kaiser, T.B. and L.D. Pearlstein, 1982, Lawrence Livermore National Laboratory Report UCRL-87659.

12. Lee, X.S. and P.J. Catto, 1981, Phys. Fluids **24**, 2010.

13. Lee, X.S., P.J. Catto and R.E. Aamodt, 1982, Phys. Fluids **25**, 1491.

14. Logan, G.B., 1981, Comments Plasma Phys. Controlled Fusion **6**, 199.

15. Myra, J.R., D.A. D'Ippolito and P.J. Catto, 1982, SAI Report SAI-254-82-174-LJ/PRI-44.

16. Nevins, W.M. and L.D. Pearlstein, 1981, Bull. Am. Phys. Soc. **26**, 984.

17. Newcomb, W.A., 1982, presented at the Sherwood Meeting on Theoretical Aspects of Controlled Thermonuclear Fusion, Santa Fe, New Mexico, paper 3A1.

18. Newcomb, W.A., 1981, J. Plasma Phys. **26**, Part 3, 529.

19. Pearlstein, L.D., T.B. Kaiser and W.A. Newcomb, 1981, Phys. Fluids **24**, 1326.

20. Rosenbluth, M.N. and C.L. Longmire, 1957, Annals of Phys. **1**, 120.

21. Ryutov, D.D. and G.V. Stupakov, 1981, in *Plasma Physics and Controlled Nuclear Fusion Research* (International Atomic Energy Agency: Vienna, Austria), **Vol. 1**, 119.

22. Strauss, H.R., S. Wollman and M. Wakatani, 1982.

23. Stupakov, G.V. 1979, Fiz.Plazmy **5**, 871 [1979, Sov. J. Plasma Phys. **5**, 486].

24. Tang, W.M. and P.J. Catto, 1981, Phys. Fluids **24**, 1314.

25. Taylor, J.B., 1963, Phys. Fluids **6**, 215.

26. Thompson, W.B., 1961, Rep. Prog. Phys. **24**, 363.

27. Turner, W.C., J.F. Clauser, F.H. Coensgen, D.L. Correll, W.F. Cummins *et al.*, 1979, Nucl. Fusion **19**, 1011.

References Section III.D

1. Berk, H.L., M.N. Rosenbluth, H.V. Wong, T.M. Antonsen, D.E. Baldwin, 1982, Proc. 9^{th} Int. Conf. Plasma Phys. & Contr. Fusion, Baltimore.

2. Kadomtsev, B.B. and D.P. Pogutse, 1970, Nucl. Fusion **11**, 67.

3. Kesner, J. and B. Lane, 1983, MIT Report PFC/JA-83-21.

References Section III.E1

1. Aamodt, R.E., D. R. Nicholson, C. S. Liu, 1979a, Phys. Fluids **22**, 114.

2. Aamodt, R.E., Y.C. Lee, C.S. Liu, L. Chen and M. N. Rosenbluth, 1979b, Bull. Amer. Phys. Soc. **24**, 956.

3. Avinash and R.K. Varma, 1983, *Theory of Electron Beam Injected Plasma*, submitted to Nucl. Fusion.

4. Baldwin, D.E., C.O. Beasley, H.L. Berk, W.M. Farr, R.C.Harding *et al.*, 1971, *Plasma Physics and Controlled Nuclear Fusion Research* (IAEA, Vienna), **vol. II**, 735.

5. Bhadra, D., 1967, Phys. Rev. **161**, 126.

6. Berk, H.L., T.K. Fowler, L.D. Pearlstein, R.F. Post, J.D. Callen, W.C. Horton, and M.N. Rosenbluth, 1969, *Plasma Physics and Controlled Nuclear Fusion Research* (IAEA, Vienna), **vol. II**, 151.

7. Berk, H.L. and M.J. Gerver, 1976, Phys. Fluids **19**, 1646.

8. Berk, H.L., L.D. Pearlstein, and J.G. Cordey, 1972, Phys. Fluids **15**, 891.

9. Callen, J.D. and G.E. Guest, 1971, Phys. Fluids **14**, 1588.

10. Callen, J.D. and G.E. Guest, 1973, Nucl. Fusion **13**, 87.

11. Casper, T.A. and G.R. Smith, 1982, Phys. Rev. Lett. 48, 1015.

12. Casper, T.A. and G.R. Smith, 1983, private communication.

13. Coensgen, F.H. *et al.*, 1975, Phys. Res. Lett. **35**, 1501.

14. Cordey, J.G. and R.J. Hastie, 1972, Phys. Fluids **15**, 2291.

15. Davidson, R.C. and J.M. Ogden, 1975, Phys. Fluids **18**, 1045.

16. Davidson, R.C., N.L. Gladd, C.S. Wu, and J.D. Huba, 1977, Phys. Fluids **20**, 301.

17. Foote, E.A. and R.M. Kulsrud, 1981, Phys. Fluids **24**, 1532.

18. Gerver, M.J., 1976, Phys. Fluids **19**, 1581.

19. Gerver, M.J., 1979a, Phys. Rev. Lett. **42**, 981.

20. Gerver, M.J., 1979b, Phys. Fluids **22**, 1510.

21. Gerver, M.J., 1980, Phys. Fluids **23**, 755.

22. Gerver, M.J., 1983, "Microstability of Tara Anchor with Belly Band," MIT Report PFC/RR–82–26.

23. Hastie., D.E., 1980, (A Linear Theory of High Beta Drift Waves), Ph.D. Thesis, MIT.

24. Horton, C.W. Jr., 1981, Phys. Fluids **24**, 1270.

25. Horton, W., 1980, Drift Mode Stability Analysis for the Tandem Mirror, Nucl. Fus. **20**, 321.

26. Kadomtsev, B.B., 1965, Plasma Turbulence, Academic Press, New York.

27. Klinkowstein, R.E., 1978, Ph.D. thesis, MIT.

28. Krall, N.A., 1968, "Drift Waves," in A. Simon and W.B. Thompson (eds.) *Advances in Plasma Physics* (John Wiley & Sons: New York), **vol. 1**, 153.

29. Krall, N.A. and T.K. Fowler, 1967, Phys. Fluids, **10**, 1526.

30. Mikhailovskii, A.B., 1962, Sov. Phys. Doklady **7**, 826.

31. Mikhailovskii, A.B., 1965, Nucl. Fusion **5**, 125 (in Russian).

32. Mikhailovskii, A.B., 1967a, Sov. Phys. Doklady **11**, 603.

33. Mikhailovskii, A.B., 1967b, Review of Plasma Physics 3, Consultants Bureau, N.Y.

34. Mikhailovskii, A.B. and A.V. Timofeev, 19xx, Sov. Phys. JETP, **17**, 626.

35. Pearlstein, L.D., 1978, Mirror Theory Monthly, Nov. issue.

36. Pearlstein, L.D., 1982, "Loss-Cone Stability," in D.E. Baldwin and B.G. Logan (eds.), *Physics Basis for an Axicell Design for the End Plugs of MFTF-B* (Lawrence Livermore Laboratory Report UCID-19359), 181.

37. Pearlstein, L.D. and H.L. Berk, 1969, Phys. Rev. Lett. **23**, 220.

38. Pearlstein, L.D., G.R. Smith, and W.M. Nevins, 1980, "Loss-Cone Instability," in D.E. Baldwin, B.G. Logan and T.C. Simonen (eds.) *Physics Basis for MFTF-B* (Lawrence Livermore Laboratory Report UCID-18496-Part 2), IV-109.

39. Post, R.F. and M.N. Rosenbluth, 1966, Phys. Fluids **9**, 730.

40. Rosenbluth, M.N., B. Coppi and R.N. Sudan.

41. Smith, G.R., 1983, "Alfven Ion Cyclotron Instability in Tandem Mirror Plasmas - I", Lawrence Livermore National Laboratory Report UCRL-89676 (submitted to Phys. Fluids).

42. Stix, T.H., 1962, *The Theory of Plasma Waves* (McGraw-Hill, New York).

43. Tang, W.M., L.D. Pearlstein, and H.L. Berk, 1972, Phys. Fluids **15**, 1153.

44. Watson, D.C., 1980, Phys. Fluids **23**, 2485.

References Section III.E.2

1. Ard, W. B., R. A. Dandl, R. F. Stetson, 1966, Phys. Fluids **9**, 1498.

2. Blanken, R. A., N. H. Lazar, 1970, Phys. Fluids **13**, 2752.

3. Casper, T. A., Yu-Jiuan Chen, R. Ellis, R. James, C. Lasnier, 1983, LLNL report no. UCID-19783.

4. Chen, Y.-J., W. M. Nevins, G. R. Smith, 1982, Bull. Am. Phys. Soc. **27**, p. 917.

5. Gladd, N. T., 1983, Phys. Fluids **26**, 974.

6. Guest, G. E., D. J. Sigmar, 1971, Nuc. Fusion **11**, 151.

7. Hewitt, R. G., D. B. Melrose, K. G. Ronnmark, 1982, Aust. J. Phys. **35**, 447.

8. Ikegami, H., I. Ikezi, M. Hosakawa, K. Takagama, S. Tanaka, 1968, Phys. Fluids **11**, 1061.

9. Lau, Y. Y., K. R. Chu, 1983, Phys. Rev. Lett. **50**, 242.

10. Melrose, D. B., K. G. Ronnmark, R. G. Hewitt, 1982, J. Geophys. Res. **87**, 4476.

11. Perkins, W. A., W. L. Barr, 1968, Phys. Fluids **11**, 388.

12. Porkolab, M., M.H. Brennan, J. Simms, 1971, Plasma Phys. **13**, 353.

13. Porkolab, M., 1983, LLNL report no. UCRL-89033, March 9, 1983.

14. Schwartz, M.J., A. J. Lichtenberg, 1972, Phys. Fluids **15**, 470.

15. Stallard, B. W., Y. Matsuda, W. M. Nevins, 1983, Nuc. Fusion **23**, 213.

16. Tsang, K. T., 1982, in Proceedings of the Annual Controlled Fusion Theory Conference, New Mexico, paper no. IC20.

17. Tsang, K. T., 1983, Science Applications, Inc. Report No. SAI-254-83-1014/PRI-63.

18. Wu, C. C., and L. C. Lee, 1979, Astrophys. et al **230**, 621.

19. Wu, C.S., H.K. Wong, D.J. Gurney, L.C. Lee, 1982, Geophys. Res. **87**, 4476.

References Section III.F

1. Breun, R. *et al.*, 1981, Phys. Rev. Lett. **47**, 1833.

2. Kesner, J. 1978, Nucl. Fusion **18**, 781.

3. Kesner, J., 1979, Nucl. Fusion **19**, 107.

4. Smith, G.R., W.M. Nevins, and W.M. Sharp, 1983, "Alfven Ion-Cyclotron Instability in Tandem Mirror Plasmas," presented at Sherwood Theory Meeting, March 21-23, Arlington, Virginia, paper 1D1.

5. Todd, A.A., 1982, Bull. Am. Phys. Soc., ms in progress.

6. Simonen, T. *et al*, 1981, "Summary of Results for the Tandem Mirror Experiment (TMX)," Lawrence Livermore National Laboratory Report UCRL-53120.

References Section III.G

1. Cutler, T.A., L.D. Pearlstein, M.E. Rensink, 1977, "Computation of the Bounce Average Code," Lawrence Livermore National Laboratory Report UCRL-52233.

2. Killeen, J., A.A. Mirin and M.E. Rensink, 1976, in *Methods in Computational Physics*, **Vol. 16**, (Academic Press: New York) 389.

3. Logan, B.G., A.A. Mirin and M.E. Rensink, 1980, Lawrence Livermore National Laboratory Report UCRL-84357.

References Section III.H

1. Bernstein, I.B., 1958, Phys. Rev. **109**, 10.

2. Cummins, W.F., Jr., and M.E. Rensink, 1983, Fifth Topical Conference on Radio Plasma Frequency Heating, Madison, Wisconsin.

3. Ferron, J. *et al.*, 1982 Bull. A.P.S., pp.

4. Golovato, S.N. *et al.*, 1982, Nucl. Fusion **22**, 741.

5. Hasegawa, A. *et al.*, 1975, Phys. Rev. Lett. **35**, 370.

6. Hershkowitz, N., 1982, Bull. A.P.S. **27**, 1013.

7. Hirose *et al.*, 1970 Phys. Fluids **13**, 2039.

8. Hosea, J.C. *et al.*, 1970, Phys. Fluids **13**, 701.

9. Kesner, J., *et al.*, 1982, Nucl. Fusion **22**, 549.

10. McVey, B., 1983, Fifth Topical Conference on Radio Frequency Plasma Heating, Madison, Wisconsin.

11. McVey, B., *et al.*, 1982, MIT Report PFC/JA–82–16.

12. Molvik, A.N. *et al.*, 1982, Bull. A.P.S. **27**, 968.

13. Nicholson, D.R. 1983, U. of Iowa Report 83-2.

14. Ono, M. *et al.*, 1983, Fifth Topical Conference on Radio Frequency Plasma Heating, Madison, Wisconsin.

15. Perkins, F.W. 1980, Bull. A.P.S.

16. Smatlack, D., 1982, Ph.D. Thesis, U. Wisconsin.

17. Smith, D.K., 1980, Ph.D. Thesis U. Wisconsin.

18. Smith, D.K. and B. McVey, 1982, Bull. A.P.S. **27**, 915.

19. Stix, T.H., 1962, *The Theory of plasma Waves* (McGraw–Hill: New York).

20. Swanson, D.G. *et al.*, 1975, Phys. Rev. Lett. **35**, 517.

IV. Advanced Tandem Mirror Concepts

The results of initial tandem mirror experiments, particularly TMX, served to confirm the principle of central cell electrostatic confinement and MHD equilibrium and stability in an "average minimum-B" system. However, TMX results also evoked continuing concern with regard to loss-cone instabilities in the neutral beam driven plugs.

At the same time, results of reactor studies indicated that it was difficult to extrapolate from tandem mirrors to pure D-T reactors as discussed above in Sec. III.A because of requirements of very high-field plugs and high energy neutral beams. Additionally, the work of Ryutov and Stupakov [1977] indicated that the nonaxisymmetry of the quadruple plugs resulted in a severe penalty to confinement.

The realization of these problems stimulated intense exploration of more novel tandem mirror end plug configurations and led to a significant reorientation of the mirror program. At a workshop in Livermore [in 1979], Baldwin and Logan presented schemes for potential enhancement by creation of nonmaxwellian plug distributions. This work led to the proposal of the thermal barrier [Baldwin and Logan, 1979] and the negative tandem mirror. The need for enhanced plug microstability rekindled interest in creating sloshing-ion distributions as had been suggested earlier [Kesner, 1973]. Such ion distributions were found to be particularly suitable for integration into thermal barrier schemes [Fowler, 1980; Kesner, 1980].

Additionally, the desire to reduce resonant transport led to interest in

various axisymmetric arrangements. Notable among these are the axicell scheme [Kesner, 1980], the cusp end cell [Logan, 1980; Shuy, 1981] and the use of an EBT-like hot electron ring scheme. Use of axisymmetry was found to be particularly desirable for thermal barriers. This result comes about because thermal barriers require a high magnetic field separating them from the central cell plasma to "throttle" the passing ion population and thereby decreasing the power requirement for thermal barrier maintenance. Attainment of the highest possible fields clearly drives one to the use of circular coils.

IV.A Thermal Barrier

In a standard tandem mirror the electrons have a Maxwell-Boltzmann energy distribution and have a uniform temperature along a field line. As the ion density rises in the plug, quasi-neutrality then requires that the potential rise as

$$\phi_c = T_e \ell n(n_p/n_c) \tag{41}$$

with $n_p(n_c)$ the plug (central cell) density and T_e the electron temperature. The above formula suggests that if the plug electron temperature could be elevated above that of the central cell, the confining potential, ϕ_c, could be produced without the need for a high plug density. The linear scaling of potential with T_e is clearly preferable to the logarithmic scaling of the density.

The magnetic field, potential, and density profiles proposed for thermal barrier formation [Baldwin, Logan, 1979] are indicated in Fig. IV.A.1. Introduction of a potential depression, $\phi_b \geq T_e$, is expected to produce the "thermal-barrier"

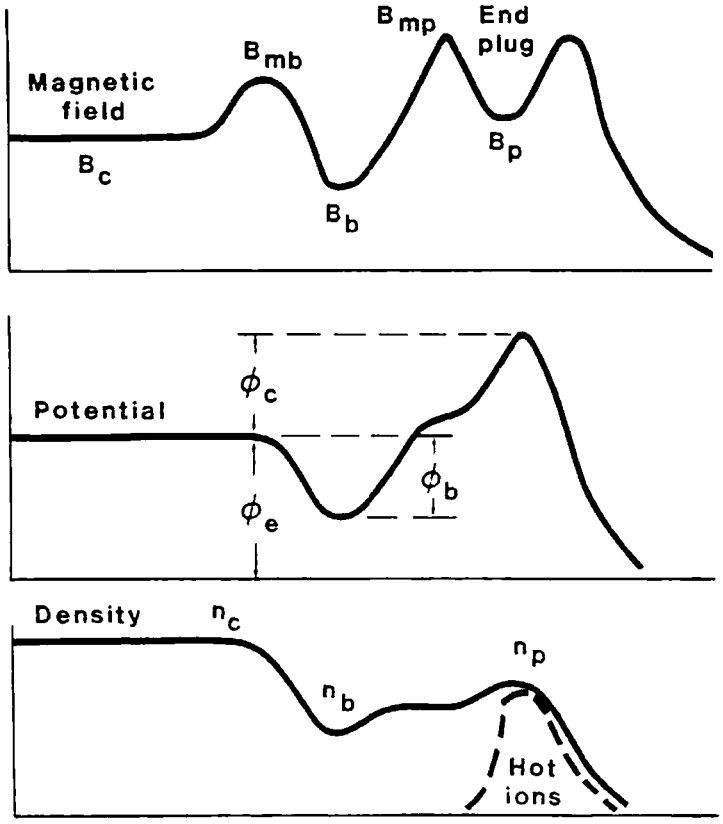

Figure IV.A.1: Curves showing the magnetic field, potential and density in the thermal barrier of a tandem mirror.

since it acts to reduce electron contact between the central cell and plug and thereby to permit the plug temperature (T_{ep}) to rise above the central cell temperature (T_{ec}) with the application of only a modest heat input. The potential depression results from a density depression and would follow a Boltzmann law

$$\phi_b = T_e \ln(\hat{n}_b/n_c) \tag{42}$$

with $\hat{n}_b$ the thermal electron density at the barrier point.

The electrons that are confined in the plug are then heated to temperatures well above the central cell values. The potential rise is expected to follow a modified Boltzmann law, namely

$$\phi_b + \phi_c = T_{ep} \ln[(n_p/\hat{n}_b)(T_{ec}/T_{ep})^{\nu}]. \tag{43}$$

This equation was originally taken to be a Boltzmann law ($\nu = 0$). Later work [Cohen et al., 1980] indicated that a more appropriate approximation would have $\nu \approx 1/2$. In this work, the Fokker-Planck equation was solved analytically subject to the assumption that the distribution function for deeply trapped "plug" electrons forms an isotropic maxwellian (at temperature T_{ep}) whereas at the trapped-passing boundary the distribution function matches that of the central cell. This finding was pessimistic, indicating that the thermal barrier was less effective than originally anticipated for creating the necessary confining potentials. (Recent work has shown, however, that in the presence of sufficiently strong ECRH heating, a more favorable potential enhancement relationship results [Cohen, 1983; Matsuda and Rognlien, 1983].)

At the same time it was understood that the depth of the thermal barrier potential could be enhanced through introduction of a hot electron component of density n_{eh} and energy $E_{eh} \gg \phi_b, \phi_c$.The presence of this "hot" species served to reduce the central cell electron penetration through the barrier. Thus, in the above equations one would take

$$\hat{n}_b = n_b - n_{eh} \equiv f_{ec} n_b, \tag{44}$$

with n_b the total density (hot plus thermal) and f_{ec} the fraction of thermal electrons at the barrier point.

The depression in ion density indicated in Fig. IV.A.1 results from maintaining a nonmaxwellian ion density in the barrier. For $\phi_b \gg T_{ic}$, the streaming (untrapped) ion density, n_{is}, can be estimated to be

$$n_{is} = (n_c/R_b)(T_{ic}/\pi\phi_b)^{1/2} \tag{45}$$

with R_b the barrier mirror ratio; $R_b \equiv B_{mb}/B_b$. Some "pumping" scheme is required to inhibit ion trapping in the potential depression which would allow the ion density, n_b, to rise as a Maxwellian–Boltzmann distribution is re–established. The ratio of the trapped to passing density, which is a measure of the pumping, can be parameterized by $g_b (g_b \equiv n_{trap}/n_{is})$.

The most straightforward pumping scheme that has been suggested would involve injection into the thermal barrier of neutral beams of sufficient energy and sufficiently small pitch angle that their charge exchange events would replace trapped ions by ions in the thermal barrier cell loss cone. Other schemes that use rf waves to cause a rapid cross–field transport of trapped ions have been

suggested [Baldwin, 1981]. The most interesting rf pumping schemes would act either on the drift or bounce time scale. It appears that these methods would be more efficient energetically, as detailed for example in the MARS study [Logan *et al.*,1983], and they are presently receiving careful scrutiny.

The ion density depression has been shown to be limited by some physics imposed constraints. Discontinuities in potential which cause enhanced scatter of passing ions have been shown to occur in the absence of trapped ions [Kesner et al., 1981]. The presence of a sufficient fraction of trapped ions was shown to eliminate this problem [R. Cohen, 1981]. Additionally, a strongly pumped ion population was seen to be subject to beam type instabilities. The stability of these modes was examined and stability requirements were found to be not overly restrictive. Generally $g_b > 2$ appeared to be desirable for microstability [Baldwin et al., 1980]. These modes become more unstable as the hot electron fraction increases.

The maintenance of the hot electron population gives rise to concerns related to ECRH penetration and damping and to hot electron equilibrium and stability. The desired hot electron population must be sufficiently dense to throttle the passing electron density which requires, typically, $n_{eh} \sim 80$ to 90% $\times n_b$. Additionally it is required that the hot electrons are not detrapped by the potential d pression, that is, $E_{eh} \gg \phi_b, \phi_c$. If the electrons "run-away" they would produce a very hot, low density population (as is often observed in ECRH-formed plasmas) which would not be sufficiently dense to aid the thermal barrier formation. To prevent this occurrence Stallard [Stallard et al., 1983] has proposed a strong localization of ECRH power to the region of the resonance

zone so that the relativistic Doppler shifts of hot electrons would prevent their further heating. In addition, the stability of the hot electron population to anisotropy-driven modes, present when $P_\perp \gg P_\parallel$, is under investigation.

Maintenance of the thermal barrier requires application of power for both ion pumping and electron heating. The former is necessary to maintain the density depression against ion trapping which would tend to fill in and thereby diminish the potential depression. The latter is necessary to a) maintain the magnetically-trapped hot electron population that throttles thermal electron contact and b) to heat the thermally-isolated plug electrons to a sufficient temperature to maintain the desired ion plugging potential. Ultimately the effectiveness of the thermal barrier (in terms of Q) depends on the ability to minimize this input power.

IV.B Sloshing Ions

Although the thermal barrier cell was first suggested as an independent mirror cell internal to the minimum-B ion plugging cell, it was quickly realized that the thermal barrier and ion plugging potential could be combined into one cell by use of so-called "sloshing ions" [Fowler and Logan, 1979; Kesner, 1980]. Sloshing ions are identified as the hot ion component,created and maintained in a deep mirror, that exhibits a local midplane density depression and symmetric density peaks on either side of the midplane. The thermal barrier would then form at the midplane potential depression and the ion plugging potential occurs at the outer ion density peak.

Such a density profile results, for example, from aiming neutral beams so that the bounce points of the injected ions are between the mirror midplane and the throat. This can be accomplished by aiming the beams at an angle (typically near 45°) at the midplane or by off midplane perpendicular injection. If the resulting ion distribution function is sufficiently peaked at the injection angle, the ion density will peak at the associated bounce points and exhibit a midplane depression. Maintenance of such a profile will require pumping, (such as that described above in Sec. IV.A), to prevent scattering of hot ions into deeply trapped pitch angles which would serve to eliminate the midplane density depression. Obtaining a sufficient midplane density depression while maintaining adequate confinement of the hot ions requires a deep mirror ratio cell; typically a mirror ratio greater than 4 and an injection angle of less than 45° to the cell axis are desired.

The sloshing ion scenario would make possible the incorporation into a single

end cell of the thermal barrier, ion plug and minimum-B "anchor" as in the TMX-U experiment [Coensgen et al., 1980]. Typical magnetic field, density, and potential profiles found in TMX-U are shown in Fig. IV.B.1. Additionally, sloshing ions make it possible to combine the thermal barrier and ion plug in a single cell, separate from the minimum-B anchor, as in the TARA axicell [Kesner et al.,1982].

The key advantage to generating sloshing ions lies in enhanced microstability of the hot ion species due to the ability of the hot ion species to self-trap a warm ion population. This approach to improved stability was suggested by the experimental observation of sloshing-ion distributions on the DECA II-B experiment [Launois et al., 1971; Nicholas et al., 1972; Kesner, 1973]. Furthermore, experiments on PR-6 [Kanaev, 1976] clearly demonstrated improved mirror microinstability stabilization resulting from self-trapping of warm plasma in a midplane potential depression formed by an ECRH-generated hot electron component. A detailed axial eigenmode analysis for DCLC and ALC modes was later carried out [Pearlstein *et al.*, 1980] using ion distribution functions that modeled neutral-beam- generated sloshing distributions. The stability range limits for these modes were clearly identified [Pearlstein, 1980; Gerver, 1982].

Use of sloshing ions appears to be particularly compatible with thermal-barrier tandem mirror end plugs. The midplane density depression produced by the sloshing ion creates a partial thermal barrier and aids in obtaining ECRH access at the cell midplane. Thus ECRH can be used to create a hot mirror confined electron component that further throttles the flow of thermal central cell electrons. This permits the heating of the electrons located beyond the

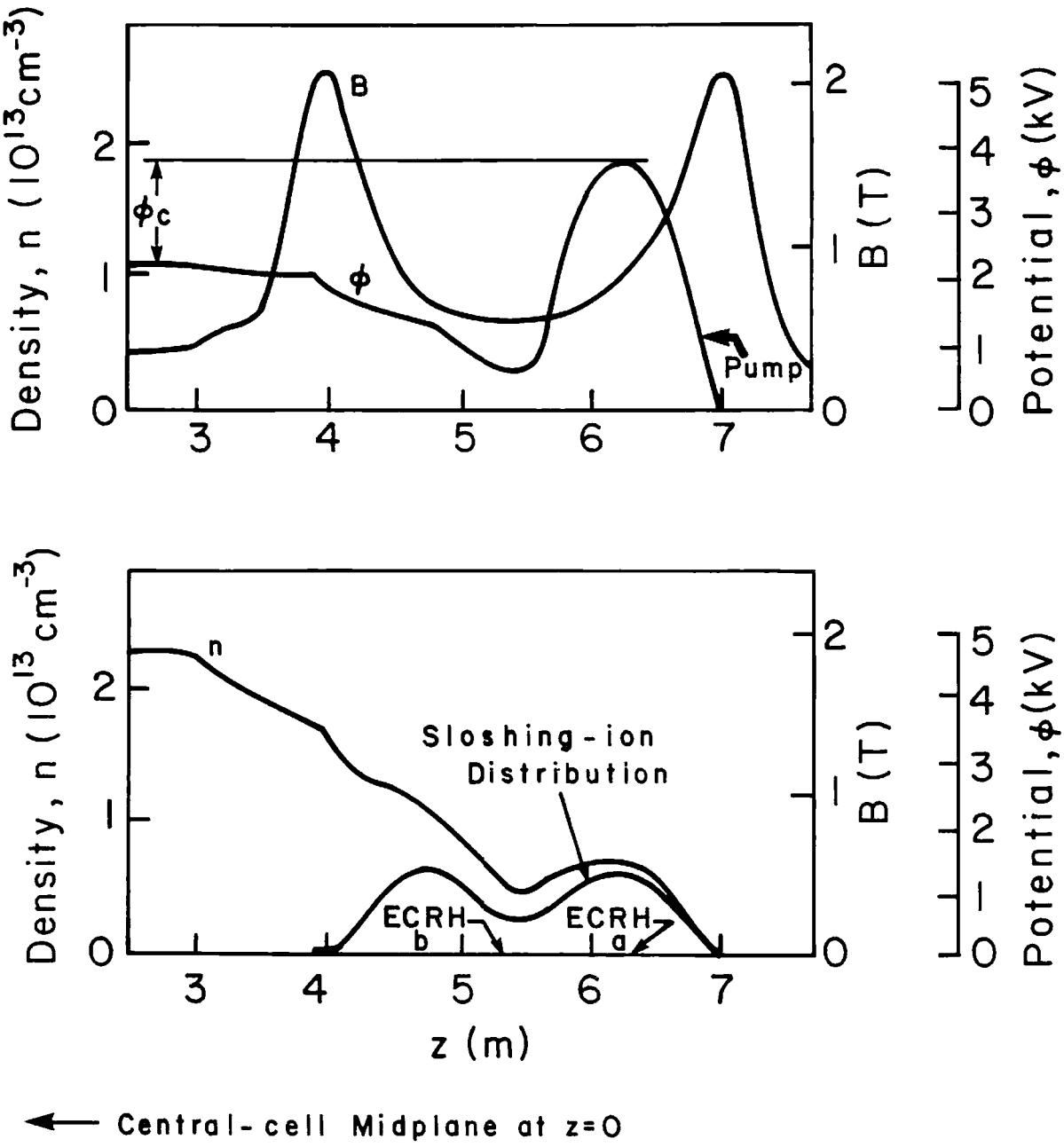

Figure IV.B.1: Contours of Magnetic Field Strength, B, Plasma Potential, ϕ, Plasma Density, n and Sloshing Ion Distribution in a TMX-U End Cell with a Full Thermal Barrier

thermal barrier and produces the accompanying potential rise. The central cell ions pass through the thermal barrier and reflect at the potential peak. These ions scatter and tend to accumulate in the potential depression. Although these warm ions aid the stability of the hot sloshing ions, additional pumping is necessary to limit their densities. To limit the pumping requirements, it is desirable to maximize the inner barrier-cell magnetic field peak and thus reflect most central cell ions before entering the thermal barrier region.

IV.C Thermal-Barrier Tandem Mirror Arrangements

The most compact plug arrangement would locate the sloshing ions in a quadruple end plug as in the TMX-U experiment (see Fig. IV.B.1) at LLNL. However, it was realized early on that enhanced performance and design versatility could be obtained by use of multiple cell plug arrangements.

To separate the sloshing-ion cell containing the thermal barrier and the ion plugging potential from the minimum-B anchor cell, the axicell design shown in Fig. IV.C.1 was proposed. A device of this type, named TARA, is being built at MIT. Here the plug and thermal barrier are positioned in a high mirror ratio axisymmetric cell located adjacent to the central cell. This arrangement serves to eliminate resonant transport (which results from nonaxisymmetric plugs) and permits the attainment of higher mirror ratio plugs due to use of circular coils. Additionally, more versatility in the design of the minimum-B anchor cell became possible as demonstrated by the proposed ECRH-heated hot-electron anchor approach used in TARA [Kesner et al., 1980]. The TARA arrangement is, however, vulnerable to trapped particle instability.

Another sloshing-ion scheme that received careful study is the MFTF-B outboard A-cell [Baldwin *et al.*, 1980] (Fig. IV.C.2) in which the tandem mirror central cell is bounded by the minimum-B yin-yang anchors, and the thermal barrier and plug form an elliptical cross section outboard cell, the so-called "A-cell." This provided a compact arrangement in which sloshing-ion stabilization was operative in the last (outboard) mirror cell. This feature was particularly desirable since the microstability problem is always most severe in the outermost

Figure IV.C.1: The axicell design shown here separates the minimum-B anchor cell from the sloshing-ion cell containing the thermal barrier and the ion-plugging potential. The TARA tandem mirror at MIT incorporates such as axicell.

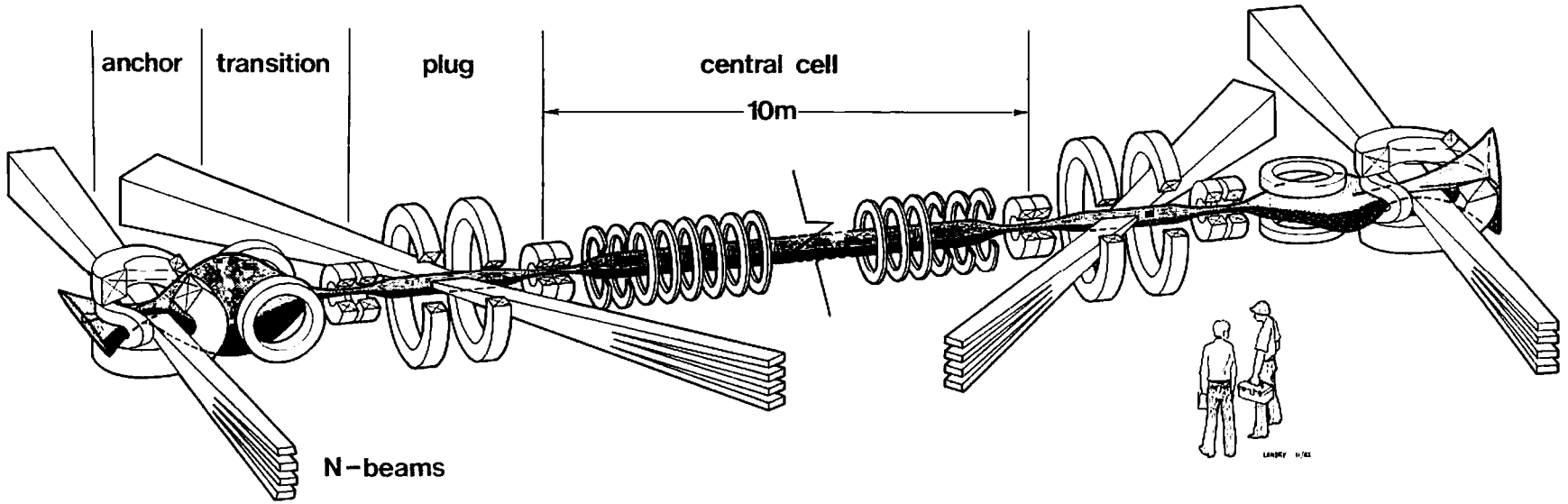

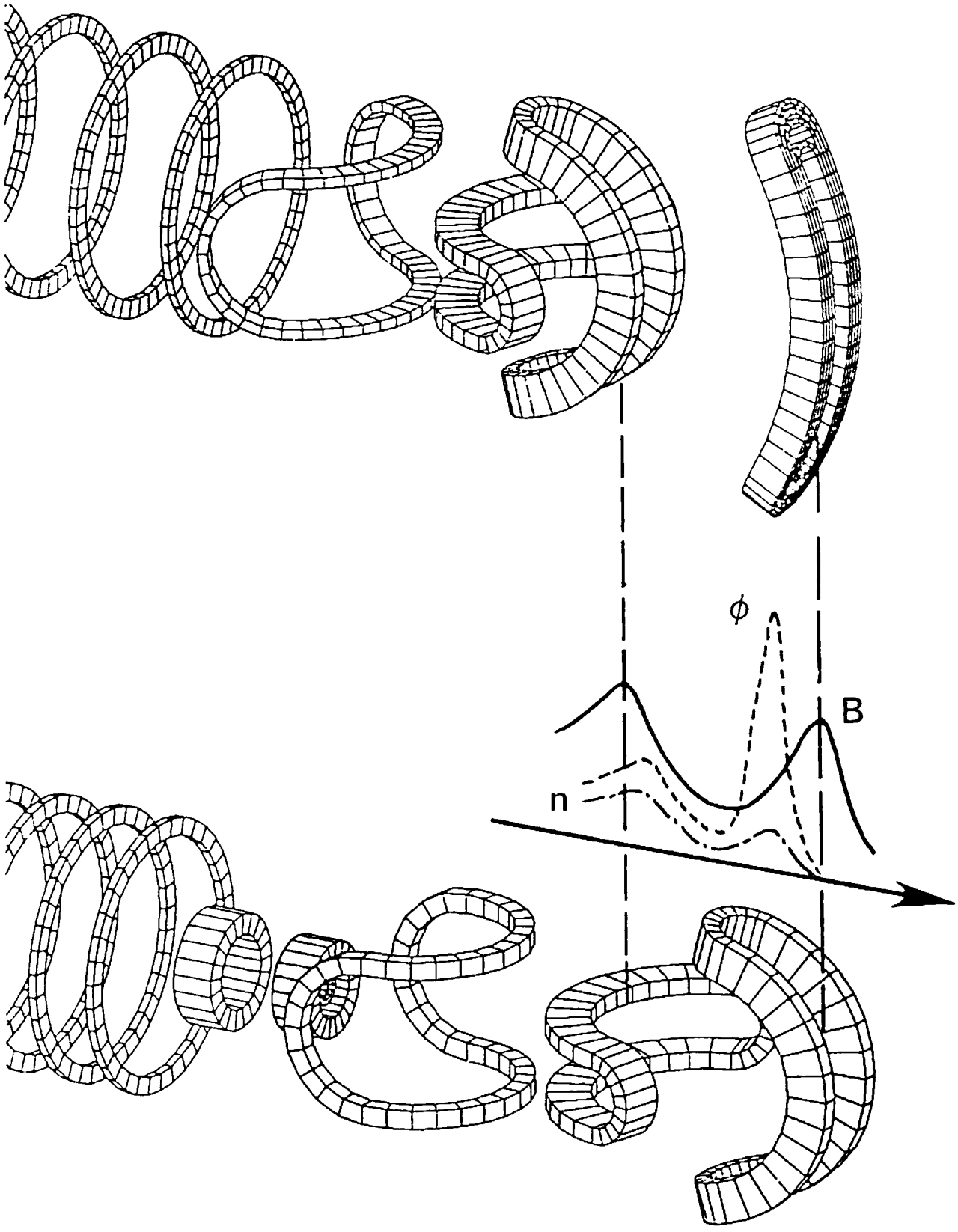

Figure IV.C.2: End cell coil arrangement for the MFTF-B tandem mirror for a) the outboard A - cell arrangement, b) the axicell arrangement

mirror cell which must support the largest potential drop. This approach, however, limits the maximum field that precedes the thermal barrier since this field occurs at the quadruple anchor cell and this feature reduces its reactor extrapolatability [Carlson et al., 1981]. Additionally, the outboard A–cell design is subject to severe resonant transport.

A third end plug arrangement that offers enhanced stabilization of trapped particle modes (Fig.IV.C.2) is to be embodied in the MFTF experiment under construction at LLNL. In this configuration, the thermal–barrier and plug form within a minimum-B end–cell containing sloshing ions as in TMX–U. The performance of this device is enhanced over the TMX–U arrangement by the positioning of an axisymmetric mirror, the so–called "axicell," between the central cell and plug. The axicell throttles the flow of passing ions into the plug and thereby permits higher central–cell densities for a given plug–thermal–barrier design. With an optimized transition design shown in Fig. IV.C.3, resonant transport due to the presence of passing ions in the transition can be effectively eliminated. Importantly, the passing ion population will provide stabilization of trapped particle modes.

Lastly, the Γ–10 arrangement (Fig. IV.C.4) being built at Tskuba University in Japan features an outboard axisymmetric plug with an inboard anchor. The central cell is bounded by an axisymmetric coil to reduce resonant transport and permit symmetric transitions to the circular flux surface on either side of the anchor. The anchor is designed to obtain beta from hot electrons so as to prevent a potential rise therein (which would generate resonant transport). This arrangement, although more complex, retains many of the key advantages of

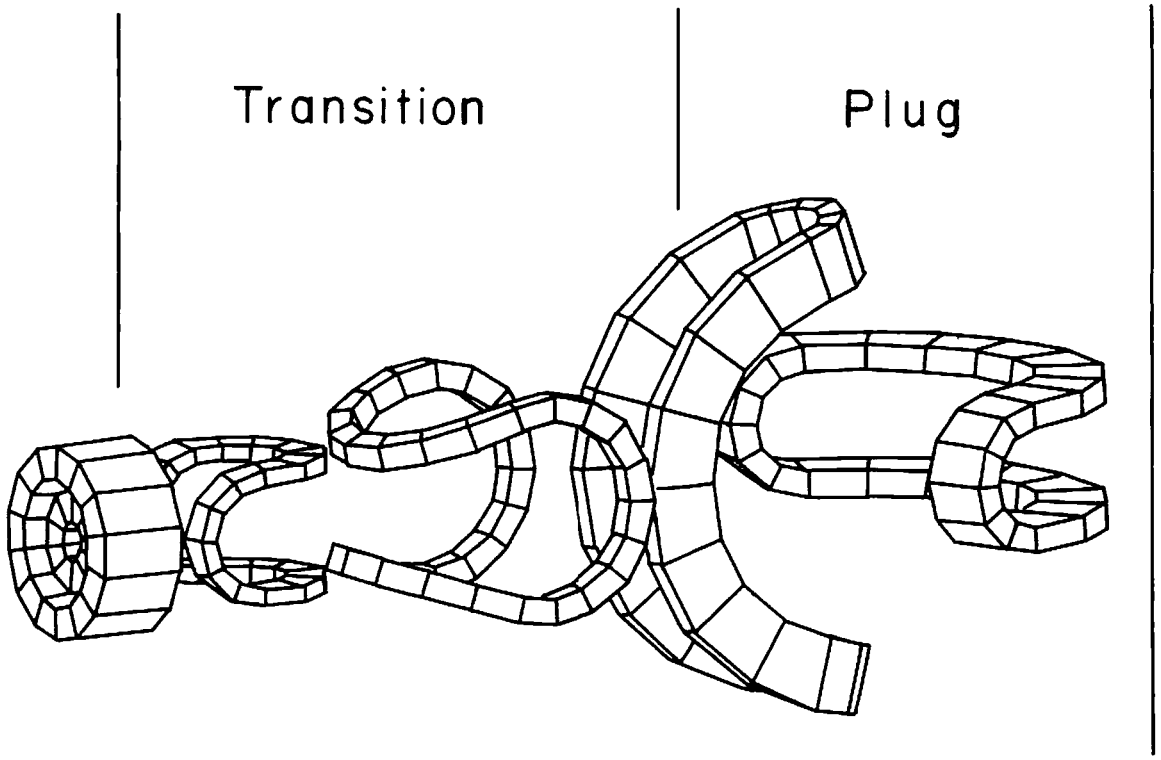

Figure IV.C.3: MFTF end plug coil design. Double Baseball transition provides cancelling geodesic curvature to minimize resonance transport for passing ions.

Figure IV.C.4: Gamma–10 tandem mirror

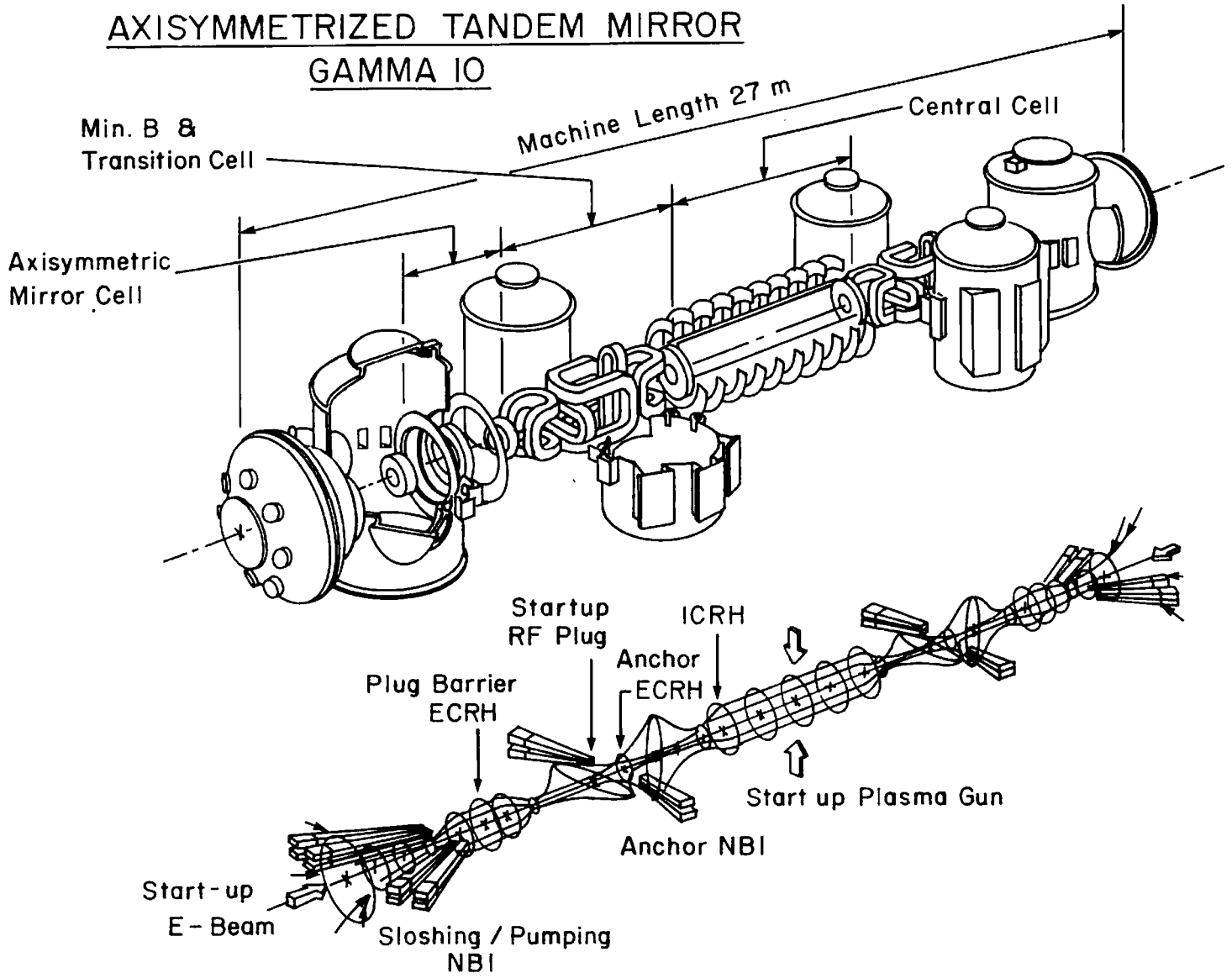

other approaches. Its chief drawback may be that a relatively high plasma beta would be located within the transition regions which could serve to degrade MHD interchange and ballooning limits.

IV.D Negative Tandem Mirror Operation

Another tandem mirror operating mode closely related to thermal barrier operation is called the negative tandem mirror. In this operating mode, the potential of the plug (which adjoins the central cell) is driven negative by a combination of electron heating (ECRH) and ion pumping as in the thermal barrier. However, the ion plugging cell (Fig. IV.A.1) is eliminated. The central cell electrons would then reflect at the midplane of the negative plugs and the central cell would float negative so that ions would reflect at the outer plug regions. The resulting potential is shown schematically in Fig. IV.D.1, which compares potentials from a simple tandem mirror, a tandem mirror with thermal barriers and a negative tandem mirror.

The principal advantage of such a scheme is the elimination of a neutral–beam–sustained ion population from the end cell with the resulting reduction in recirculating power and neutral beam efficiency. Furthermore, the electrostatically–confined ion population is now not susceptible to either loss–cone or anisotropy–driven instabilities. Pumping requirements are reduced compared to sloshing–ion schemes since the pumping of the sloshing species is eliminated. The pumping requirement for central cell ions that trap in the negative potential depression is comparable to levels required in the sloshing ion scheme.

The primary difficulty of the negative tandem mirror rests in maintaining the hot electron population. A simple negative tandem scheme which included high density hot electron plugs was considered early on by Fowler but was abandoned due to the relatively high electron collisionality. It was later realized by Logan [Logan, 1979] in the development of the thermal barrier concept that

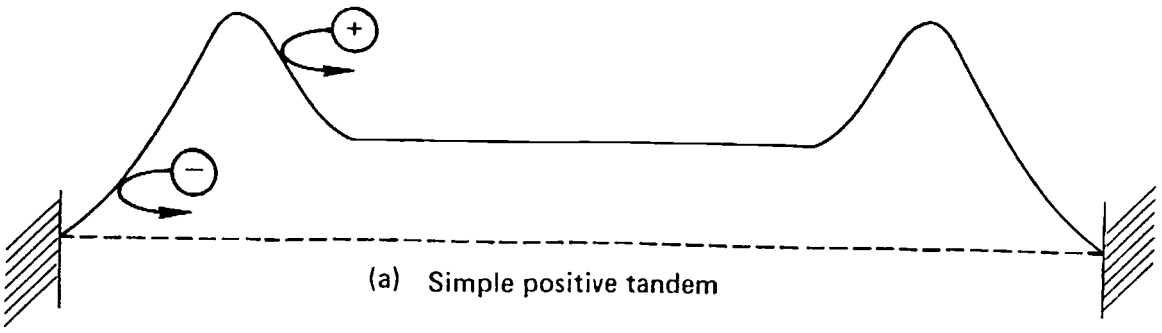

(a) Simple positive tandem

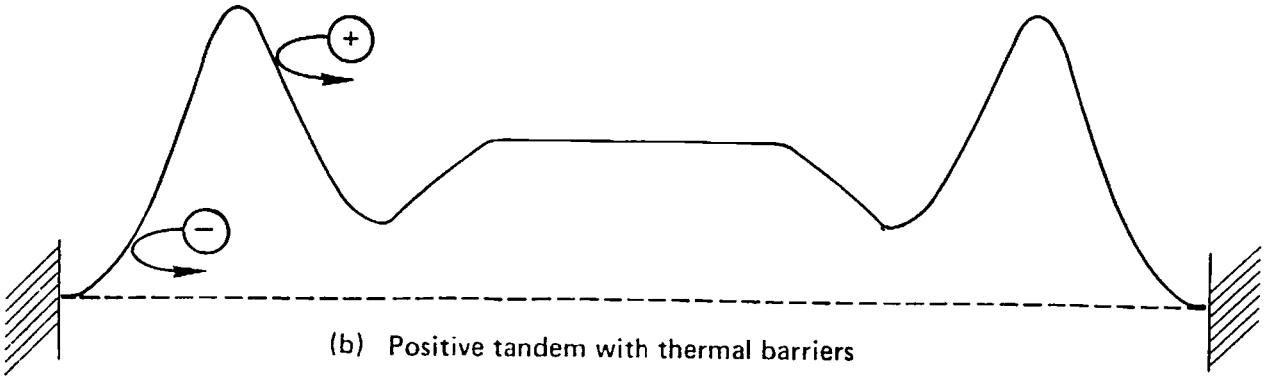

(b) Positive tandem with thermal barriers

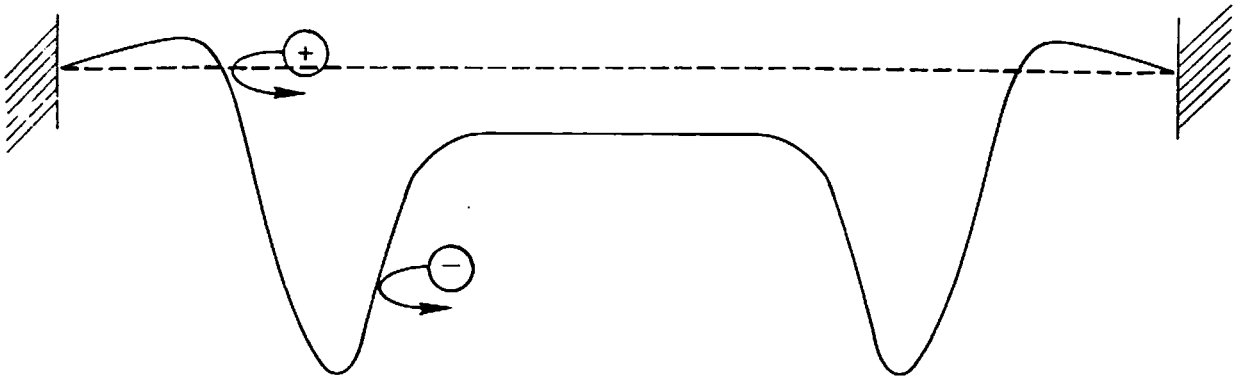

(c) Negative tandem mirror

Figure IV.D.1: Axial potential profiles of tandem mirrors.

pumping of the ion species that traps in the negative plug would permit a large negative potential to develop with much reduced plug densities, thereby greatly reducing the hot electron loss rate.

As in the converse hot ion plug case, cold electrons are expelled from the negative plugs and a hole and loss cone will develop in the electron distribution. The hot electrons are thus susceptible to both loss cone and anisotropy driven instabilities. Unlike the ion case, the electron dielectric constant $(\omega_{pe}^2/\omega_{ce}^2)$ is necessarily less than unity (to permit ECRH access) which should serve to reduce instability growth rates. However, parallel wave lengths tend to be smaller, enhancing the danger of convective modes. The most dangerous modes that have been suggested are the upper hybrid loss cone mode [UHLC] and the electromagnetic anisotropy driven Whistler and Timofeev modes. The UHLC instability has been subject to detailed study for plasma parameters appropriate to the earth's magnetosphere [Ashour-Abdalla and Kennel, 1978]. Detailed analyses of these modes relevant to tandem mirrors remain to be performed, but it appears difficult to avoid the parameter ranges of these instabilities [Y. Chen *et al.*, 1981]. The degree of deterioration of energy and particle confinement resulting from the presence of a marginally-stable level of turbulence of these modes remains to be obtained.

Another question that has been addressed is that of the limitations on ion pumping required to sustain the desired potential profiles. It has been shown in a thermal barrier context that obtaining a self-consistent continuous potential depression places limitations on the ion pumping rate which are seen to be more severe in the negative tandem mirror case. These calculations did not consider

the presence of a hot electron species. Nevertheless, it has been shown that for sufficient hot electron density and trapped thermal central cell ion population, the desired potential profiles can be self-consistently generated [Poulsen et al., 1982].

The production of a hot electron population with a desired energy and density is crucial to this scenario. The hot electron population must be both fueled and heated by ECRH, a process that is more subtle in its interrelationship with the central cell sustenance and ion pumping than the comparable neutral beam driven hot ion plugs.

The negative plug fueling problem is rendered more difficult than in the thermal barrier case by the absence of central cell confined electrons beyond the mirror midplane. Thus, the feed must be localized on the central cell side of the midplane. The ability to obtain a required electron feed is similar to the comparable ion ICRF fueling [Kesner,1978] which was successfully demonstrated by the Phaedrus experiment [Breun et al., 1980]. (It should be noted that, in the Phaedrus experiment, ICRF fueling appears to result from single-pass ion trapping whereas in the desired negative plugs such trapping would result from a multiple pass diffusive process.) Phaedrus results are discussed in more detail in Sec. V.C.

The key to the fueling process is to place the rf resonance zone at a mod-B surface located between the plug midplane and inner (central cell side) mirror throat . Ion pumping and ECRH diffusion must be adequate to produce a potential profile that is self-consistently generated to peak at the plug midplane as shown in Fig. IV.D.1. In this situation, a passing electron must first become

Yushmanov trapped, that is trapped between the inner magnetic field peak at z_1, and the plug midplane potential peak at z_2 and then be further heated to become magnetically trapped.

Additionally, the same ECRH heating constraints apply to the negative mirror as they do the thermal barrier, *i.e.*, the electrons must be sustained at the desired energy and beta. To avoid electron runaway and thus ensure MHD-like electron behavior and sufficient density, the heating zone must be well localized at the plug midplane.

References Sections IV and IV.A

1. Baldwin, D.E., 1981, Bull. A.P.S. **26**, 1621.

2. Baldwin, D.E. and B.G. Logan, 1979, Ch. 3-A.

3. Baldwin, D.E. *et al.*, 1980, in Proc. 8^{th} Int. Conf. on Plasma Physics and Cont. Fus. (IAEA: Vienna).

4. Cohen, R., 1981, Nucl. Fusion **21**, 209.

5. Cohen, R.H., 1983, Lawrence Livermore National Laboratory Report UCRL-88778.

6. Cohen, R.H., I.B. Bernstein, J.J. Dorning and G. Rowlands, 1980, Nucl. Fusion **20**, 1421.

7. Fowler, T.K., 1980, in Mirror Theory Monthly, Lawrence Livermore National Laboratory.

8. Fowler, T.K. and B.G. Logan, 1979, in Mirror Theory Monthly, Lawrence Livermore National Laboratory.

9. Kesner, J., 1973, Plasma Physics **15**, 577.

10. Kesner, J., 1980, Nucl. Fusion **20**, 557.

11. Kesner, J., G. Knorr, D.R. Nicholson, 1981, Nucl. Fusion **21**, 1265.

12. Logan, B.G., 1980, Comments Plasma Physics and Cont. Fus., **5**, 271.

13. Logan, B.G. *et al.*, 1983, Mirror Advanced Reactor Study, Interim Design Report, Lawrence Livermore National Laboratory Report UCRL-53333.

14. Matsuda, Y. and T.D. Rognlien, 1983, Lawrence Livermore National Laboratory Report UCRL-89124.

15. Ryutov, D.D. and G.V. Stupakov, 1977, JETP Lett. **26**, 174; 1978 Fiz. Plazmy 4, 501; 1978, Dukl. Akad. Nauk. SSSR **240**, 1086.

16. Stallard, B.R., Y. Matsuda, W.M. Nevins, 1983, Nucl. Fusion, in press.

17. Shuy, G.W., 1981, Comments Plasma Phys. and Cont. Fus. **6**, 155.

References Section IV.B

1. Coensgen, F., T.C. Simonen, A.K. Chargin, B.G. Logan, 1980, Lawrence Livermore National Laboratory Report LLL–Prop–172.

2. Fowler, T.K. and B.G. Logan, Nov. 1979, in Mirror Theory Monthly, Lawrence Livermore National Laboratory.

3. Gerver, M.J. *et al.*, 1982, see III-e.

4. Kanaev, B.I., 1976, (PR–6) Ch. II.

5. Kesner, J., 1973, Plasma Physics **15**, 577.

6. Kesner, J., 1980, Nucl. Fusion **20**, 557.

7. Kesner, J., R.S. Post, D.B. McVey and D.K. Smith, 1982, Nucl. Fusion **22**, 549.

8. Launois, D., P. Lecoustey, J. Tachon, J. Kesner and N. Nicholet, 1971, Proc. 4^{th} Int. Conf., Madison (IAEA: Vienna), p. 575.

9. Launois, D., P. Lecoustey, J. Tachon, J. Kesner and M. Chattellier, 1973, Nucl. Fusion **17**, 775.

10. Nicholet, N. *et al.*, 1972.

11. Pearlstein, L.D. *et al.*, 1980, "Loss-Cone Stability," in D.E. Baldwin and B.G. Logan, (eds.), Physics Basis for MFTF-B, Lawrence Livermore National Laboratory Report UCID-18496 Pt 2, pp. 11-109.

References Section IV.C

1. Baldwin, D.E., B.G. Logan, T.C. Simonen, eds. 1980, Lawrence Livermore National Laboratory Report UCID-18496.

2. Carlson, G. *et al.*, 1981, Lawrence Livermore National Laboratory Report UCID-19271.

3. Kesner, J. *et al.*, 1980

4. Kesner, J., R.S. Post, D.K. Smith, D.E. Baldwin and Y.C. Lee, 1982, Nucl. Fusion **22**, 577.

References Section IV.D

1. Ashour-Abdalla, M. and C.F. Kennel, 1978, J. Geophys. Res. **83**, 1531.

2. Breun, R. *et al.*, 1981 Phys. Rev. Lett. **47**, 1833.

3. Chen, Y.-J., W.M. Nevins and G.R. Smith, 1981, in *Proc. Workshop on Hot Electron Ring Physics*, San Diego, CA, Oak Ridge National Laboratory Report Conf-811203, **Vol. 2**.

4. Guest, G.E. and D.J. Sigmar, 1971, Nucl. Fusion **11**, 151.

5. Kesner, J., 1978, Nucl. Fusion **19**, 107.

6. Logan, B.G., 1979, Mirror League Workshop, Lawrence Livermore National Laboratory, Livermore, CA.

7. Poulsen, P. *et al.*, 1982, Lawrence Livermore National Laboratory Report UCID–19341.

V. SURVEY OF EXPERIMENTAL FACILITIES

V.A Introduction

The design and construction of four tandem mirror devices began shortly after the invention of the tandem mirror in 1976. Gamma-6 (Γ-6) became operative at Tskuba University in Japan early in 1978, TMX at Lawrence Livermore National Laboratory began operation in 1978, Phaedrus, at the University of Wisconsin, in 1979 and the AMBAL experiment at Novosibirsk (U.S.S.R.) is expected to begin operation in 1983. Table V.A.1 indicates the parameters achieved in experiments in operation and those predicted for experiments under construction.

Additionally, after the invention of the thermal barrier as a means of potential enhancement and the understanding that sloshing ion distributions would improve ion microstability, a second generation of experiments was proposed and is nearing completion. These include the TMX-Upgrade experiment at Livermore, TARA at MIT and Gamma-10 (Γ-10) at Tskuba University (Japan). Additionally, the MFTF experiment, which had been designed as a large single-cell minimum-B mirror experiment, was redesigned to form a tandem device capable of producing parameters in the fusion reactor range. In this chapter the results and conclusions from the TMX and Phaedrus experiments are reviewed briefly.

DESIGNATION	Phaedrus		TMX	TMX-U[a]	STM[a]	TARA[a]	MFTF-B[a]	GAMMA 6	GAMMA 10[a]	AMBAL[a]
COUNTRY	USA		USA	USA	USA	USA	USA	JAPAN	JAPAN	USSR
STARTUP YEAR (NEW TANDEMS)				1982	1982	1984	1985		1983	1982
TYPE	ICRH	NB[a]		Thermal barrier	Axisym-metric	Thermal barrier	Thermal barrier Mars mode		Thermal barrier	
Central Cell										
Magnetic field strength (T)	0.25 to 0.1		0.2	0.3	0.25 to 0.59	0.2	1.0	0.15	0.4	0.15
Mirror-to-mirror length (cm)	450	450	530	800	71	1000	1580	240	640	350
Plasma radius (cm)	12	12	30	20	*	12	30	2.8 x 37[b]	25	30
Neutral-beam average particle energy (keV)	--	--	--	11(H°)	*	—		--	--	0.2(D°)
Neutral-beam current (A)	--	—	--	240	*	--	--	--	--	20
Duration (ms)	13	30	--	75	*	30	3×10^4	—	--	500
ICRH rf power (kW)	200	200	--	--	--	1000	800	--	1000	--
Plasma density (cm^{-3})	2×10^{12}	2×10^{13}	3×10^{13}	2×10^{13}	$<1 \times 10^{12}$	4×10^{12}	4×10^{13}	1×10^{13}	1×10^{13}	1×10^{13}
Ion temperature (keV)	0.01	0.2	0.25	0.9	1.0(max)	0.4	15	0.04	1.0	0.5
Electron temperature (keV)	0.03	0.05	0.2	0.6	*	0.4	9	0.015	1.0	1.0
Ion-confining potential (kV)	0.01	0.07	0.3	2.2	*	2.2	30	0.05	2.5	1.1
Confinement parameter ($cm^{-3}.s$)	5×10^9	5×10^9	1×10^{11}	4×10^{11}(total) 1×10^{12} (P)	*	3×10^{11}(P)	5×10^{13}(P)	5 to 10×10^9	1×10^{12}(P)	3×10^{11}

End cells						Anchor	Axicell	Anchor	Axicell		Anchor	Axicell	
Midpoint magnetic (T)	0.3	0.4	1.0	0.5	*	0.4	0.5	1.0	4	0.4	0.7	0.6	1.0
Mirror magnetic field (T)	0.51	0.69	2.0	2.0	*	0.8	3.0	3.0	12,6	0.92	2.2	3.3	2.0
Mirror-to-mirror length (cm)	115	115	115	300	71	115	200	510	200	75	160	248	100
Plasma radius (midplane)(cm)	5.5	5.5	10	15	*	9	8	30	15	3	18	20	12
Neutral-beam average particle energy (keV)	--	4.5	13	11(H°)	*	15	15	70	60	10	50	25	20(H°)
Neutral-beam current (each plug)(A)	--	150	250	360	*	100	63	75	25	10	25	50	300,100
Duration (ms)	13	30	25	75	*	30	30	3 x 10	3 x 10	1	100	100	100,500
ICRH (each plug)(kW)	200	200	--	--	--		1000	--	--	4	500	--	—
ECRH (each plug)(kW)	50	--	--	400	5.0		200	800	--	REB	200	400	--
Plasma density (cm^{-3})	4×10^{12}	10^{13}	4×10^{13}	7×10^{12}	$<1 \times 10^{12}$	6×10^{12}	10^{13}	$\sim 5 \times 10^{12}$	$\sim 10^{14}$	5×10^{13}	1.5×10^{13}	5×10^{12}	3×10^{13}
Average plasma ion energy (keV)	0.8	4.5	13	10	--	9	9	70	70	0.04	30	20	20
Electron temperature (keV)	0.03	0.05	0.26	1.4	-.030	0.7	0.7	70,500	9	0.02	1.0	2.5	1.0

[a]Predicted plasma parameters

[b]Oval cross section

(P) Pastukhov nτ includes only those ions that are lost axially and reach the end plate.

*Information not available

V.B The TMX Experiment[a]

V.B.1 Introduction

The TMX experiments at Lawrence Livermore National Laboratory demonstrated the fundamental tandem mirror principles, as summarized in Table V.B.1. Table V.B.2 lists the maximum plasma parameters achieved in TMX. The main result was that TMX generated electrostatic confining potentials that significantly improved central-cell plasma confinement. These data established a new method of scaling ion confinement by ambipolar potential in magnetic mirror systems and provided the impetus for the initiation of both TMX-Upgrade, a tandem mirror in which potential confinement is increased through the use of thermal barriers, and MFTF-B, a larger tandem mirror that will extend the TMX-Upgrade results to thermonuclear temperatures.

---

[a]This section contains the executive summary from "Summary of Results from the Tandem Mirror Experiment," [T. Simonen *et al.*, 1981].

TABLE V.B.1

Summary of TMX Results

- Generated tandem mirror configuration:
  - -Configuration sustained for full 25-ms shot duration.
  - -Plug microstability maintained with solenoid outflow.
  - -Central-cell MHD stability (40% maximum beta with neutral-beam injection).
- Demonstrated central-cell electrostatic plugging:
  - -Measured electrostatic potential well.
  - -Direct evidence by measurements made when one end plug was turned off.
  - -Measured factor-of-9 electrostatic enhancement.
  - -Radial confinement exceeds axial confinement.
- Improved electron confinement:
  - -Electron temperature higher than in 2XIIB.
  - -Low density at end wall.
  - -Dominant power loss to end walls.
  - -Low levels of impurities.

TABLE V.B.2

Maximum plasma parameters achieved in TMX with deuterium fuel and a central-cell magnetic field strength of 0.1 T. These parameters were not achieved simultaneously on the same shot.

Plug density	4×10^{13} cm^{-3}
Plug ion energy	13 keV
Plug electron temperature	0.26 keV
Plug radius	10 cm
Central-cell density	3×10^{13} cm^{-3}
Central-cell ion energy	0.25 keV
Central-cell radius	30 cm
Plug plasma potential	1 kV
Central-cell confining potential	0.3 kV
Central-cell axial-confinement parameter	10^{11} cm$^{-3} \cdot$ s
Electrostatic enhancement in confinement	9
Central-cell beta (0.07 without central-cell neutral-beam injection)	0.40

V.B.2 Initial TMX Results

Tandem Mirror Configuration

One of the predicted tandem mirror characteristics verified by TMX was that the density of the plasma in the end plug could be sustained at a higher level than that of the central-cell plasma, and that this produced higher electric potentials in the end plugs than in the central cell. These densities were controlled by varying the end-plug neutral-beam current and the central-cell gas-feed current. The density peaks generate potential peaks, as shown in Fig. V.B.1, which also shows that relatively small end-plug plasmas can electrostatically confine a much larger central-cell plasma.

The density and temperature of the TMX plasma are within a factor of 2 of those predicted by theoretical codes. Calorimeter measurements showed that most of the neutral-beam power deposited on the axis was carried to the end walls by ions.

Gross MHD stability and microstability were achieved. Finite-beta plasma was confined in the central cell with minimum-B end plugs. The outflow of central-cell plasma provided end-plug microstability.

Improved Plasma Confinement

The TMX end plugs improve confinement of the central-cell plasma by up to a factor of 9 over that which would have been attained if the end-plug plasmas had not been present. Typical enhancements were in the range of 3 to 7 times. Central-cell axial confinement of ions is near that predicted by our theoretical

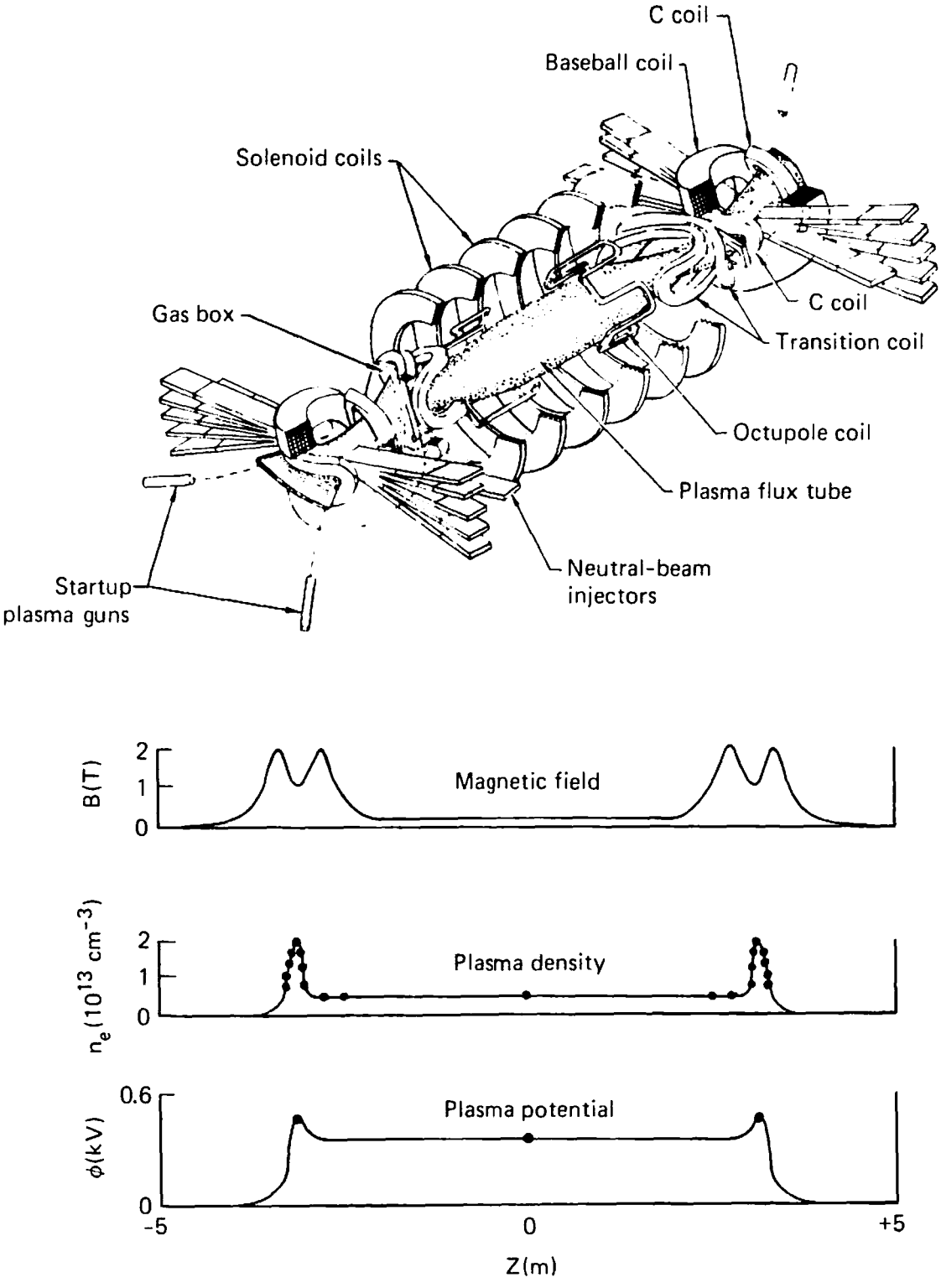

Figure V.B.1 TMX Magnet Geometry and Measured Axial Plasma Profiles

models.

TMX plasma confinement can be explained by classical coulomb theoretical models, over a certain range of parameters. However, there must be sufficient warm plasma to stabilize the plugs. If insufficient low-energy plasma flows through the end plug, then fluctuating electric fields develop at the end-plug ion-cyclotron frequency and confinement of central-cell ions is reduced. Theoretical models that have been developed on the basis of these experiments describe TMX performance over a wide range of operation.

A second measure of improvement in the tandem mirror over the single mirror is the electron temperature that can be achieved with a given amount of input neutral-beam power. TMX end plugs achieved electron temperatures up to 260 eV, three to four times higher than the electron temperatures of the similar single-cell mirror machine 2XIIB when operated with comparable neutral-beam input power. Since TMX has such a large central-cell plasma, this electron temperature increase indicates a hundred-fold improvement in electron energy confinement. This improvement arises from the fact that the low-energy plasma required for end-plug microstability is supplied from the TMX central cell rather than from the ends, as in 2XIIB, thus reducing the electron energy loss to the end walls.

V.B.3 Later TMX Results

During much of the last period of TMX operation (December 1979 through September 1980), poor vacuum conditions caused lower electron temperatures

than had been achieved earlier (although at times temperatures above 200 eV were still observed). Therefore, our progress during the later phases of TMX operation was in gaining physics understanding rather than in increasing plasma parameters. This increase in understanding results from more extensive diagnostic instrumentation, new data analysis, and improved theoretical understanding. Highlights of these recent results are summarized below.

Tandem Configuration

Plasma potential measurements carried out as a function of radius have shown that the electrostatic potential well is not just localized near the axis but extends across the central cell. The well-diagnosed plasmas had 150-V well depths, as expected for the measured electron temperature and densities. Other cases had well depths about twice as high.

End-plug potentials exceeding 1 keV have been generated and maintained in TMX.

Methods for controlling the radial profiles have been demonstrated. Operation of TMX over a wide range of central-cell gas feeds has shown that the radial density profiles which usually peak on-axis can be changed to inverted profiles peaked off-axis. Additional diagnostic channels allowed measurement of these radial density profiles in more detail than was previously possible.

Plasma Confinement

Under proper operating conditions, the confinement of the central–cell plasma is in agreement with the theoretical coulomb values. The highest confinement parameter achieved was $n\tau = 10^{11}$ cm^{-3} ·s. When end–plug fluctuation levels are significant, confinement is degraded in agreement with Monte–Carlo calculations. These fluctuations limited the range over which TMX could be operated but did not prevent us from demonstrating the basic features of tandem mirrors.

Power Balance

It is possible to account for the neutral–beam power input by using multiple diagnostic rays.

Near the axis, most of the trapped neutral–beam power is lost axially, indicating good radial confinement. Near the edge, more power is lost radially. Radial arrays of calorimeters on the TMX end wall show that the power is more concentrated on the axis than was previously assumed. Radial end–loss analyzer measurements indicate that this concentration is due to the radial profiles of both the end–loss current and the plasma potential.

Plasma Beta Measurements

After TMX was shut down, an extensive calibration of the diamagnetic loop was carried out. With this new calibration, it was determined that a maximum

central-cell beta of 0.4 was achieved with neutral-beam injection.

This calibration has also enabled us to conclude that the central-cell ion distribution has a nonmaxwellian component, as had been expected, because of ion-cyclotron heating by plug fluctuations.

Radial Transport

In TMX, radial particle confinement exceeds axial confinement near the axis. Near the edge, radial transport processes are more important.

Resonant-neoclassical-ion-transport theory is consistent with the experimental measurements, but the measurements cannot resolve factor-of-3 uncertainties in the theory nor can comparable amounts of ambipolar radial transport be resolved.

Radio-Frequency Measurements

Wavelength and polarization measurements of the end-plug ion-cyclotron fluctuation indicate wave properties more similar to the Alfven ion-cyclotron (AIC) mode than to the drift-cyclotron loss-cone (DCLC) mode. In comparison to 2XIIB, the AIC mode is theoretically more unstable in TMX, while the DCLC mode is less unstable. Theoretically, the AIC mode is expected to be much more stable in the low-ion-beta end plugs of the TMX Upgrade and MFTF-B, as is the DCLC mode.

Turbulent noncoherent central-cell fluctuations up to 0.5 MHz, possibly associated with drift waves, have been detected in the central cell. No correlation with plasma confinement has been identified.

Coherent low-frequency 7 kHz ($m = 1$) and 12 kHz ($m = 0$) oscillations have been observed in the central cell. The $m = 0$ mode is correlated with bursts of end-plug ion-cyclotron fluctuations and thus would not be expected in TMX Upgrade with microstable sloshing-ion end plugs. The $m = 1$ mode exists at large amplitude near the edge when sufficient central-cell gas input causes large density gradients near the edge. The $m = 1$ mode can be controlled by modifying central-cell radial profiles by controlled central-cell fueling and heating.

Impurity Studies

Further analysis continues to indicate remarkably low central-cell impurity levels (0.5%), resulting in less than 10% power loss by impurity radiation. Recent data analysis shows that the lower ionization states of the prevalent oxygen impurity are localized near the plasma edge and the higher ionization states near the axis, as expected.

High-resolution spectroscopy has provided Doppler-broadening measurements of impurity radiation that corroborate the 100-to-200 eV diamagnetic-loop measurements of central-cell ion temperature.

Sandia Surface-Probe Studies

Surface probes have been employed to characterize plasma-wall interactions and to determine TMX plasma properties. Passive solid-state probe measurements of particle fluxes and energies at the central-cell walls corroborate other central-cell diagnostic measurements.

The probes collected the expected number of particles on the end walls. The major component of end losses comes from the central cell. The end-plug contribution is also in agreement with theoretical calculations.

End-Wall Plasma Characteristics

The TMX plasma has been decoupled successfully from the end walls. This was a necessary accomplishment for future higher-temperature machines. A very low density (2×10^9 cm^{-3}), cool (5 eV) plasma exists near the end wall. This density is four orders of magnitude less and this electron temperature 40 times cooler than the density and electron temperature of the end plug plasmas.

Secondary electrons emitted from the end wall are detected but the power losses are small, consistent with a model developed for MFTF-B end-wall processes.

V.C The PHAEDRUS Experiment

The PHAEDRUS experiment at the University of Wisconsin was proposed by R.S. Post [Post, 1977] as an experiment dedicated to the development of ion cyclotron resonance heating techniques in tandem mirrors. It was envisioned that ICRF applied at the fundamental frequency could serve to trap and heat central-cell plasma that entered the plugs [Kesner, 1979] leading to an rf-sustained tandem mirror. Furthermore, second harmonic heating was recognized as a means to heat high energy ions preferentially, thus lessening the deleterious tendency of rf to diffuse low energy ions into the loss cone. It was expected that rf heating in combination with neutral beams would serve to reduce neutral beam energy requirements [Kesner, 1978]. Thus the Phaedrus experiment was equipped with the capability for both neutral beam- and rf- sustained operation. The Phaedrus experiment began operation in 1979.

V.C.1 Experimental Results

A summary of Phaedrus experimental results as of 1982 is contained in Table V.C.1 [Hershkowitz *et al.*, 1982]. Two separate modes of operation have been developed. The rf sustained mode is operated with resonant ICRF in the end plugs [Breun *et al.*, 1981]. In this operating mode ICRF serves the dual function of trapping the central cell stream and heating the end plug ions. Table V.C.2 lists the experimental parameters for the rf-sustained operating mode.

Table V.C.1

Summary of Phaedrus Results

- Generated an rf-sustained tandem mirror configuration
  - -The plugs are fueled by ICRF trapping of the central-cell stream.
  - -Plasmas have been sustained for as long as 25 ms.
  - -With low levels of nonresonant ICRF power in the central cell, the equilibrium is consistent with theoretical interchange limits.
  - -Central-cell ion confinement has been enhanced by a factor of three over free flow.
  - -The radial potential profiles are hollow.
- A central cell stand-alone mode was developed.
  - -At high resonant ICRF power levels, the central-cell plasma can be sustained (20 ms) with insignificant pressure in the plugs.

Table V.C.2

Phaedrus Parameters

Plug	
length (mirror-to-mirror)	1 m
plasma radius	6 cm
density	$1\text{–}10\times10^{12}$ cm^{-3}
ion temperature	0.4–1 keV
electron temperature	15–30 eV
ion confinement time	$\sim 250\ \mu$s
Central Cell	
length (mirror-to-mirror)	4.3 m
plasma radius	12 cm
density	$1\text{–}10\times10^{12}$ cm^{-3}
ion temperature	35 eV
electron temperature	12–40 eV
ion confinement time	$\geq 400\ \mu$s
beta	$\leq 8\%$
Confining potential	0–40 V
Potential to ground	60–100 V

At higher resonant ICRF power levels in the central cell, it was observed that the central-cell plasma was inherently stable by itself [Ferron *et al.*, 1982]. The stability mechanism for this mode of operation is currently under investigation. Recent developments in the neutral-beam systems for Phaedrus add the prospect of investigating combined beam–ICRF operating modes [Conrad *et al.*, 1982].

Initial experiments on Phaedrus were concerned with the development of ICRF heating techniques in a tandem mirror. A number of separate experiments were performed in the end plugs at $\omega = \omega_{ci}$ and at $\omega = 2\omega_{ci}$ and in the central cell. A novel antenna design [Smith, 1980] was particularly successful in trapping a gun plasma (of temperature $T_i \sim 100$ eV) and heating the ions up to a mean energy of 1 keV with a coupling efficiency of $\sim 90\%$ [Breun *et al.*, 1981]. Heating experiments at $2\omega_{ci}$ indicated good coupling efficiency and led to the clear observation of tail heating [Golovato *et al.*, 1982]. ICRF heating ($\omega = \omega_{ci}$) of the stream gun plasma in the central cell resulted in betas in excess of 25% [McVey, 1982]. The observed heating characteristics were interpreted as deriving from cyclotron damping of the near fields of the antenna.

V.C.2 Details of the Rf-Sustained Mode of Operation

The rf-sustained mode is operated with a particle source of neutral gas in the central cell, resonant ICRF power in the plugs, and nonresonant ICRF power input to the central cell. The plug plasmas are maintained by ICRF trapping of the central cell stream. Monte Carlo test particle modeling of this process compares favorably with the experimental parameters [Hershkowitz *et al.*, 1982; Todd, 1982]. This mode of operation has the following practical limitation. As the central-cell confining potential rises, the stream is throttled, and the ion fueling of the plug diminishes. Plug to central cell density ratios in the range of 1 to 2 have been obtained. End loss measurements suggested a factor of three enhancement of the ion confinement due to electrostatic plugging. The rf-sustained mode of operation is characterized by radial potential profiles that are hollow. This is suggestive of surface heating by the ICRF, and this hypothesis is reaffirmed by antenna field pattern calculations. The potential confinement of central-cell ions can be dynamic with the axial profiles changing during a shot [Hershkowitz *et al.*, 1982b].

MHD stability limits were measured by observing the onset of the rf-sustained mode [Molvik *et al.*, 1982]. A minimum central-cell field was necessary to generate an equilibrium plasma after stream gun turn-off. Below this threshold magnetic field, the plug beta was not sufficient to stabilize the central cell pressure. The low-frequency (3–5 kHz) fluctuations were measured to be an $m = 1$ flute-like perturbation. The experimental results were consistent with interchange stability theory [Kaiser, 1980].

References Sec. V.B

1. Simonen, T. (ed.) 1981, "Summary of Results from Tandem Mirror Experiment (TMX)", Lawrence Livermore National Laboratory Report UCRL–53120.

References Sec. V.C

1. Breun, R. *et al.*, 1981, Phys. Rev. Lett. **47**, 1833.

2. Conrad, J.R. *et al.*, 1982, Bull. A.P.S. **27**, 959.

3. Ferron, J.R. *et al.*, 1982, Bull. A.P.S. **27**, 958.

4. Golovato, S.N. *et al.*, 1982, Nucl. Fusion **22**, 741.

5. Hershkowitz, N. *et al.*, 1982a, "Plasma Physics and Controlled Nuclear Fusion Research," **Vol. 1** (IAEA: Vienna).

6. Hershkowitz, N. *et al.*, 1982b, Phys. Rev. Lett. **49**, 1489.

7. Kaiser, 1980.

8. Kesner, J., 1979, Nucl. Fusion **19**, 107.

9. Kesner, J., 1978, Nucl. Fusion **18**, 781.

10. McVey, B.D., 1982, MIT Report PFC/JA–82-16.

11. Molvik, A.W. *et al.*, 1982, Phys. Rev. Lett. **48**, 742.

12. Post, R.S., 1977, "Investigation of RF Heating for Tandem Mirror Experiments," proposal submitted to U.S. Dept. of Energy.

13. Todd, D.A., 1982, Bull. A.P.S. **27**, 914.

14. Smith, D.K., 1980, "Fundamental Resonance Ion Cyclotron Heating in the Phaedrus Plug Mirrors," Ph.D. Thesis, U. Wisconsin.